GRIDS 2026

Graduate Instrumentation and Detector School

Solid States Detectors

(with a very strong bias towards photon detection)

Serge A. Charlebois

Université de Sherbrooke, Sherbrooke (Québec), Canada

Institut interdisciplinaire d'innovation technologique UdS

Université de Sherbrooke

Outline

- Review of semiconductor properties and of the diode
- ~~SPAD~~ photodiode structure and properties*
  - Impact on wavelength sensitivity
  - Impact on timing
- Dark count and correlated noise sources
  - Extracting count rate and afterpulsing from data
- The wavelength spectrum detectable using silicon
  - Using other semiconductors
  - Detecting UV an VUV with silicon
- Geiger mode operation of an avalanche photo diode
- Large area photon counting systems (including Photon-to-Digital Converter)
- Solid state particle detectors: LGAD and MAPS

Main references used in the document

UDS

- B. G. Streetman and S. Banerjee, Solid State Electronic Devices. Pearson, 2015.
- Semiconductor Devices: Physics and Technology, 3rd Edition, Simon M. Sze, Ming-Kwei Lee, 2016. ISBN: 978-0-470-53794-7
- Physics of Semiconductor Devices, S.M. Sze, Kwok K. Ng, 2006
  - Print ISBN:9780471143239 |Online ISBN:9780470068328 |DOI:10.1002/0470068329
- Much inspired by an excellent tutorial at ISSW 2024 – SPAD sensor school (Trento) by Prof. Angelo Gulinatti (Politecnico di Milano) and Prof. Alberto Tosi (Politecnico di Milano) « SPAD principle, main performance parameters, and device structures »

Review of semiconductor properties

Review on semiconductors – A focus on column IV

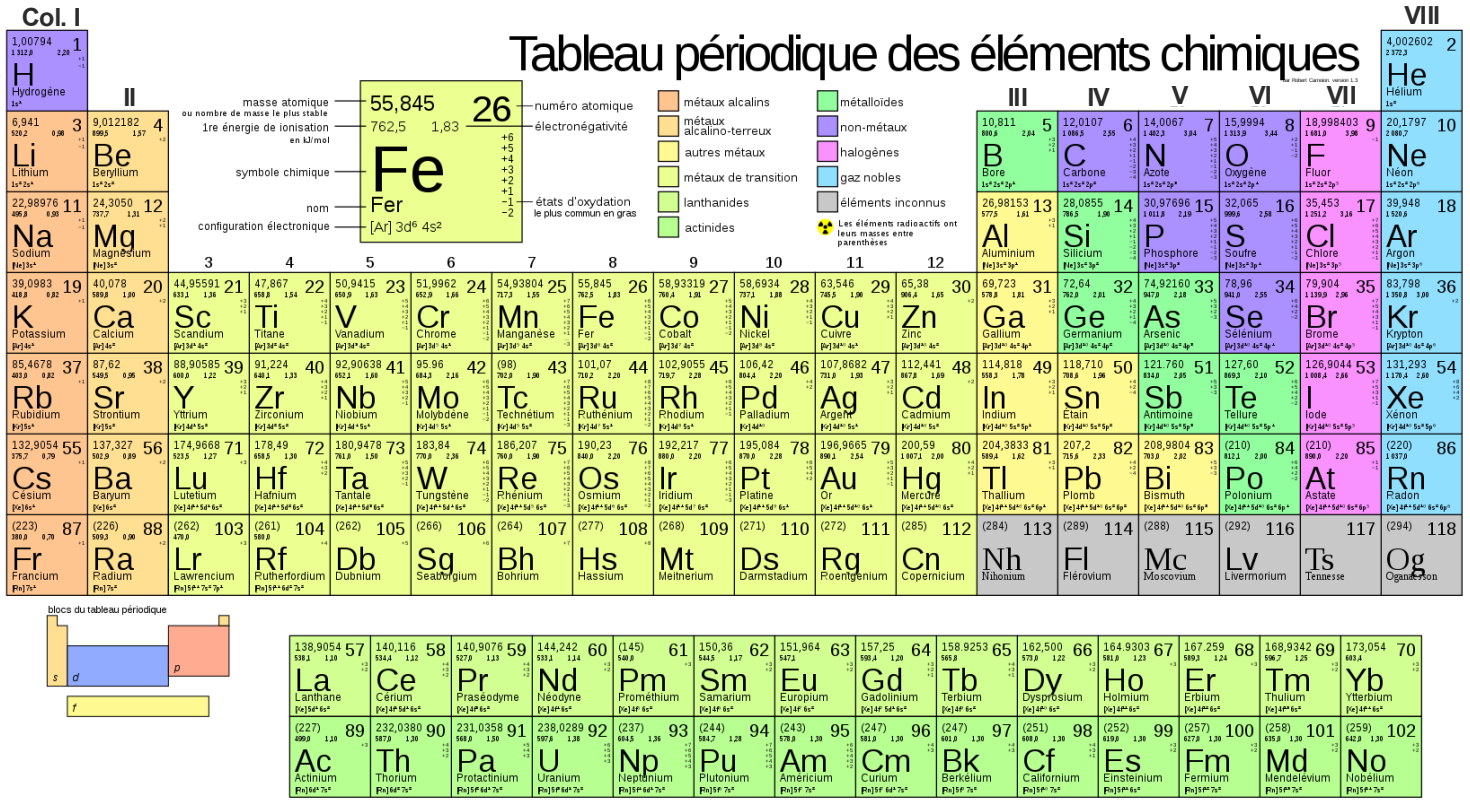

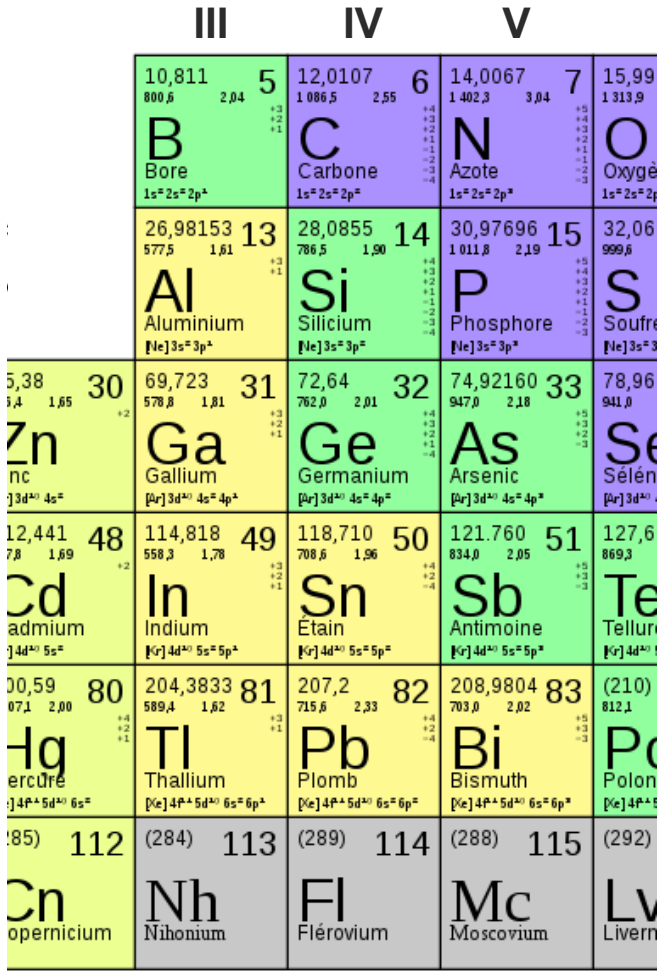

serge.charlebois@usherbrooke.ca

Review on semiconductors – The diamond and zincblende structure

- Face-centered cubic
  decorated by 2 atoms
  in a tetrahedral bonding with 4 neighbors

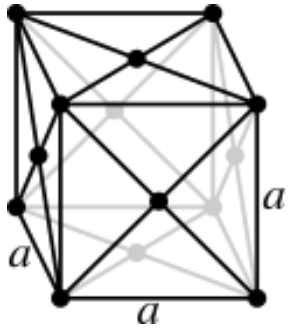

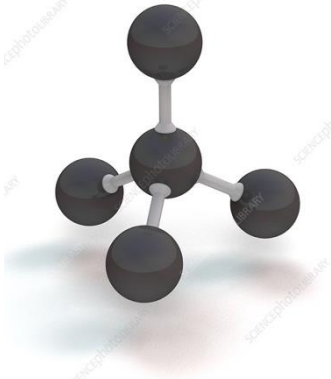

- We say diamond structure when the two atoms are identical:
  - C, Si, Ge, Sn
- We say zincblende otherwise
  - ZnS, SiGe, GaAs, InP…

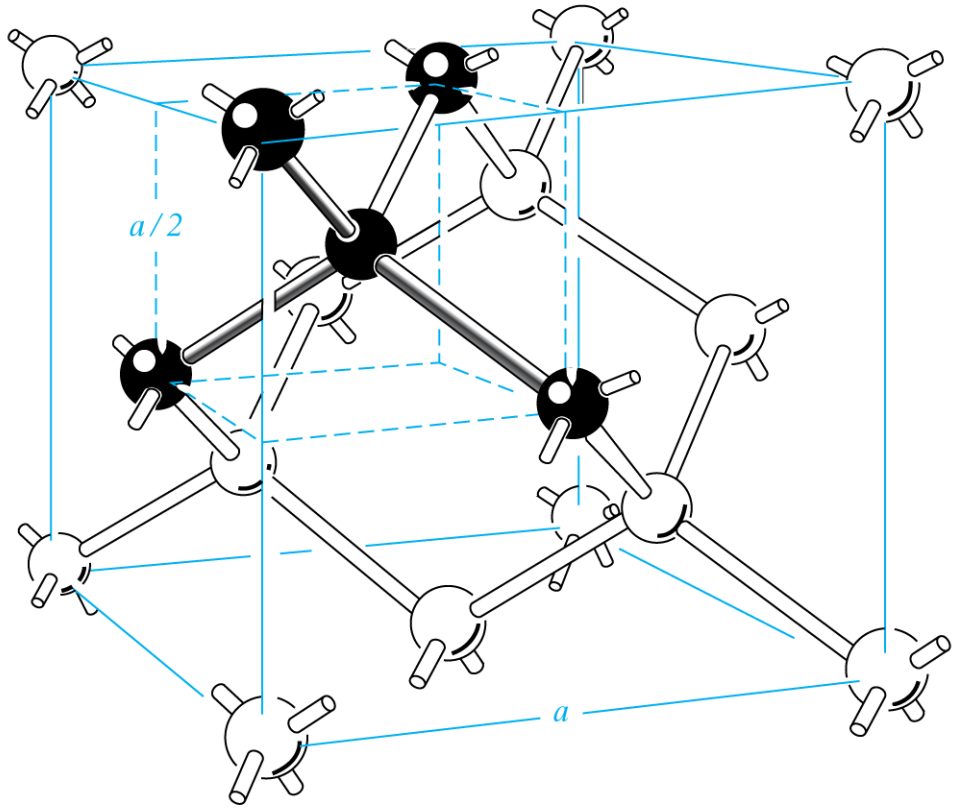

Figure 1.9

Diamond lattice unit cell, showing the four nearest neighbor structure.

(From *Electrons* and *Holes in Semiconductors* by W. Shockley, © 1950 by Litton Educational Publishing Co., Inc.; by permission of Van Nostrand Reinhold Co., Inc.)

28.0855 14

Si

[Ne] $3s^2$ $3p^2$

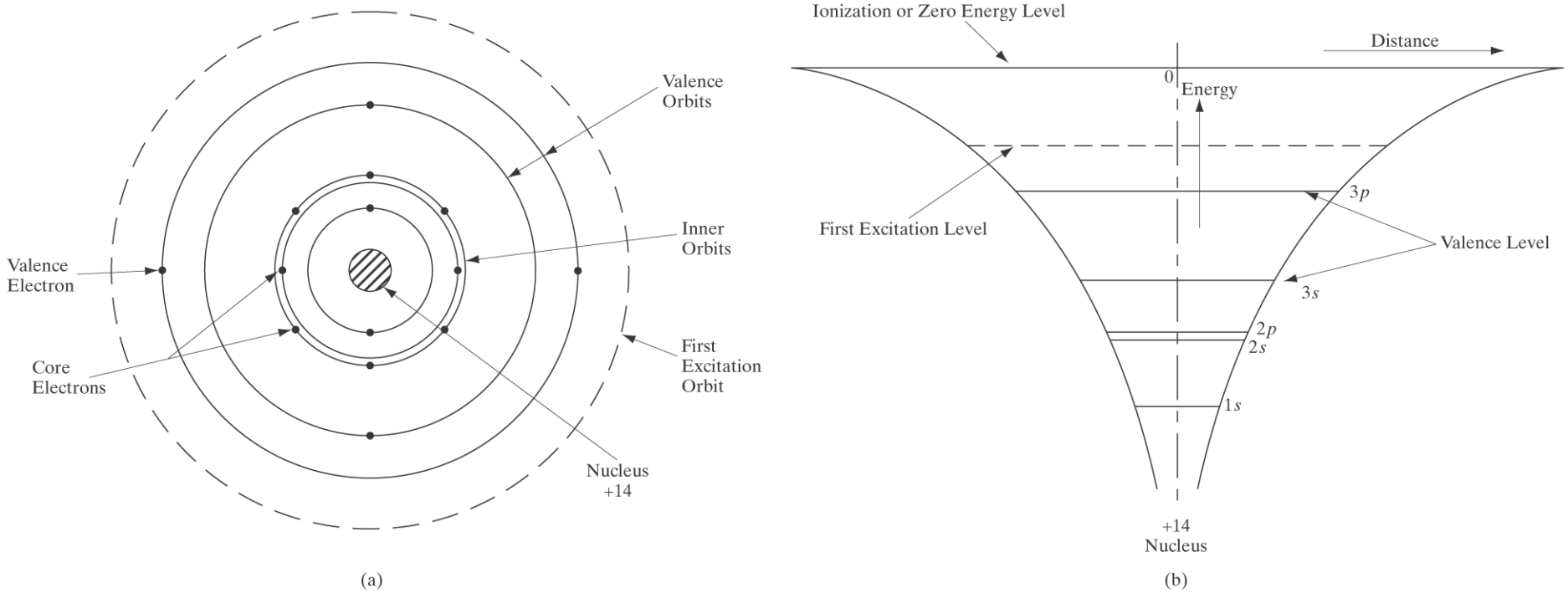

Figure 2.8

Electronic structure and energy levels in a Si atom: (a) The orbital model of a Si atom showing the 10 core electrons (**n** = 1 and 2), and the 4 valence electrons (**n** = 3); (b) energy levels in the coulombic potential of the nucleus are also shown schematically.

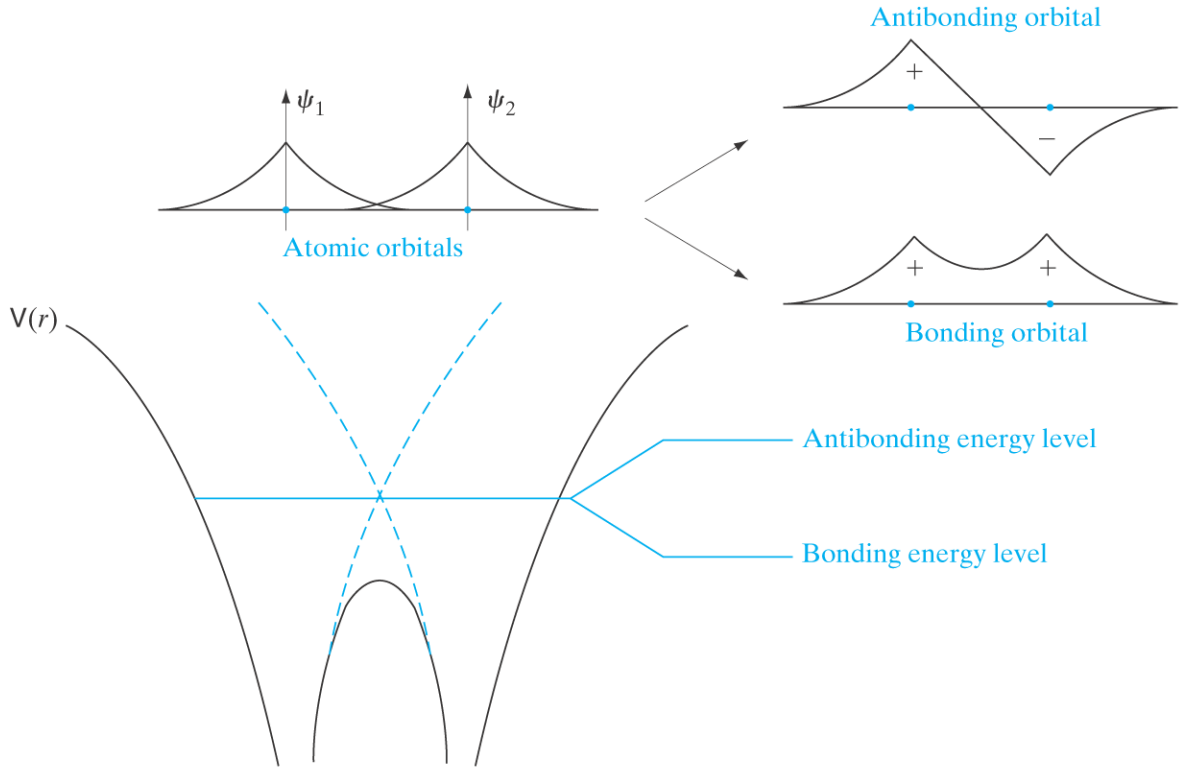

Figure 3.2

Linear combinations of atomic orbitals (LCAO): The LCAO when 2 atoms are brought together leads to 2 distinct "normal" modes—a higher energy antibonding orbital, and a lower energy bonding orbital. Note that the electron probability density is high in the region between the ion cores (covalent "bond"), leading to lowering of the bonding energy level and the cohesion of the crystal. If instead of 2 atoms, one brings together N atoms, there will be N distinct LCAO, and N closely spaced energy levels in a band.

serge.charlebois@usherbrooke.ca

Review on semiconductors – sp^3 hybridization

28.0855 14

Si

[Ne] $3s^2$ $3p^2$

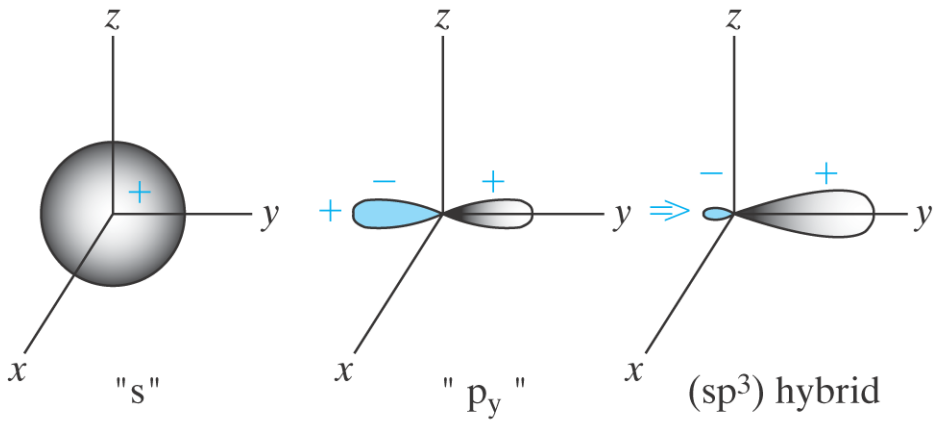

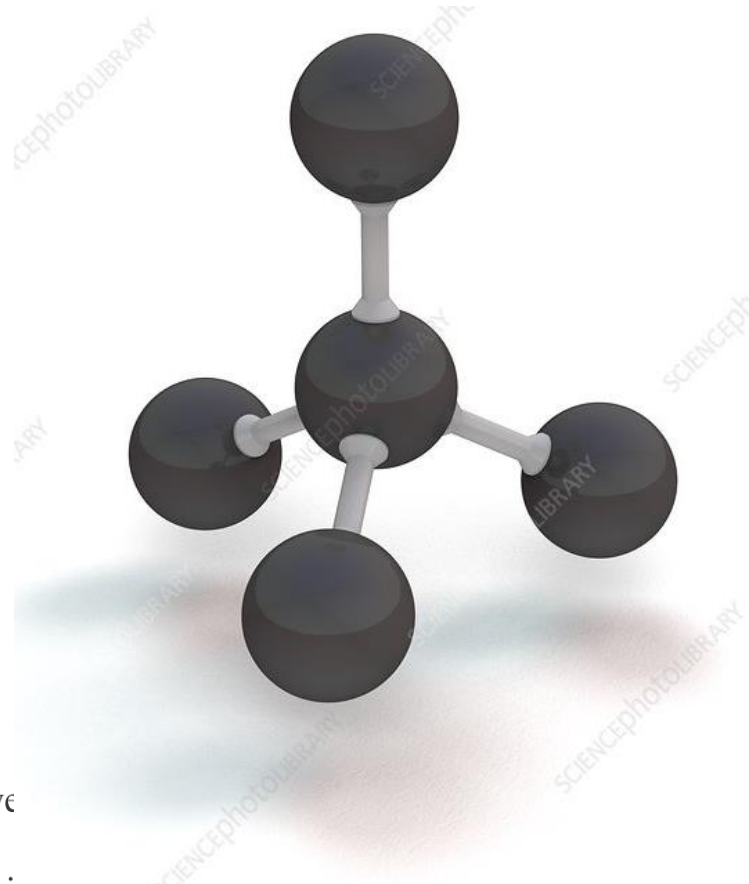

Figure 2.9

Orbitals in a Si atom: The spherically symmetric "s" type wave functions or orbitals are positive while the three mutually perpendicular "p" type orbitals (p_x, p_y, p_z) are dumbbell shaped and have a positive lobe and a negative lobe. The four sp^3 "hybridized" orbitals, only one of which is shown here, point symmetrically in space and lead to the diamond lattice in Si.

See also: https://youtu.be/k_tFJin_YoQ
https://youtu.be/wPw_LCmyjnI?si=OSmpLIyGTUG-ZsCr
https://youtu.be/hQk9xNU_2nU?si=mCVTAMogQo3O8Spg

serge.charlebois@usherbrooke.ca

Review on semiconductors – Evolution of hybridization with atomic distance

UDS

- We can have a feeling of this by using hydrostatic pressure
  - Few to 10s meV/GPa
  - Note: some indirect gaps have opposite behavior

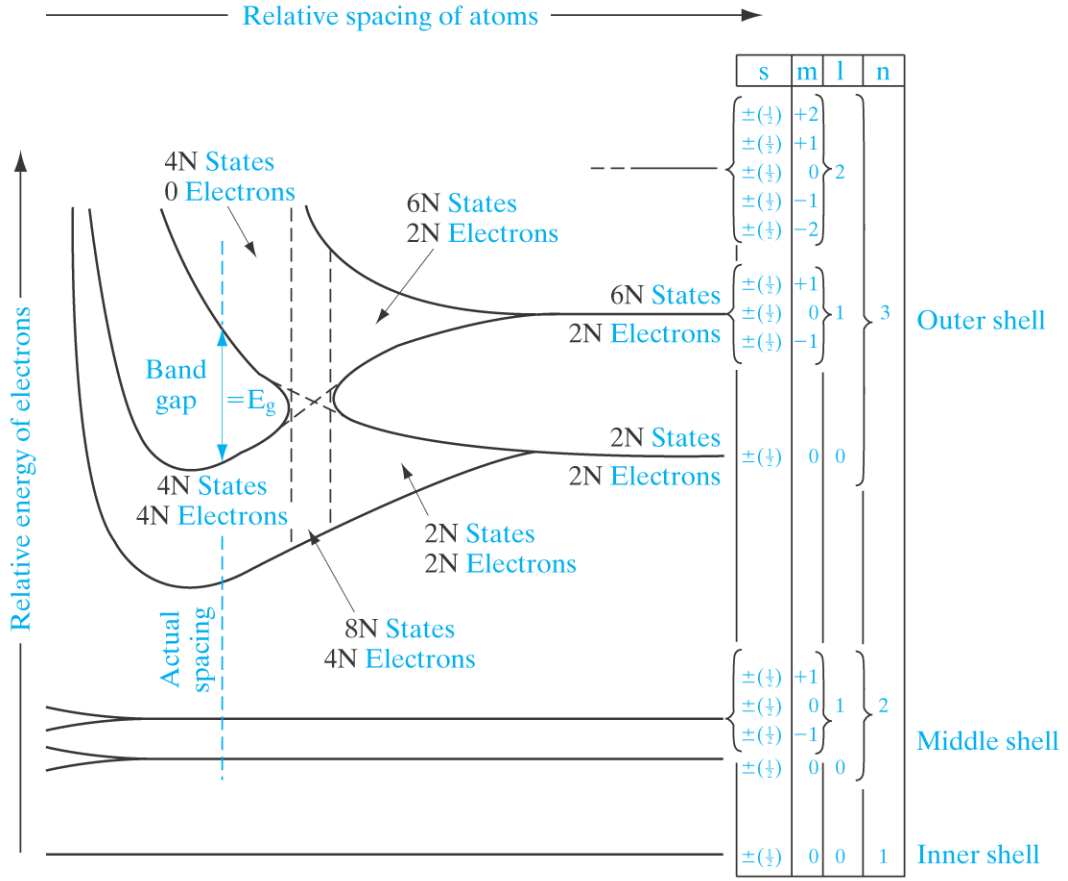

Figure 3.3

Energy levels in Si as a function of interatomic spacing. The core levels (**n** = 1,2) in Si are completely filled with electrons. At the actual atomic spacing of the crystal, the 2*N* electrons in the 3*s* subshell and the 2*N* electrons in the 3*p* subshell undergo sp^3 hybridization, and all end up in the lower 4*N* states (valence band), while the higher-lying 4*N* states (conduction band) are empty, separated by a band gap.

serge.charlebois@usherbrooke.ca

Voir aussi Sze&Lee Ch.1 Fig. 9 et 11

Review on semiconductors – Evolution of hybridization with atomic distance

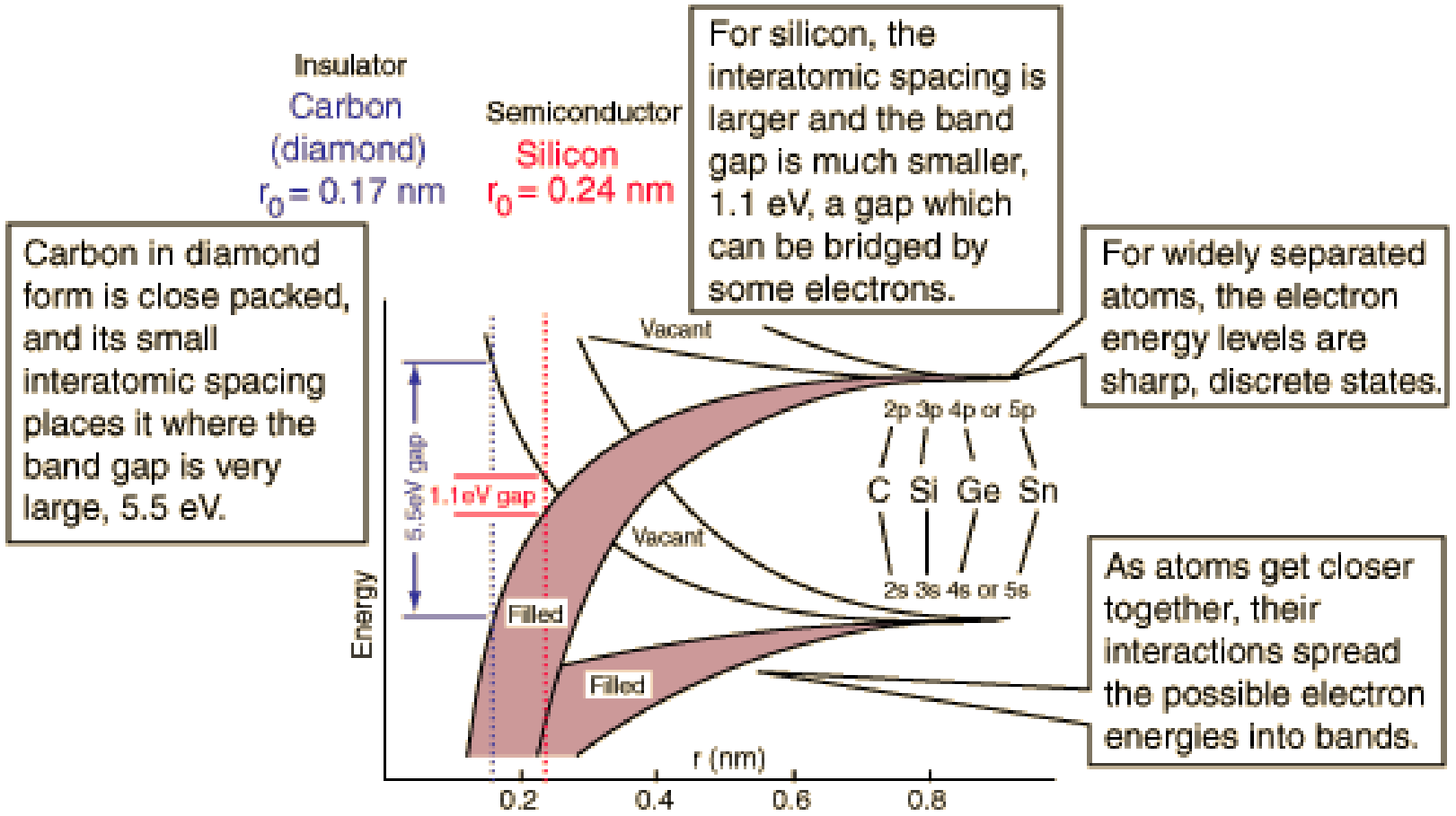

At low temperatures, electron energy levels are filled up to the Fermi level. For insulators and semiconductors, the Fermi level is in a band gap so that outer electrons are not free to move through the material in response to an electric field.

Review on semiconductors – Evolution of hybridization with atomic distance

UDS

- A close-up of the “4” monoatomic semiconductors
  - Carbon, in its diamond allotrope
  - Silicon
  - Germanium
  - Tin (yes! But in crystal form)

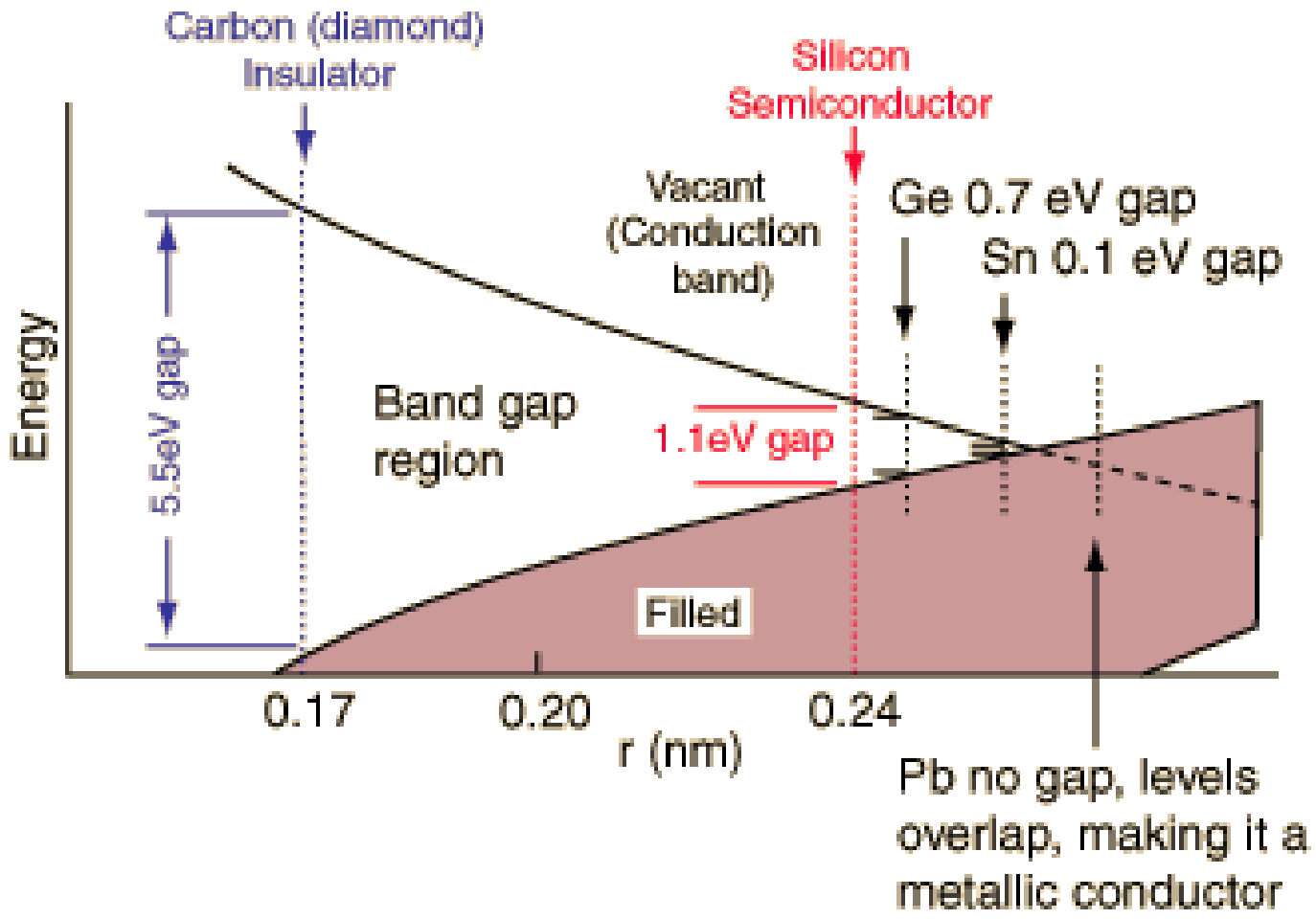

http://hyperphysics.phy-astr.gsu.edu/hbase/Solids/band2.html#c1

Review on semiconductors – A very wide family of materials

UDS

TABLE 2 Semiconductor Materials[2]

General Classification	Semiconductor	
	Symbol	Name
Element	Si	Silicon
	Ge	Germanium
Binary compound		
IV-IV	SiC	Silicon carbide
III-V	AlP	Aluminum phosphide
	AlAs	Aluminum arsenide
	AlSb	Aluminum antimonide
	GaN	Gallium nitride
	GaP	Gallium phosphide
	GaAs	Gallium arsenide
	GaSb	Gallium antimonide
	InP	Indium phosphide
	InAs	Indium arsenide
	InSb	Indium antimonide
II-VI	ZnO	Zinc oxide
	ZnS	Zinc sulfide
	ZnSe	Zinc selenide
	ZnTe	Zinc telluride
	CdS	Cadmium sulfide
	CdSe	Cadmium selenide
	CdTe	Cadmium telluride
	HgS	Mercury sulfide
IV-VI	PbS	Lead sulfide
	PbSe	Lead selenide
	PbTe	Lead telluride
Ternary compound	$Al_xGa_{1-x}As$	Aluminum gallium arsenide
	$Al_xIn_{1-x}As$	Aluminum indium arsenide
	$GaAs_{1-x}P_x$	Gallium arsenic phosphide
	$Ga_xIn_{1-x}N$	Gallium indium nitride
	$Ga_xIn_{1-x}As$	Gallium indium arsenide
	$Ga_xIn_{1-x}P$	Gallium indium phosphide
Quaternary compound	$Al_xGa_{1-x}As_ySb_{1-y}$	Aluminum gallium arsenic antimonide
	$Ga_xIn_{1-x}As_ySb_{1-y}$	Gallium indium arsenic phosphide

Review on semiconductors – A very wide family of materials

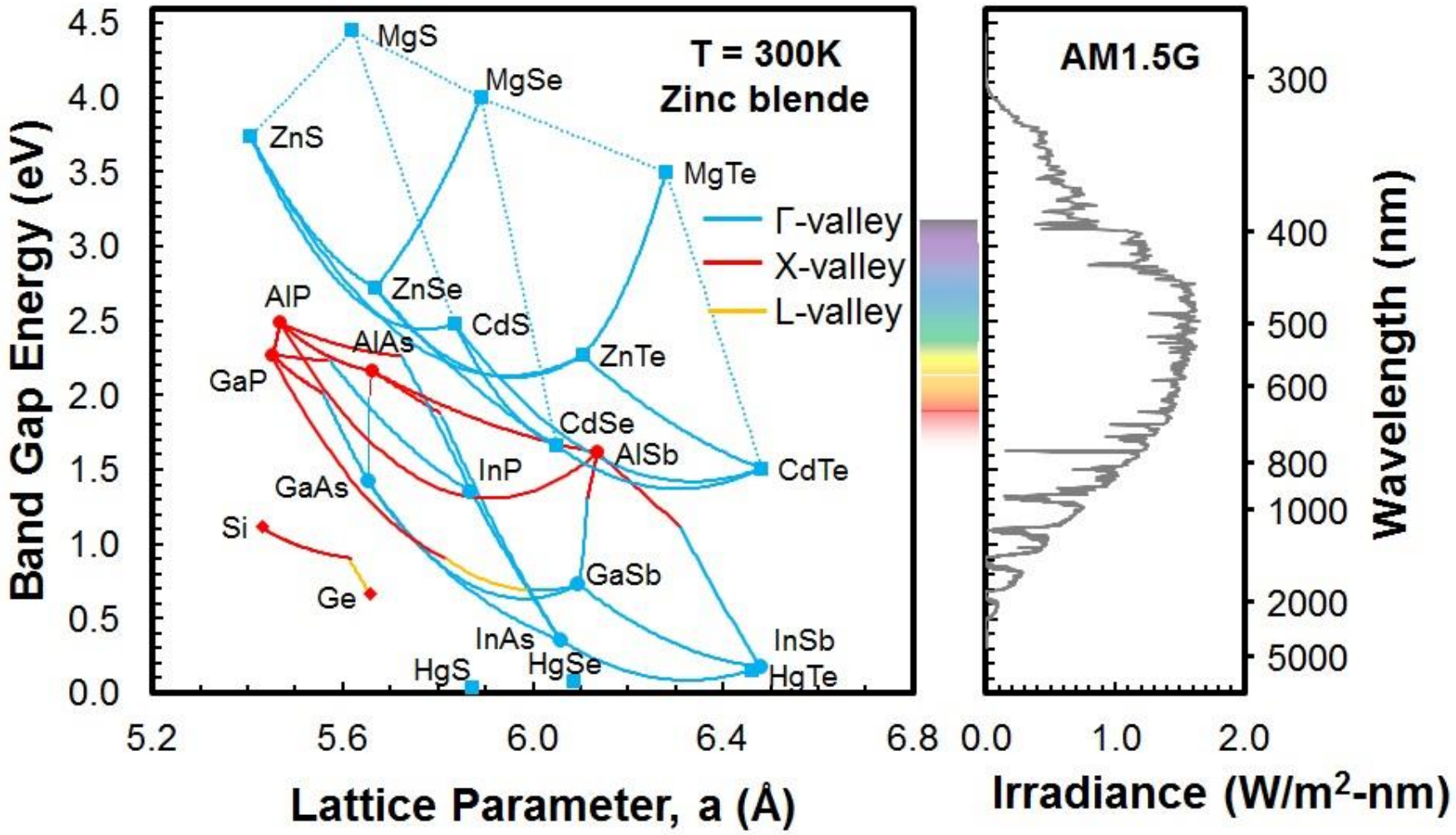

Review on semiconductors – Using semiconductors other than Si or Ge

UDS

- The crystal quality of Si and Ge is unrivaled
  - Dark noise depends on defects
  - Dielectric strength also
- Ternary and quaternary materials
  - Alloy disorder
- GaN and AlN
  - Hexagonal wurtzite crystal structure
  - Very different band properties
  - Piezoelectric material

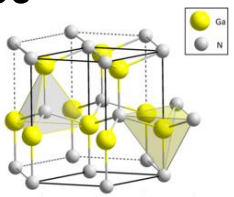

Material	Typical dislocation / defect density (cm^{-2})	Best reported (cm^{-2})
Si	< 10^2 – 10^3	< 10 (CZ/FZ)
Ge	10^3 – 10^4	~10^3 (HPGe)
4H-SiC	10^3 – 10^5 (total)	TDD < 3,500 Micropipe < 0.01
GaAs	10^3 – 10^5	~28–100 (In/B-doped)
GaAlAs	~10^3 – 10^5	~10^2 – 10^3 (homoepitaxial)
GaN	10^8 – 10^{10}	~10^6 – 10^7 (ELO/HVPE)
AlN	10^9 – 10^{10} (heteroepitaxial)	~10^2 – 10^3 (bulk boule)

Review on semiconductors – Representations with increasing complexity

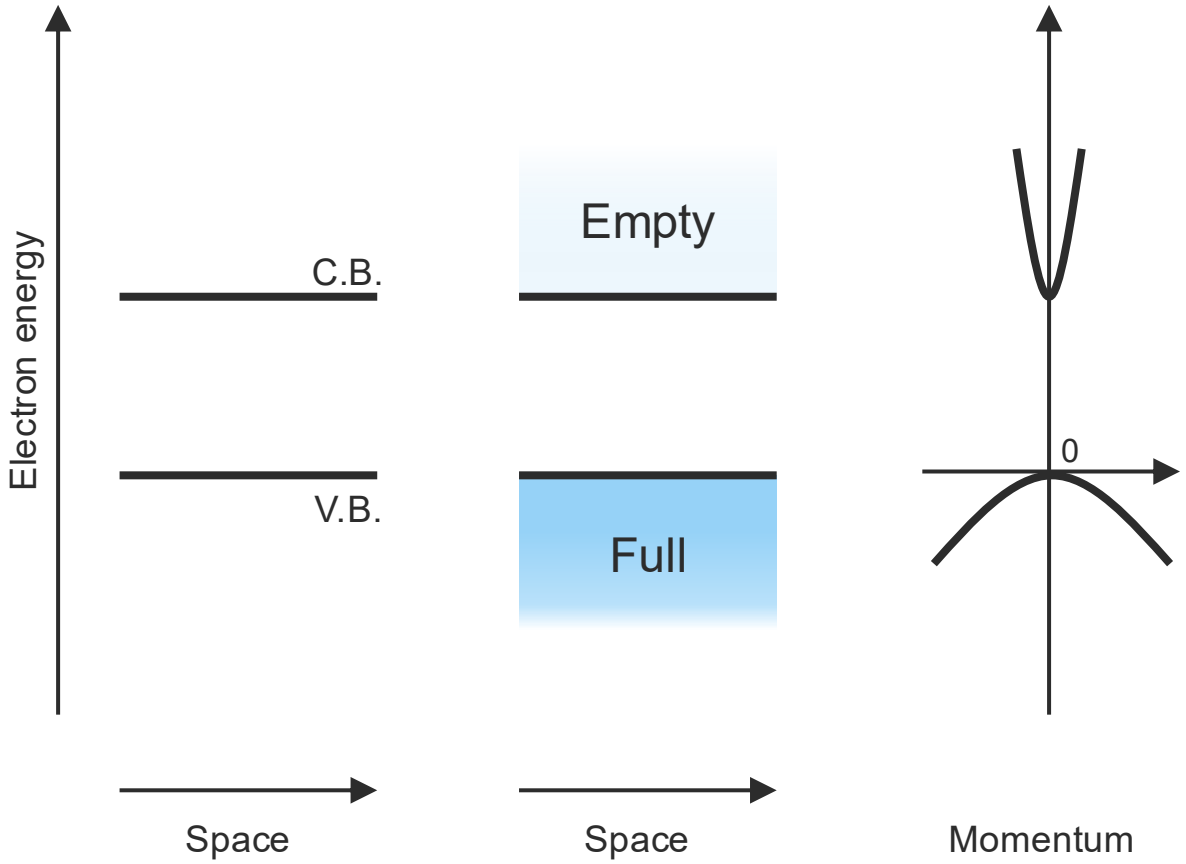

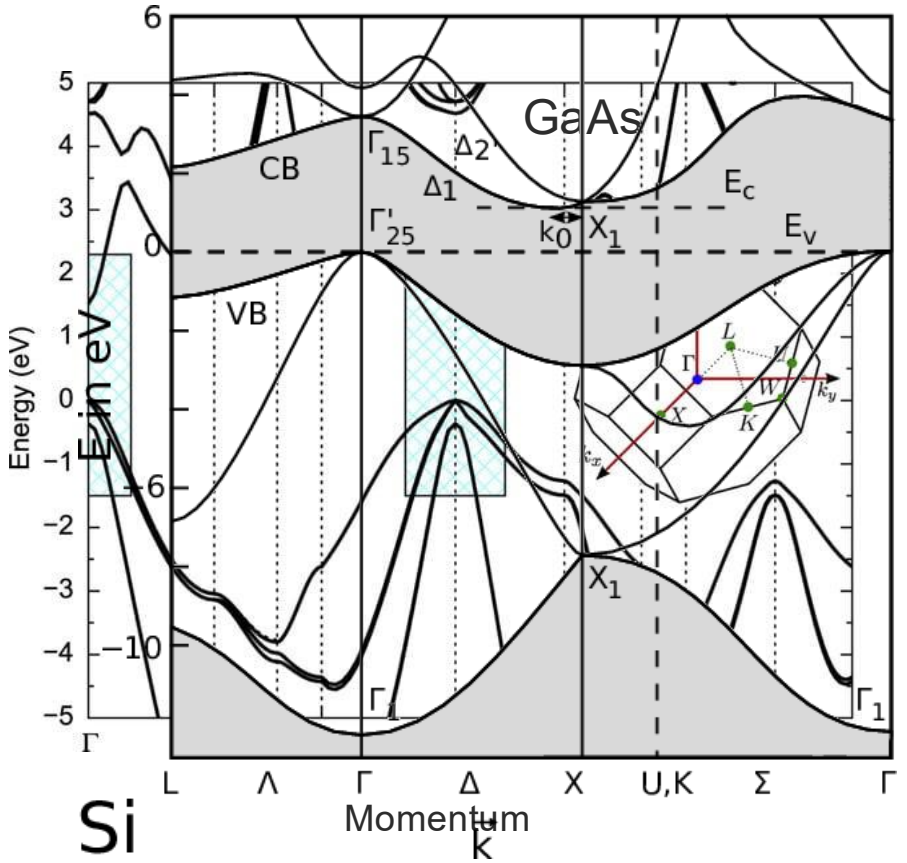

https://doi.org/10.1088/0268-1242/31/10/105002

Review on semiconductors – Direct versus indirect band gap

UDS

Ge
indirect band gap

Si
indirect band gap

GaAs
direct band gap

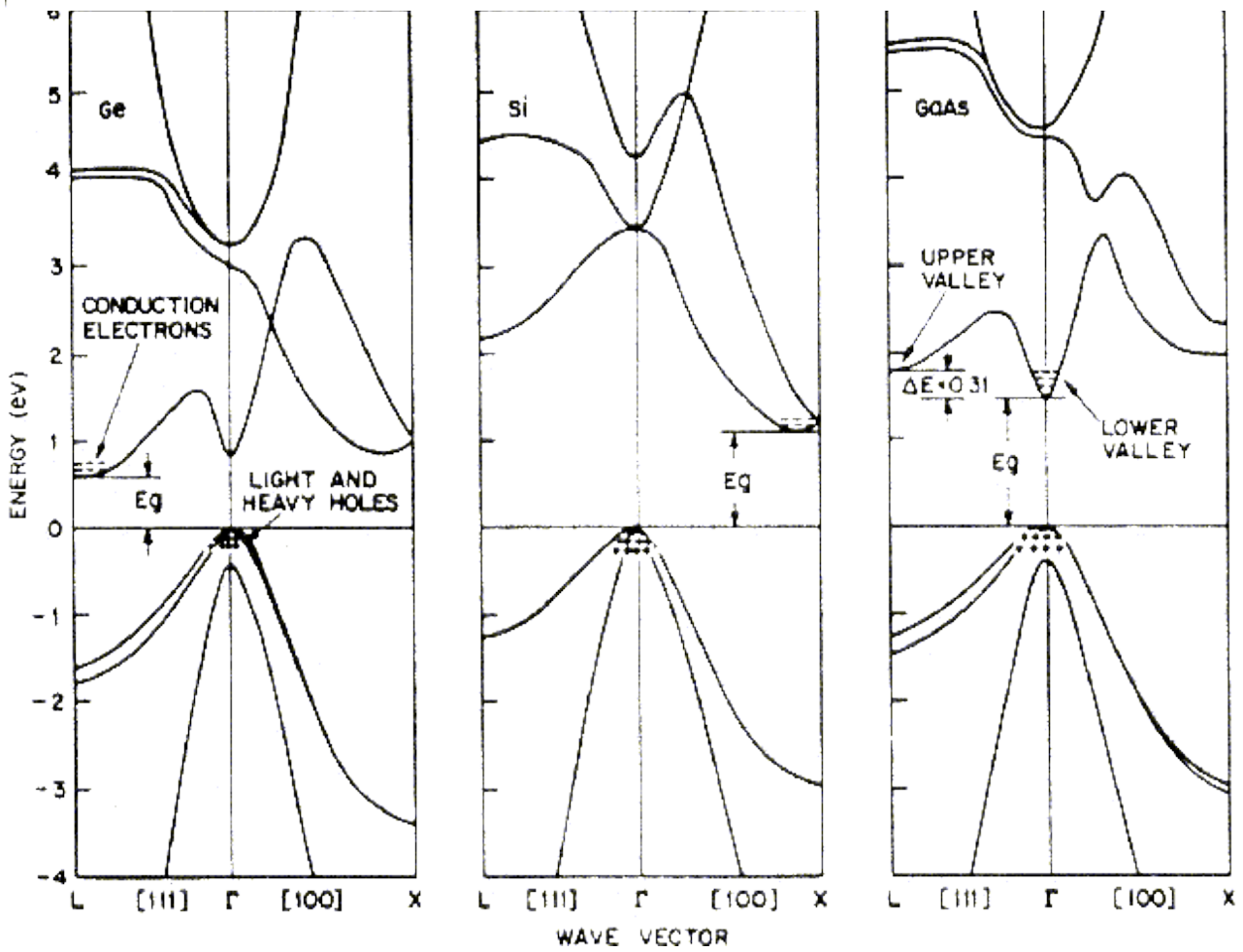

$E_g = E_L = 0.65$ eV
$\lambda = 1907$ nm
$E_{\Gamma 1} = 0.75$ eV

$E_g = E_X = 1.11$ eV
$\lambda = 1110$ nm
$E_{\Gamma 1} = 3.4$ eV

$E_g = E_{\Gamma 1} = 1.42$eV
$\lambda = 873$ nm

TABLE 1–3 • Electron and hole effective masses, m_n and m_p, normalized to the free electron mass.

	Si	Ge	GaAs	InAs	AlAs
m_n/m_0	0.26	0.12	0.068	0.023	2.0
m_p/m_0	0.39	0.30	0.50	0.30	0.3

Review on semiconductors – Doping

Example of n-type doping

- Arsenic has 5 valance electrons (column V)
  - And 5 corresponding protons

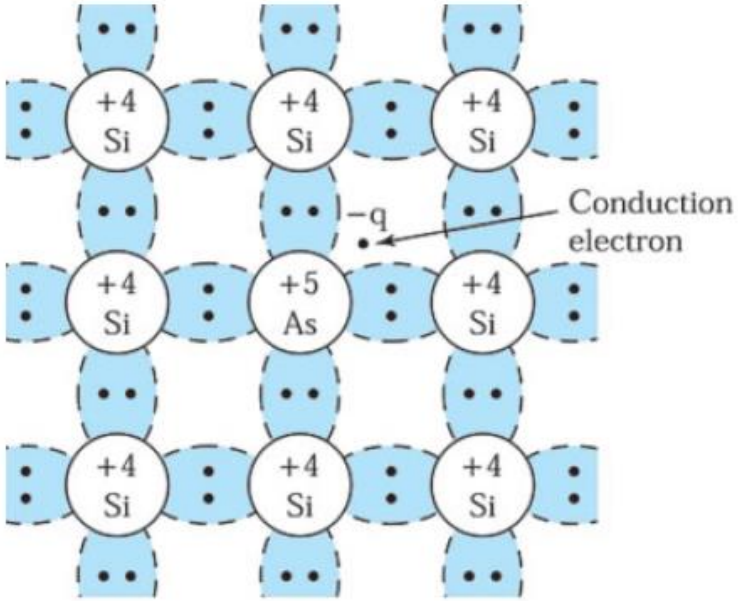

- If the extra electron is moved away by a field (e.g. in a diode)
  - One of the 5 protons will be unmatched conferring a **positive fixed charge** to the depleted volume

Example of p-type doping

- Boron has 3 valance electrons (column III)
  - And 3 corresponding protons

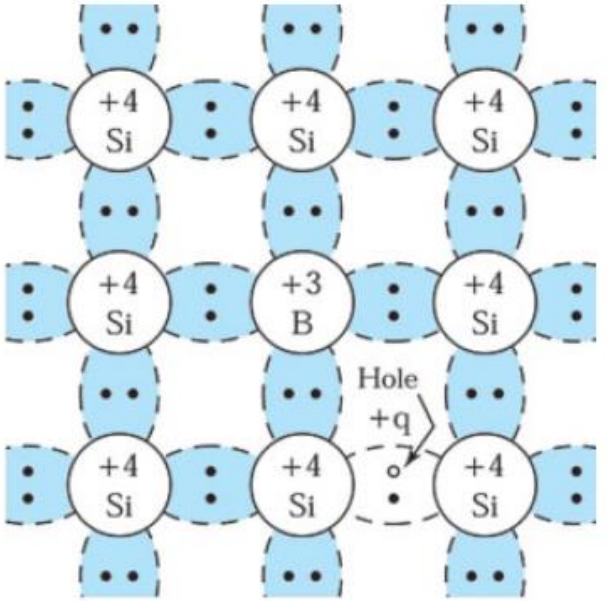

- If the extra hole is moved away by a field, i.e. “replaced” by an electron in the valence band
  - This extra electron in the vicinity of the 3 protons of boron will be unmatched conferring a **negative fixed charge**, fixed because the boron atom is fixed

Review on semiconductors – Dopants produce states in the forbidden gap

- Above mid-gap lie donor states (giving electrons to the C.B.). Below mid-gap lie acceptor states (removing electrons from the V.B. thus generating holes)
  - Some dopants produce confused states: donor near the valence band (and v-v), double ionized states (giving 2 electrons or holes)… We do not want such elements near our devices: Au, Cu, S, Zn, Ni
- Shallow traps have energies near a band at scale comparable to $k_B T$ ~ 30 meV at room temperature
- Deep states near the mid-gap are dominant in the dynamics of depletion zones: Shockley-Read-Hall

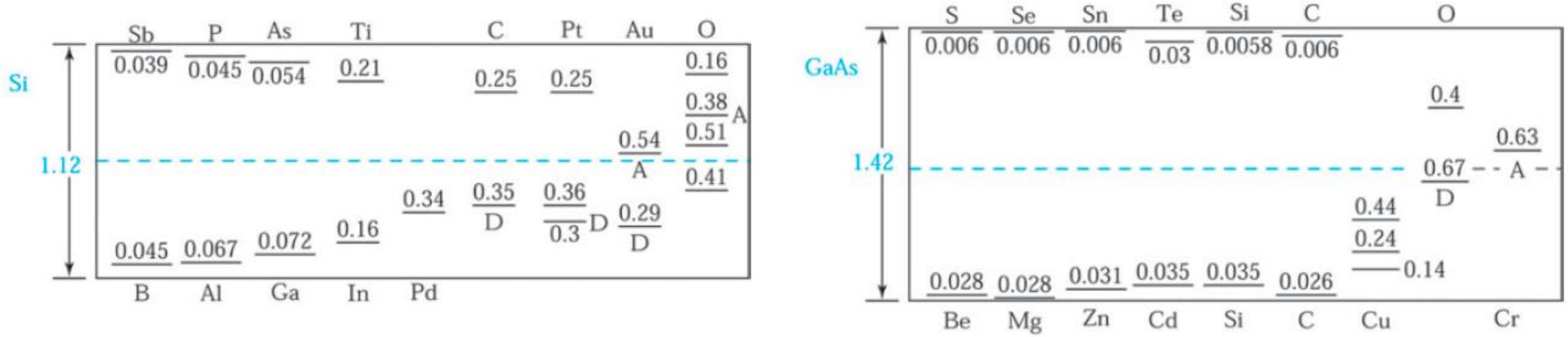

Fig. 20 **Measured ionization energies (in eV) for various impurities in Si and GaAs. The levels below the gap center are measured from the top of the valence band and are acceptor levels unless labeled by *D* for donor level. The levels above the gap center are measured from the bottom of the conduction band and are donor levels unless indicated by *A* for acceptor level.[8]**

Review on semiconductors – Fermi level and state occupation in the bands

- The density of states at the band edges is 0, $\propto \frac{k^2}{dE/dk} \propto \left|E - E_{C,V}\right|^{1/2}$
  - Note: the inverse of the curvature is linked to the effective mass $\propto \left(\frac{d^2E}{dk^2}\right)^{-1}$

Free particle model

- The Fermi level provides the occupation statics of the states
- Electrons (holes) occupy the bottom (top) of the bands tailing of as a Boltzmann distribution
- These are (part of) the equations semiconductor device simulation software solve for us

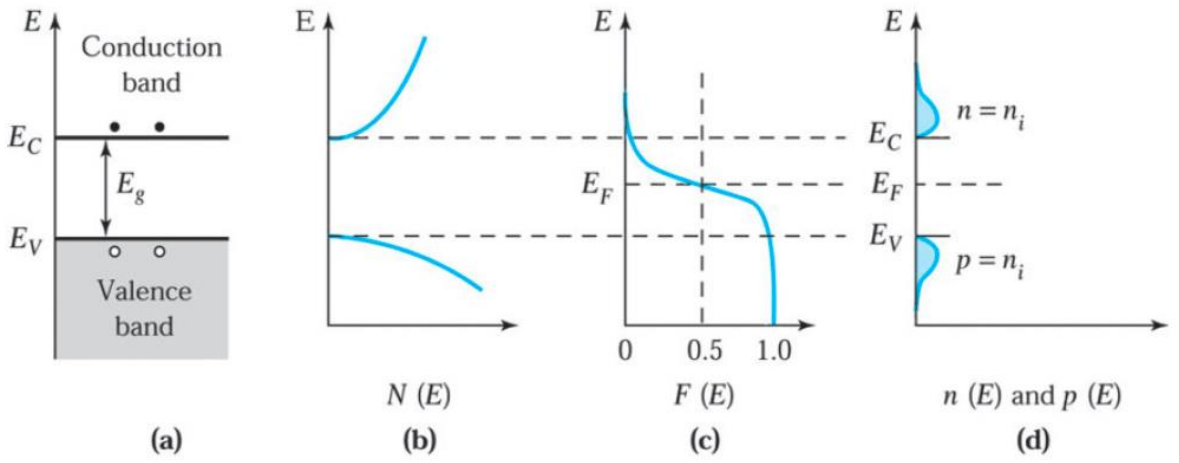

Fig. 17 **Intrinsic semiconductor. (*a*) Schematic band diagram. (*b*) Density of states. (*c*) Fermi distribution function. (*d*) Carrier concentration.**

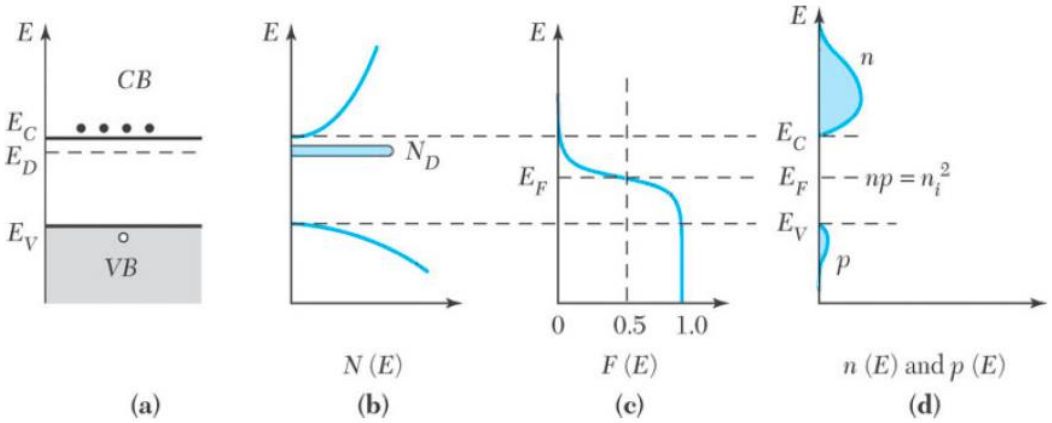

Fig. 22 ***n*-Type semiconductor. (*a*) Schematic band diagram. (*b*) Density of states. (*c*) Fermi distribution function. (*d*) Carrier concentration. Note that $np = n_i^2$.**

- Even at low electric field, carriers **are not** continuously accelerated in an electric field
  - Dissipate their kinetic energy as they "collide with atoms" at a rate – Drude model

$$\mu = q\frac{\tau}{m^*}$$

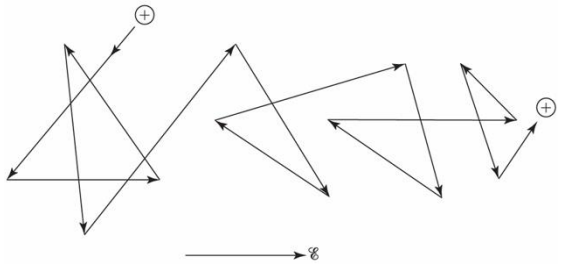

- At high field the collision rate increases to a good coupling with optical phonons (strong dipole)
  - Approximated as a "saturation speed"

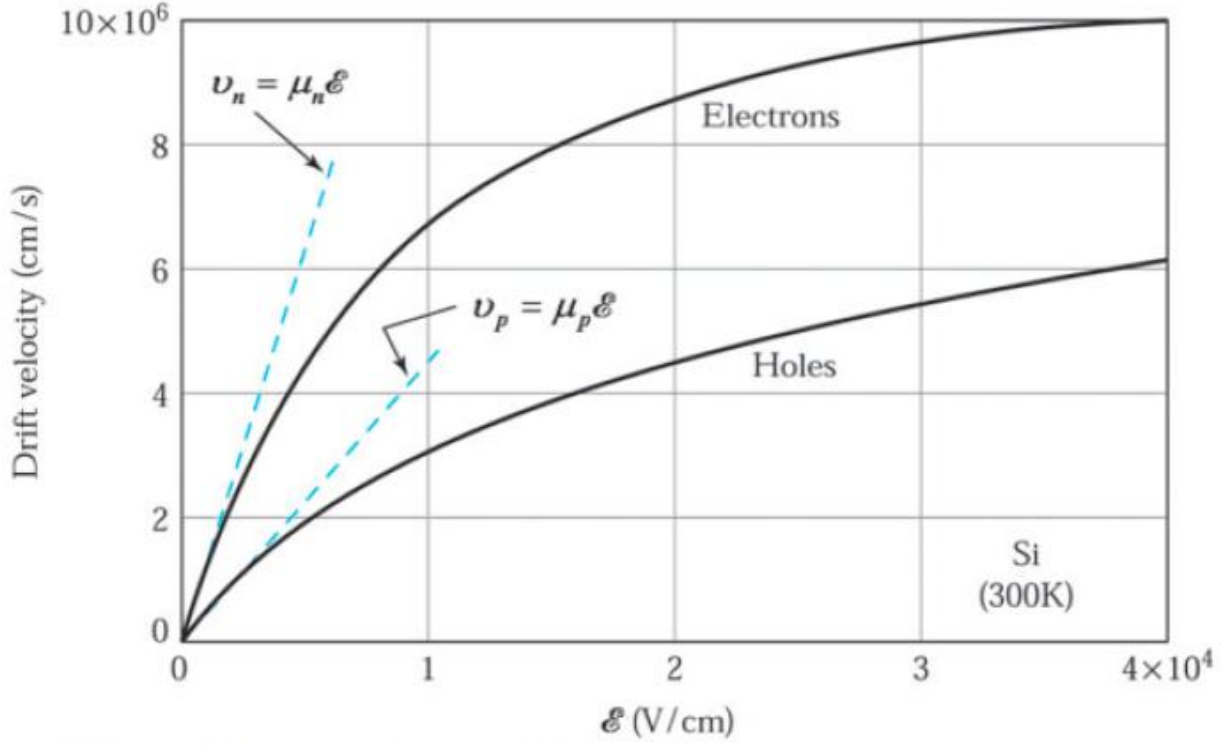

Fig. 22 **Drift velocity versus electric field in Si.**[8]

- Only on short time scale or short distances do carriers accelerate
  - The ballistic transport along very short channel transistor

Review on semiconductors –Intervalley Scattering

- The electric field, the distribution of carriers has a non-zero average k vector
  - The band diagram does not change but there are more carriers on one side than on the other
- At sufficiently high field, electrons transfer to other band minima
  - These minima typically have higher effective mass (smaller curvature in the E-k diagram)
  - This is how the complexity of the band structure shows up in the mobility of some semiconductors (e.g. GaAs)
- Provides a “negative” differential resistivity used in resonance-based devices (GUNN diodes)

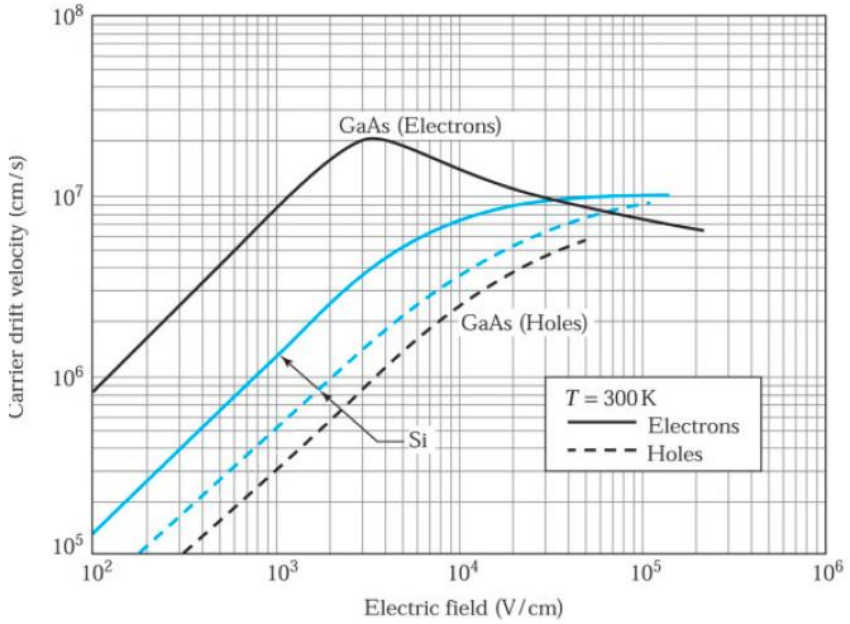

Fig. 23 **Drift velocity versus electric field in Si and GaAs. Note that for *n*-type GaAs; there is a region of negative differential mobility.[8,9]**

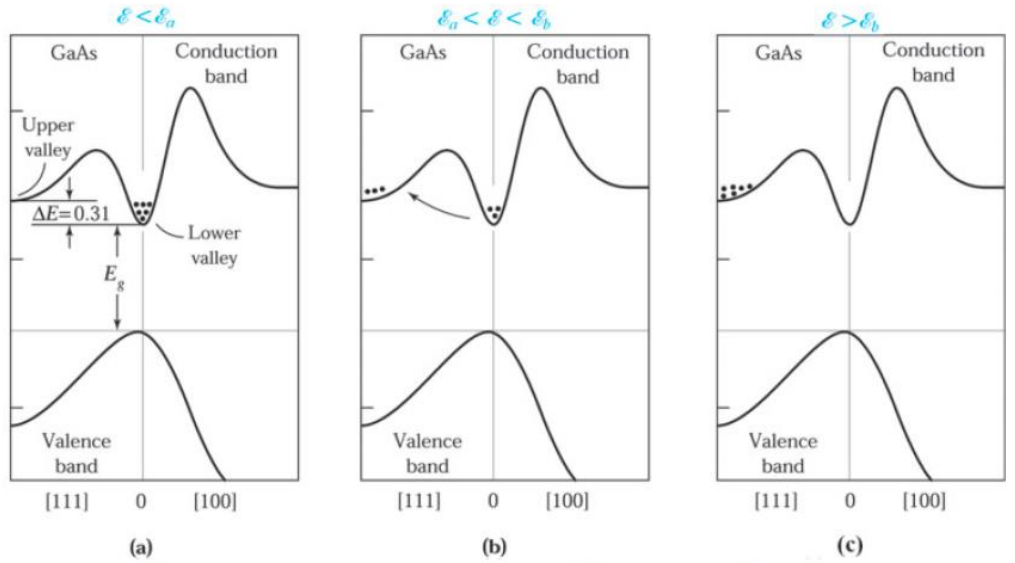

Fig. 24 **Electron distributions under various conditions of electric fields: (a) $\mathscr{E} < \mathscr{E}_a$, (b) $\mathscr{E}_a < \mathscr{E} < \mathscr{E}_b$, and (c) $\mathscr{E} > \mathscr{E}_b$ for a two-valley semiconductor.**

The pn junction – at the heart of the diode

- Free carriers diffuse to regions of less density
  - Holes to the n side
  - Electrons to the p side
- Free carriers recombine near the junction leaving behind the unscreened charge of the dopant atoms
  - Positive ions on the n side (4 electrons for 5 protons)
  - Negative ions on the p side (4 electrons for 3 protons)
- This space charge region creates an electric field that opposes the diffusion of carrier
- An equilibrium is reached

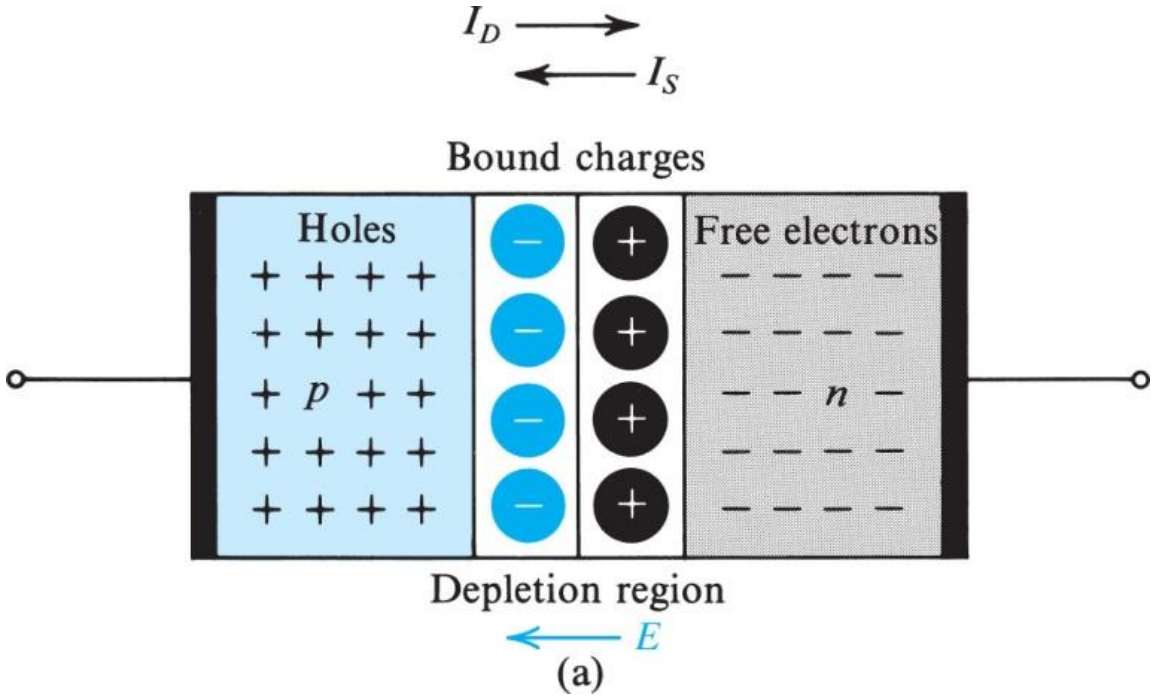

The pn junction – at the heart of the diode

- The charge on each side of the depletion region is equal in magnitude

$$Q_J = |Q_+| = |Q_-|$$
$$N_A\, x_p = N_D\, x_n$$
$$W = x_p + x_n$$

- The maximum electric field lies at the junction
  - At 0 bias: typically 10 kV/cm to 100 kV/cm

- Integrating the electric field, you get the contact potential (i.e. the barrier height)
  - Typically 0.5 to 0.8 E_g
  - It depends not on the detail of the charge distribution

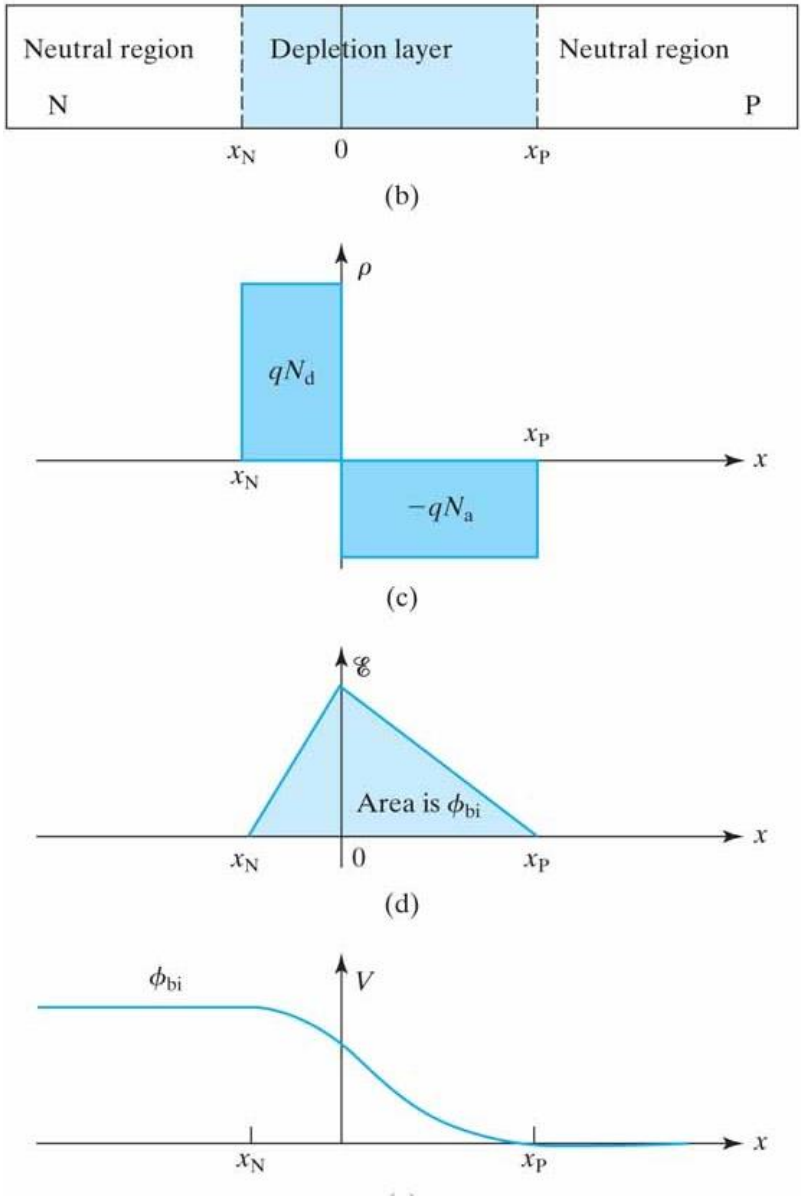

Reverse saturation current and Charge injection by photon absorption

- In reverse bias
  - Electrons (holes) in the p (n) side move to the depletion zone
  - The electric field sweeps them across the junction
  - The current is proportional to the density of minority carriers
    - It is thus independent of the voltage bias
    - Inversely dependant on doping

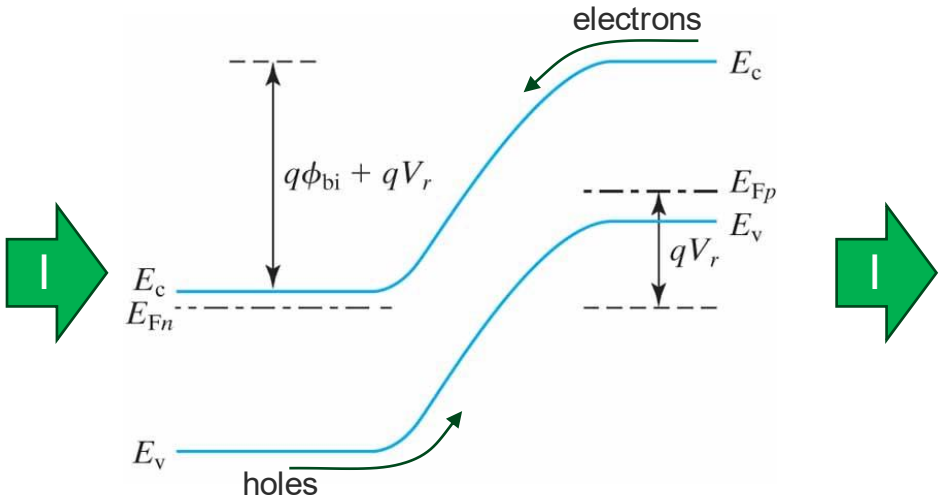

- Photons absorbed in the depletion region are swept by the enormous electric field
  - 1 photon creates 1 electron-hole pair (for visible photons)
  - It induces a current → photocurrent

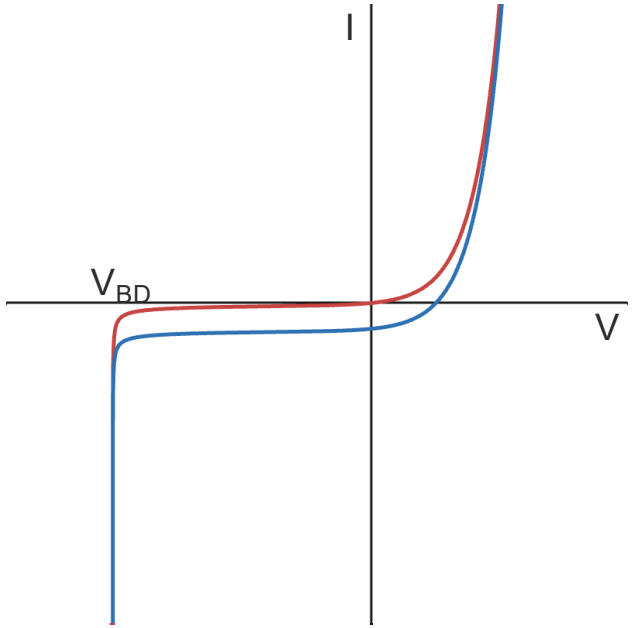

- The photocurrent is additive to the reverse bias current and essentially independent on the biasing
  - Only on the photon flux (if everything else were to stays the same)

Shockley-Read-Hall contribution from the depletion zone

- In reverse bias
  - Any carrier appearing in (or about) the depletion zone will contribute to the reverse bias current

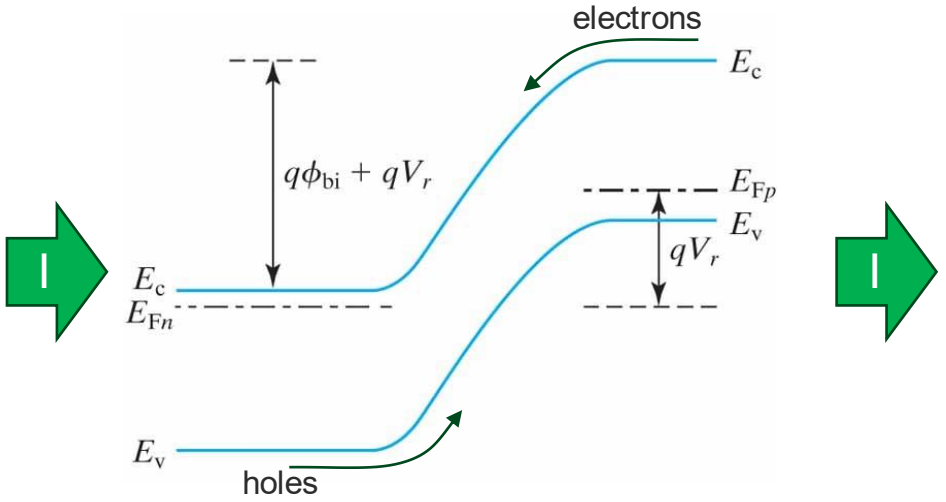

- Such contributions are
  - Pair generation across the full band gap
  - Trap assisted pair generation
  - And variants of these: field enhanced trap assisted generation

- The largest contribution comes from traps in the middle of the forbidden gap
  - Shockley-Read-Hall (and variants)
  - Depends on the volume of the depletion zone giving a bias $\sqrt{V}$ dependance to the current

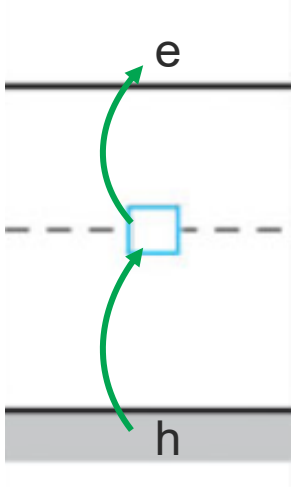

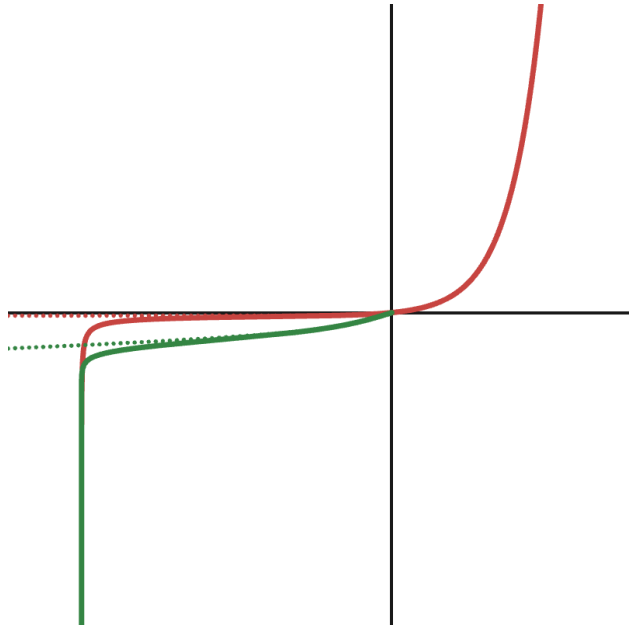

~~SPAD~~ Photodiode structure and properties

3D SPAD Array: Backside Illumination (BSI) vs Frontside Illumination (FSI)

UDS

Backside illumination

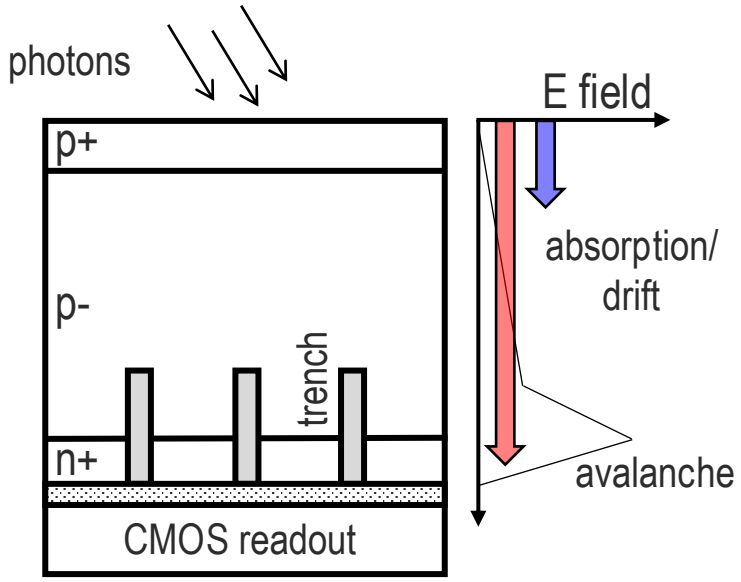

PROS

- λ range: red-NIR
- high fill factor (FF)
- easy access to backside surface

CONS

- photoelectron drift (limited timing)
- cross-talk

Frontside illumination

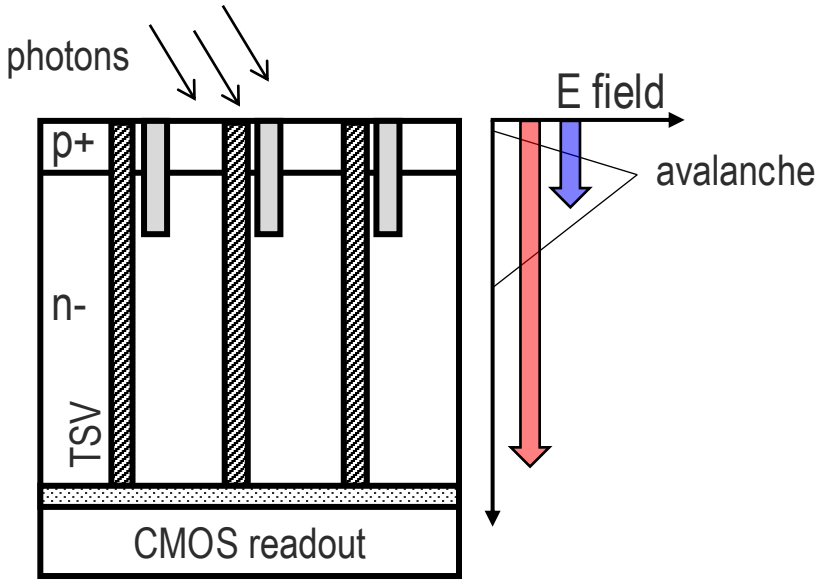

PROS

- λ range: blue-UV
- planar SPAD for timing resolution

CONS

- through silicon vias (lower FF, parasitics)

Thinned
(full trench isolation - FTI)
FSI or BSI

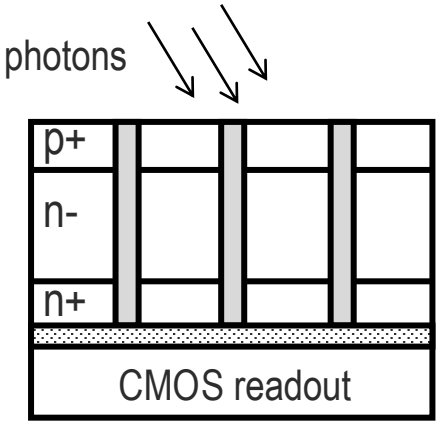

PROS

- λ range: UV-VIS-NIR
- planar SPAD for timing resolution
- high FF
- less photoelectron drift
- no through silicon vias

An example of p⁺n silicon diode with photon entry on the p⁺ side

UDS

Electric field in a p+n junction

Avalanche probability by electrons and holes

$\alpha_e > \alpha_h$ (in Si)

Compound avalanche probability

Because most of the absorption in IR would occur on the n-type side, holes would be triggering avalanche but with a lower probability than if electrons were.

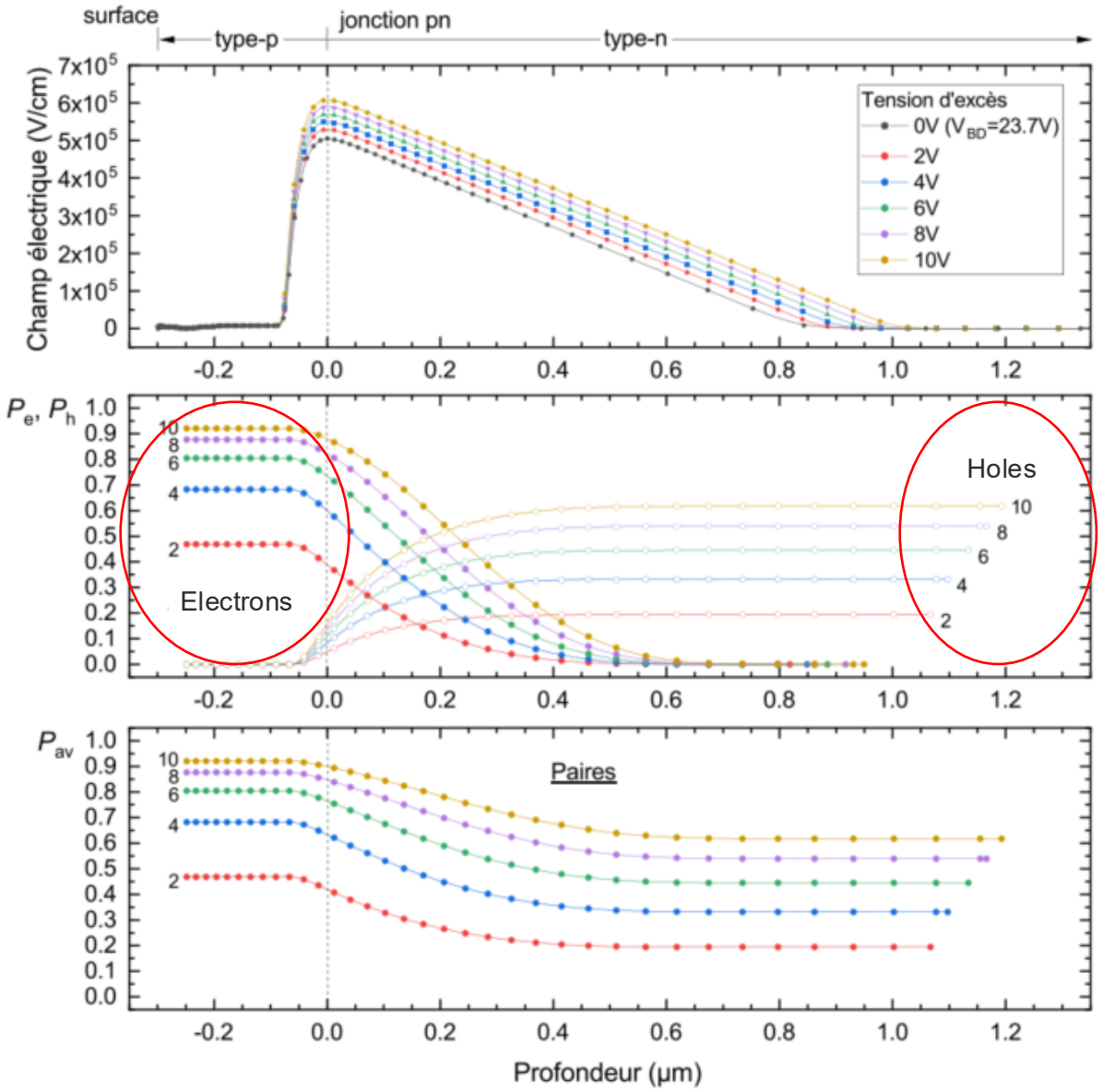

F. Vachon, thesis, U. de Sherbrooke

NIR Silicon Photomultipliers: p^+n versus n^+p junction

UDS

- Penetration depth of NIR > UV-VIS
  - Need large absorption region

- Probability of triggering avalanche is larger for electrons than holes
  - Doping profile such that electrons initiate avalanche

$$\alpha_e > \alpha_h \text{ (in Si)}$$

- Need a large absorption region of type p → n^+p

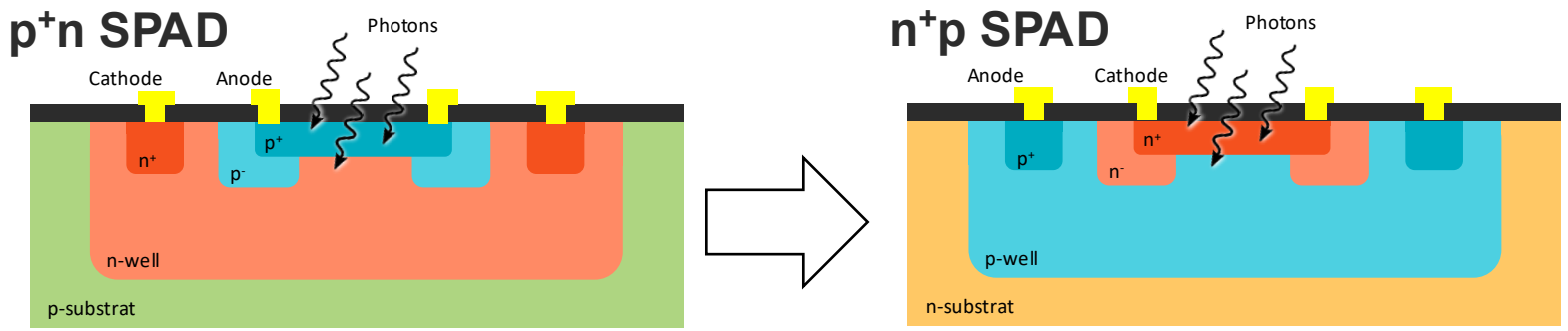

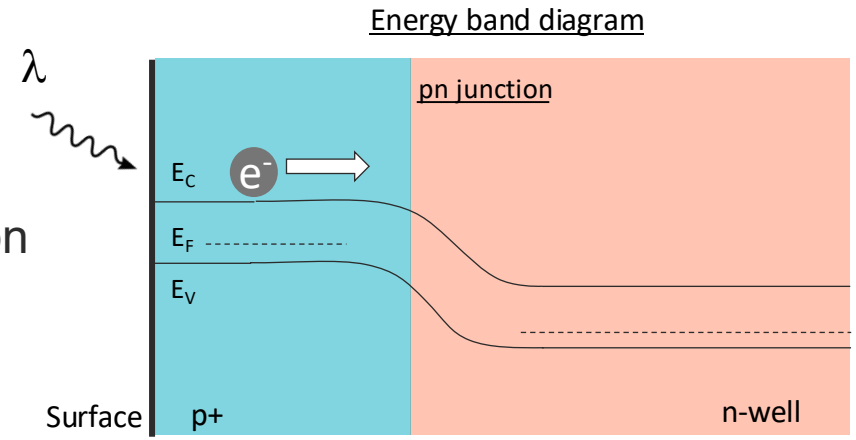

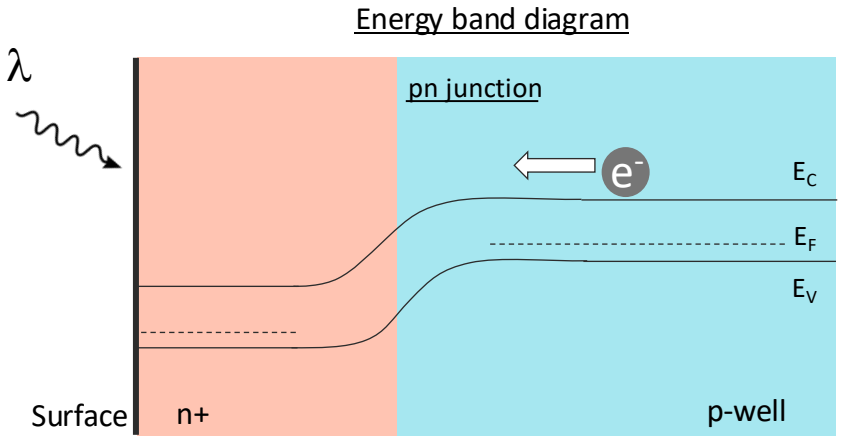

Penetration depth in Si

Visible (400-700 nm) : 100 nm to 5 µm

IR (800-1550 nm) : 10 µm to 40 µm

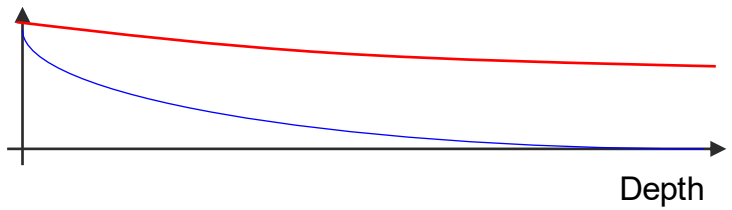

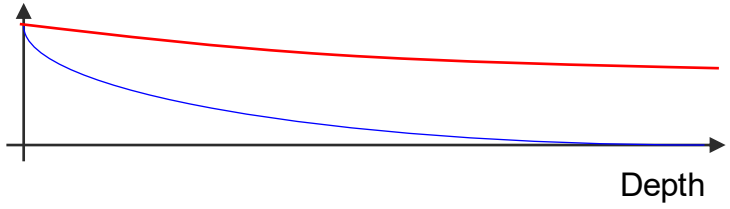

Typical SPAD structures

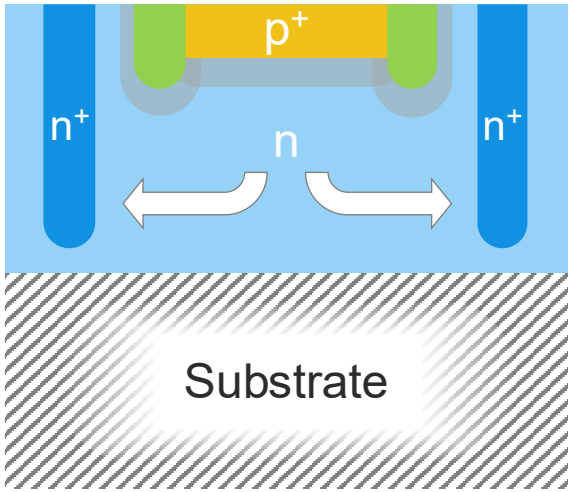

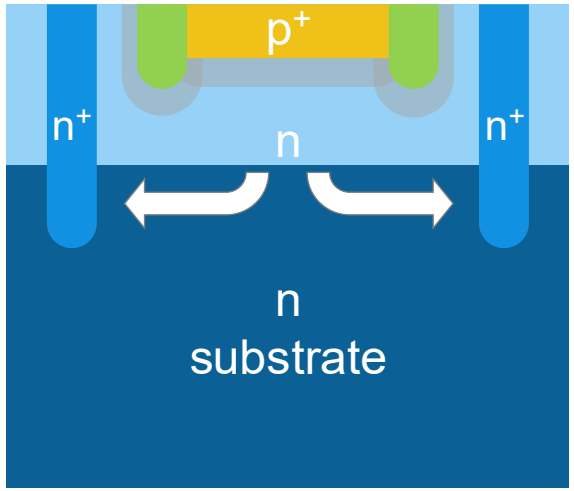

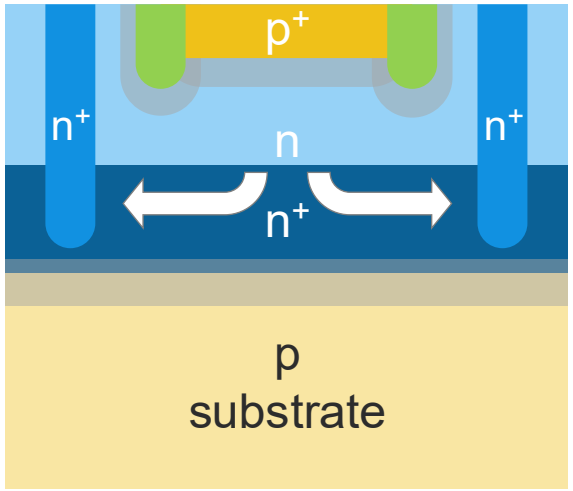

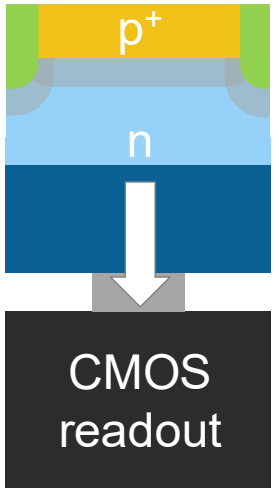

Planar structure

- Higher series resistance
- Substrate usually common to all diodes

Planar structure that uses the substrate

- Lower series resistance
- Substrate common to all diodes
- Large volume for carriers to diffuse

Planar structure with reduced volume

- Lower series resistance
- Substrate out of the active volume
- Reduced volume for carriers to diffuse

Vertical structure

- Lower series resistance
- More laterally uniform electric fields
- Can reduce volume as much as technology allows

Impact of the low field regions on detection efficiency and timing jitter

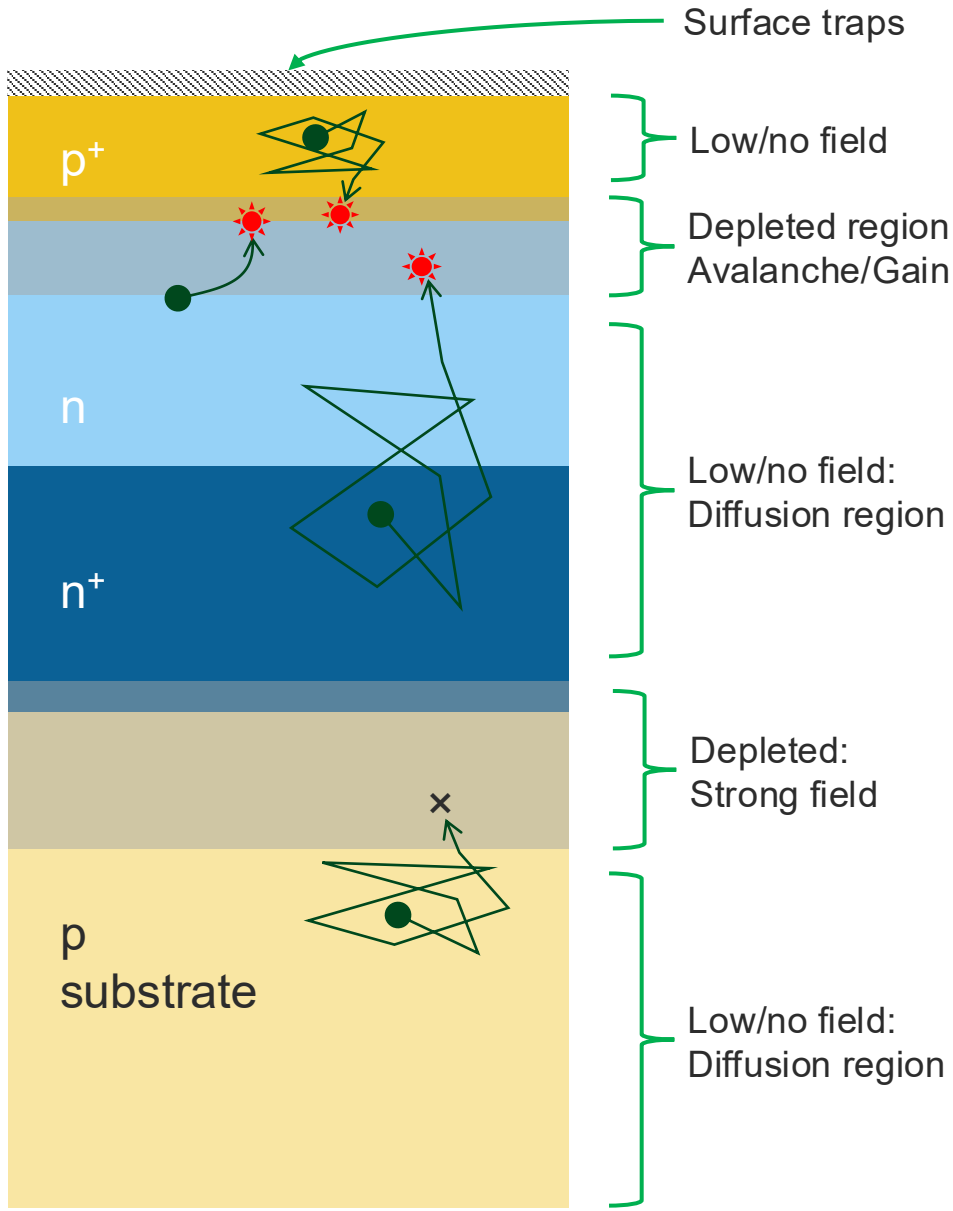

- Generating the electron-hole pair in the high field region
  - Provides highest efficiency
  - Provides lower timing jitter

- Generation in the low field volumes
  - Carriers need to diffuse to high field regions
    - i.e. drift is not the dominant process
  - Carriers can recombine before reaching avalanche region
    - Reduced detection sensitivity/efficiency
  - Diffusion is stochastic and time before avalanche varies from event to event
    - Increased timing jitter

Impact of the low field regions on timing jitter

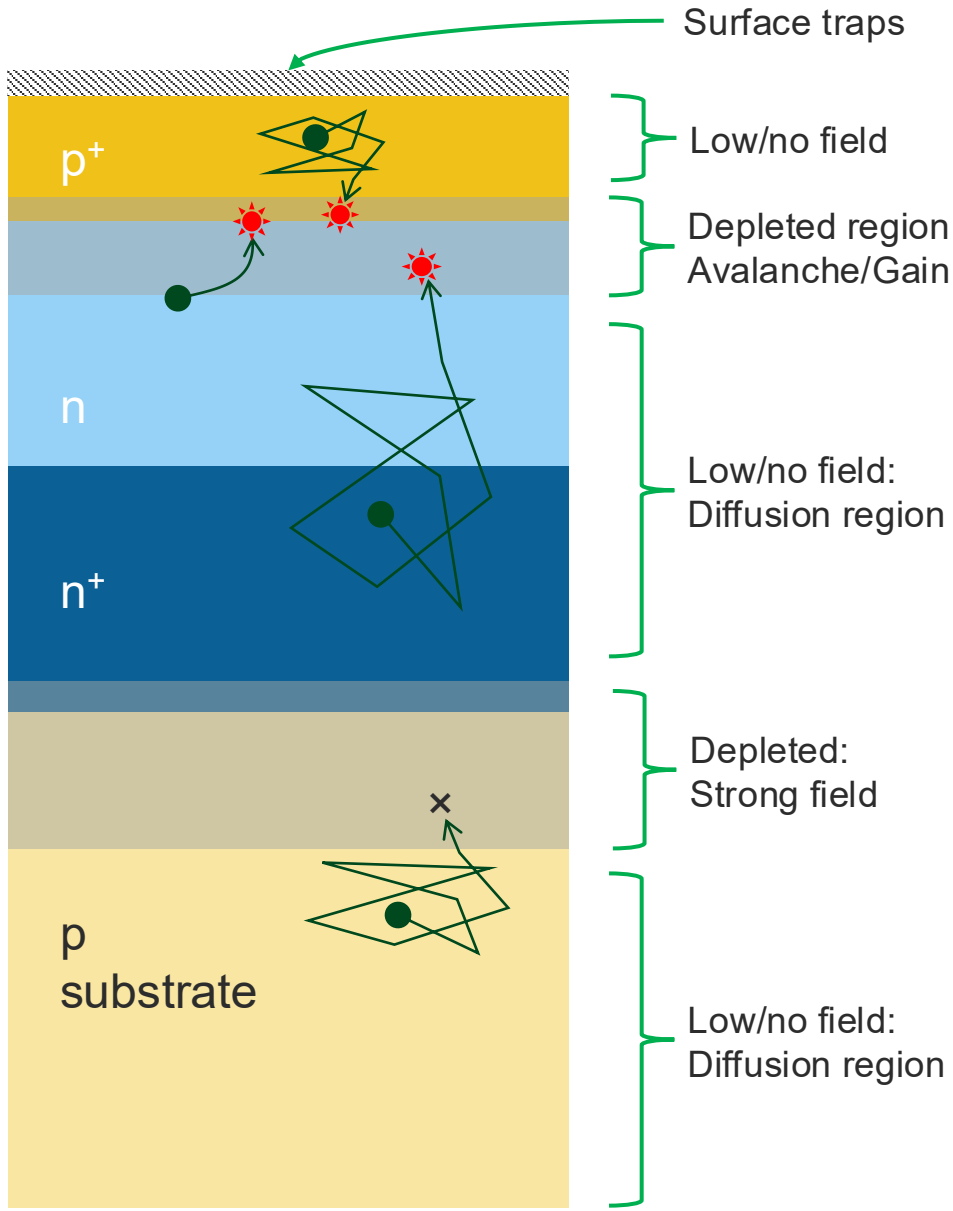

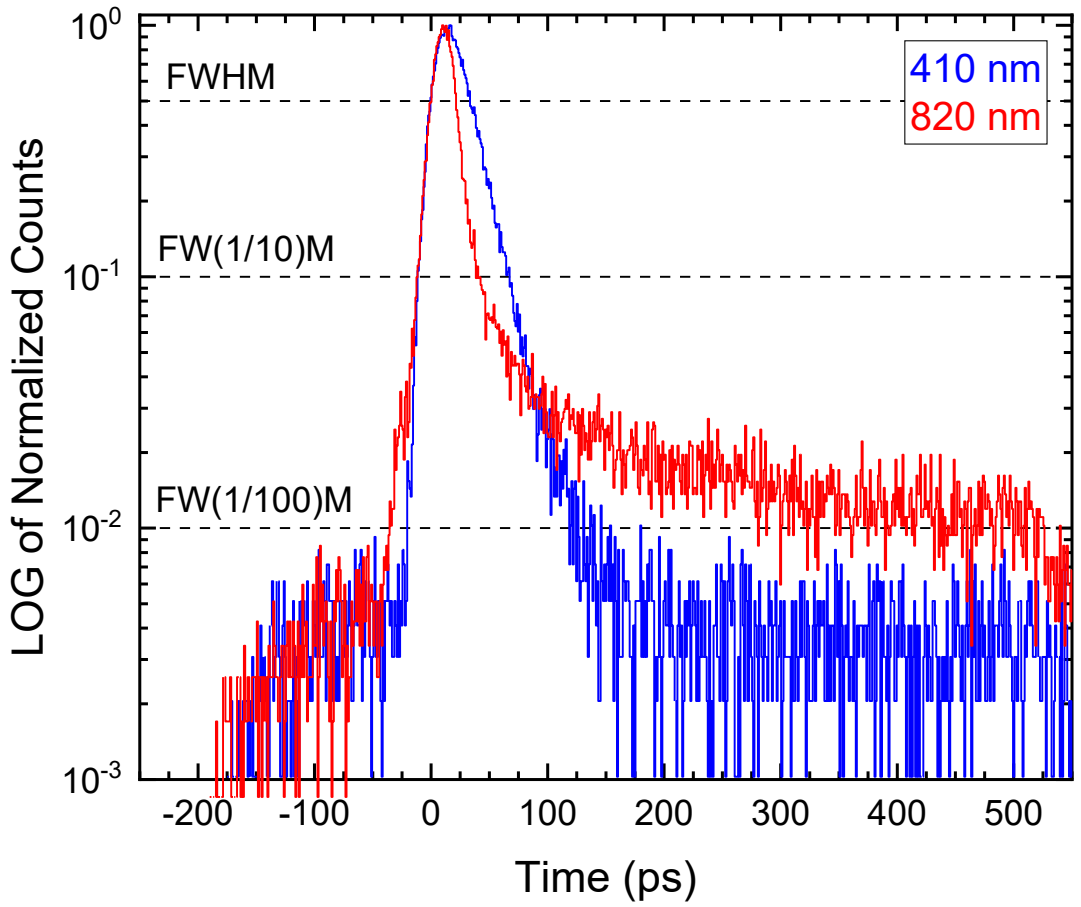

serge.charlebois@usherbrooke.ca

Impact of the low field regions on timing jitter

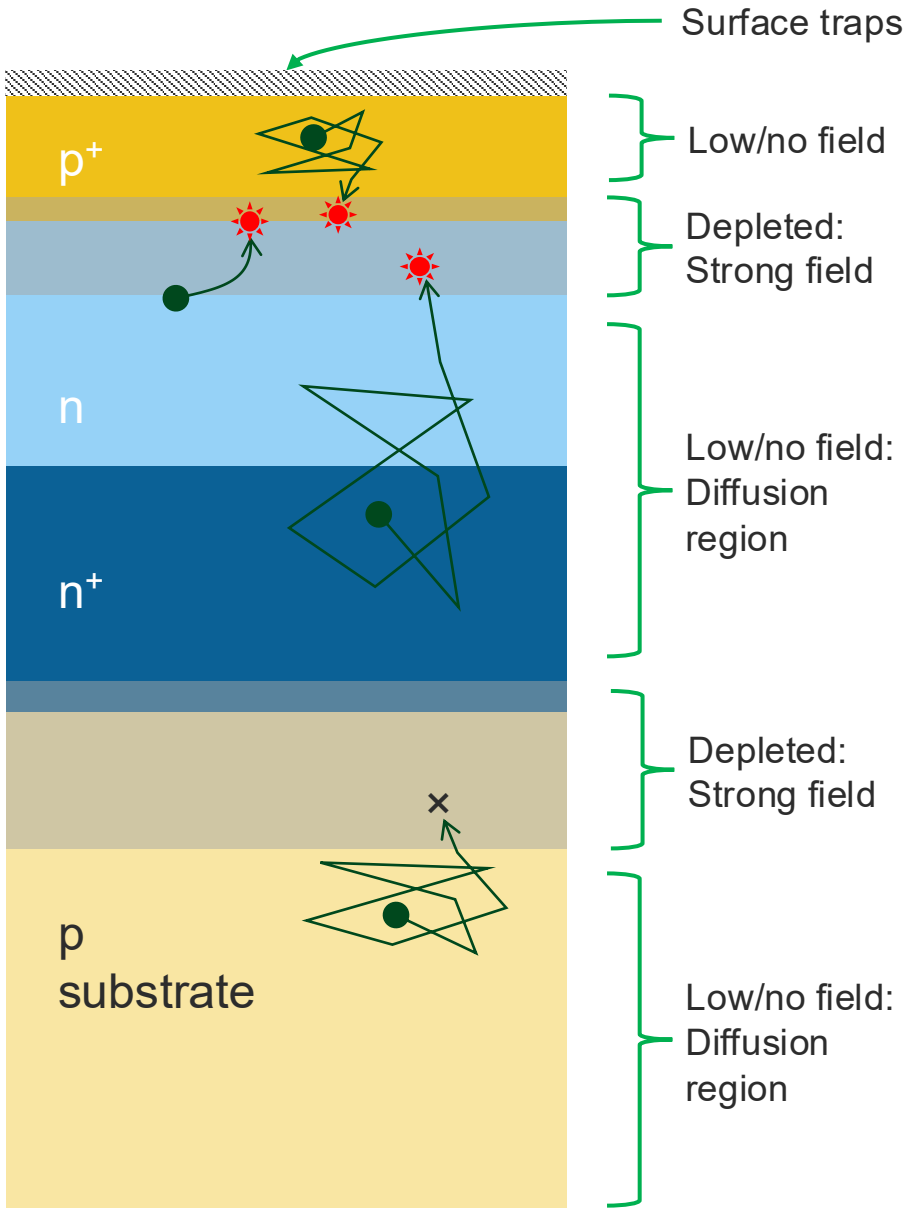

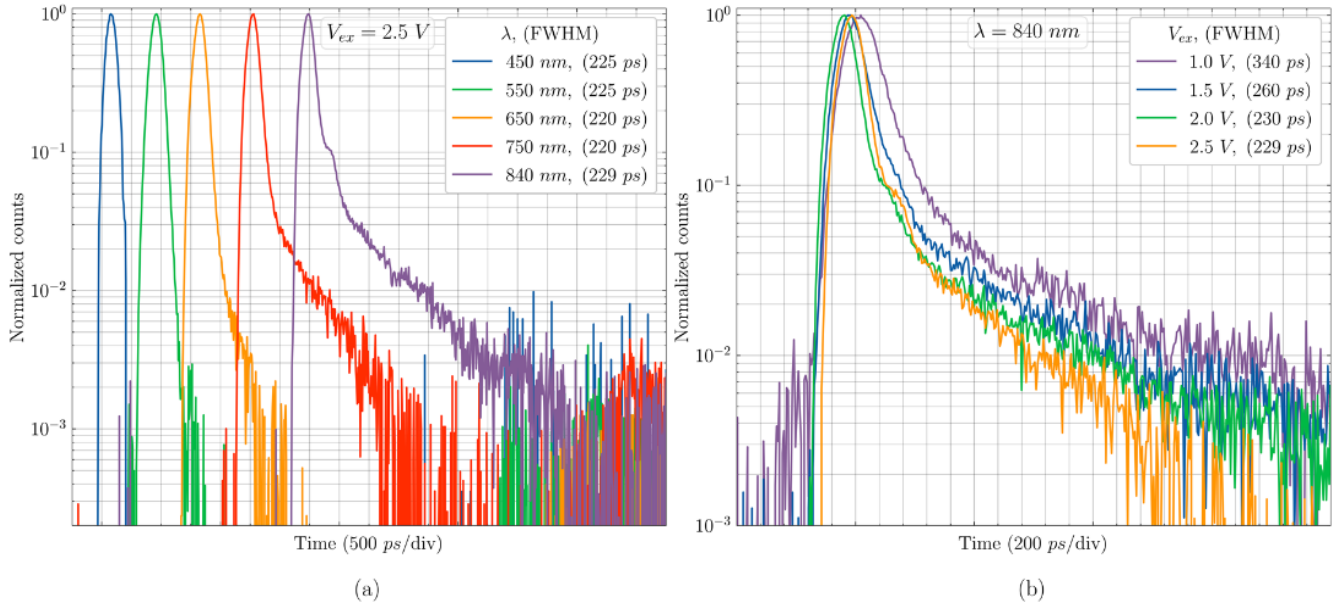

Figure 11. (**a**) Timing histogram measured at an excess bias of 2.5 V for 5 different wavelengths. (**b**) Timing histogram measured at wavelength of 840 nm for 4 different excess bias voltages. The full width half maximum represents timing jitter.

Jegannathan, G. *et al.* 2020 (https://doi.org/10.3390/s20247105)

Lateral variation of timing jitter on a SPAD

- Measuring with a focused pulsed light beam allows to scan the surface of a SPAD and study the uniformity of the triggering time
  - Depends on the field uniformity
  - Position of the contacts

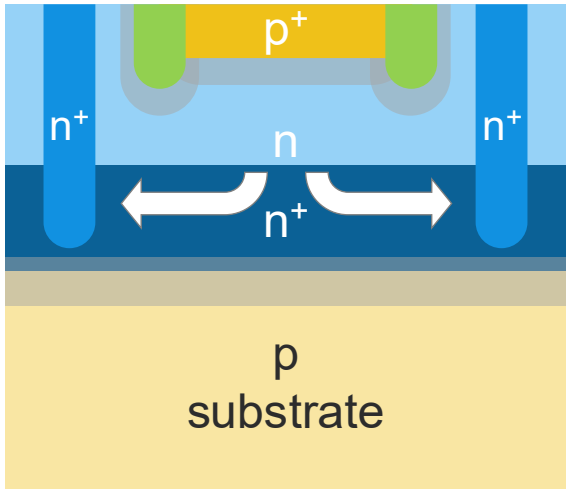

Timing jitter map of
the active area of a large SPAD

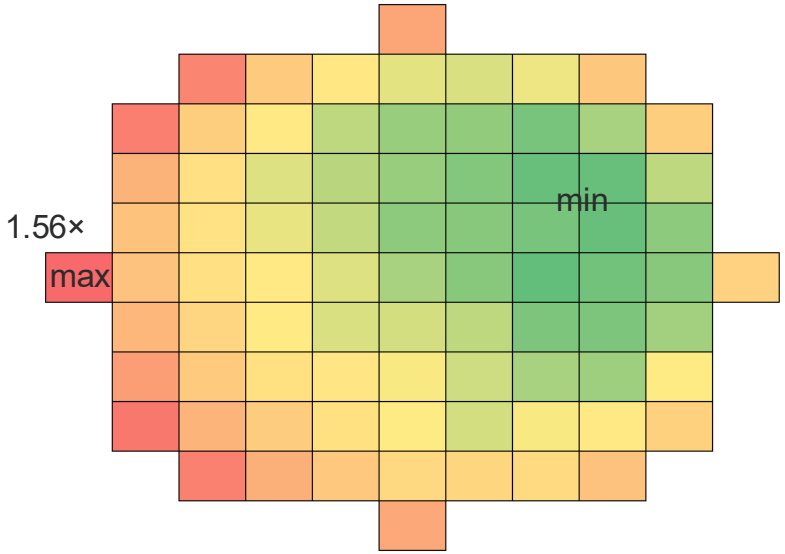

Variation range 56%

Characterization of a commercial SPAD. Unpublished.

Dark count
and correlated noise sources

Origine of Noise in SPADs

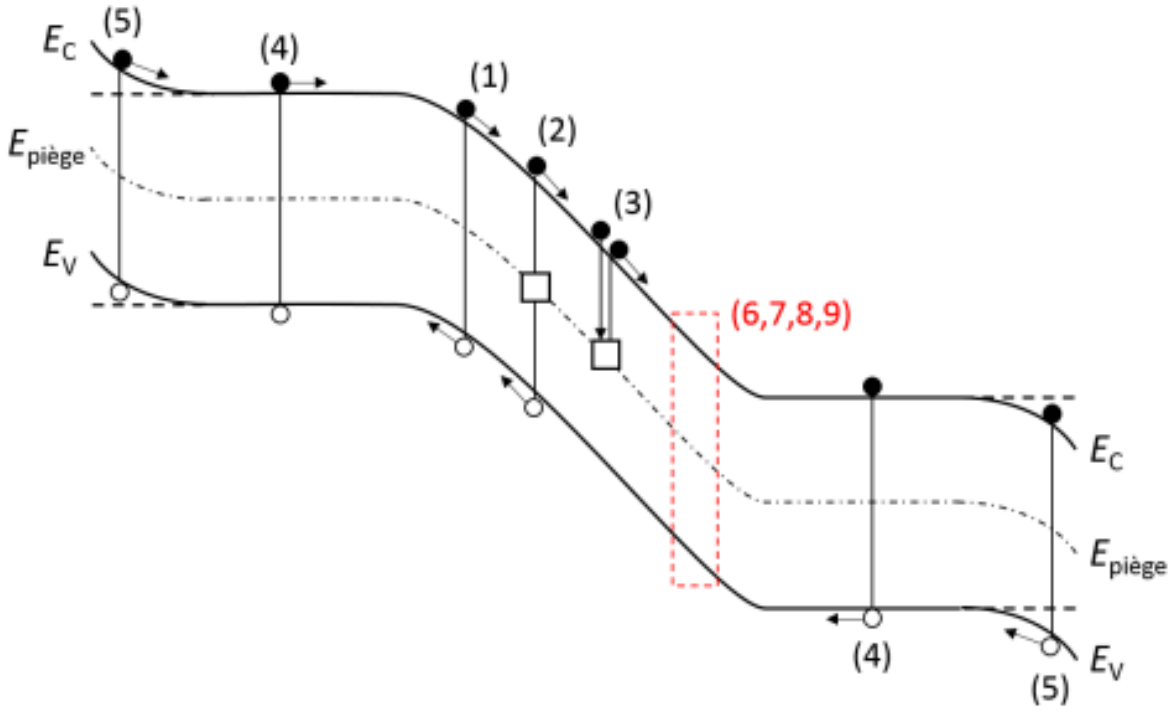

1. Thermal generation

2. Trap assisted thermal generation
   Shockley-Read-Hall

3. Trap liberating a carrier after a previous detection – afterpulsing generation — **Correlated noise**

4. Diffusion of carriers towards a junction — **↑ jitter**

5. Drift from other junctions
   (then needs to diffuse to the avalanche region) — **↑ jitter**

6,7,8,9 on next slide

[80] Ghioni, Massimo, et al. "Large-area low-jitter silicon single photon avalanche diodes." *Quantum Sensing and Nanophotonic Devices V*. Vol. 6900. SPIE, 2008.

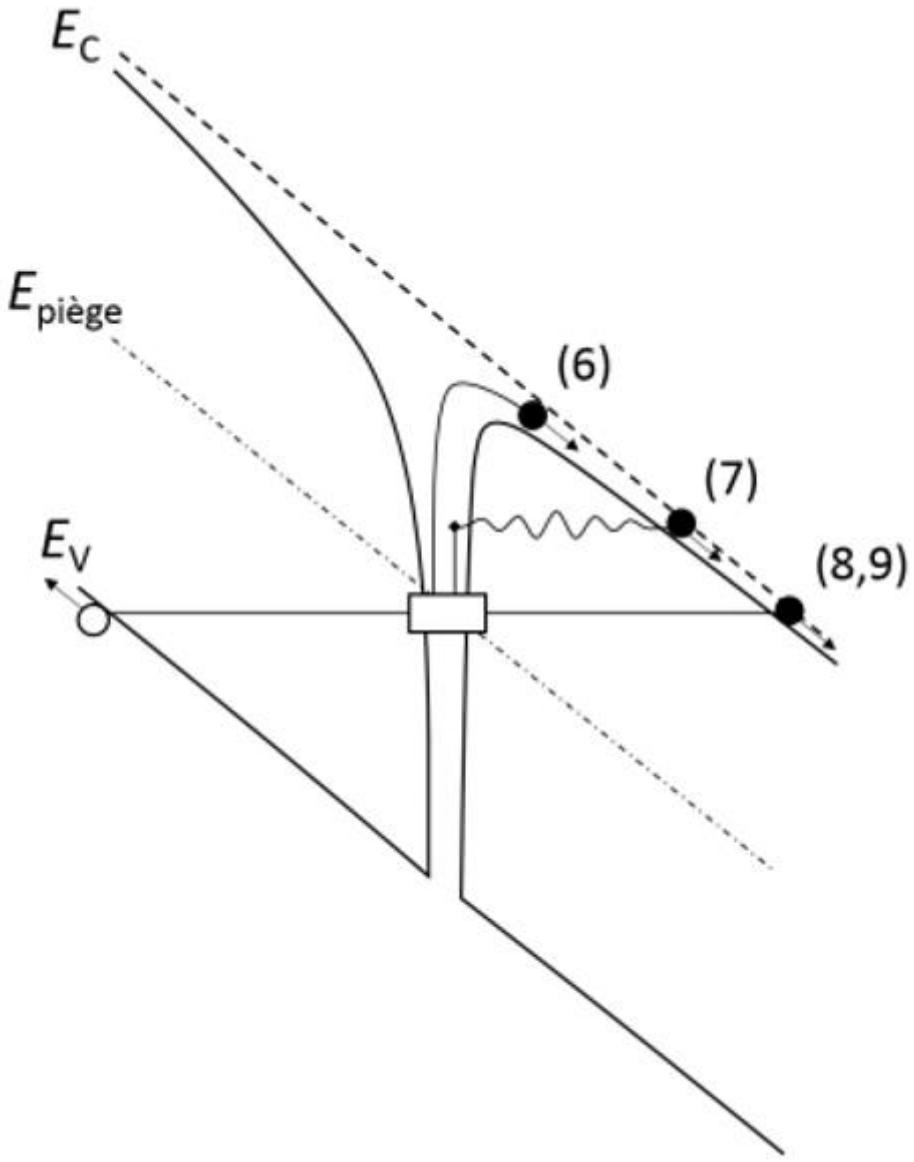

In the depletion zone – strong field

6. Field enhanced Shockley-Read-Hall generation

7. Tunnel assisted Shockley-Read-Hall generation

8. Band-to-band tunneling
   - Not thermally activated

9. Trap assisted band-to-band tunneling
   - Some thermal dependance

serge.charlebois@usherbrooke.ca

[80] Ghioni, Massimo, et al. "Large-area low-jitter silicon single photon avalanche diodes." *Quantum Sensing and Nanophotonic Devices V*. Vol. 6900. SPIE, 2008.

Noise in SPAD Arrays

UDS

- Uncorrelated noise (dark count rate – DCR):
  - Thermal noise: Shockley-Read-Hall + trap assisted + field-enhanced
  - As we cool down, noise is dominated by band-to-band tunneling (BTBT) + trap assisted.
- Correlated noise
  - Afterpulsing
  - Optical crosstalk

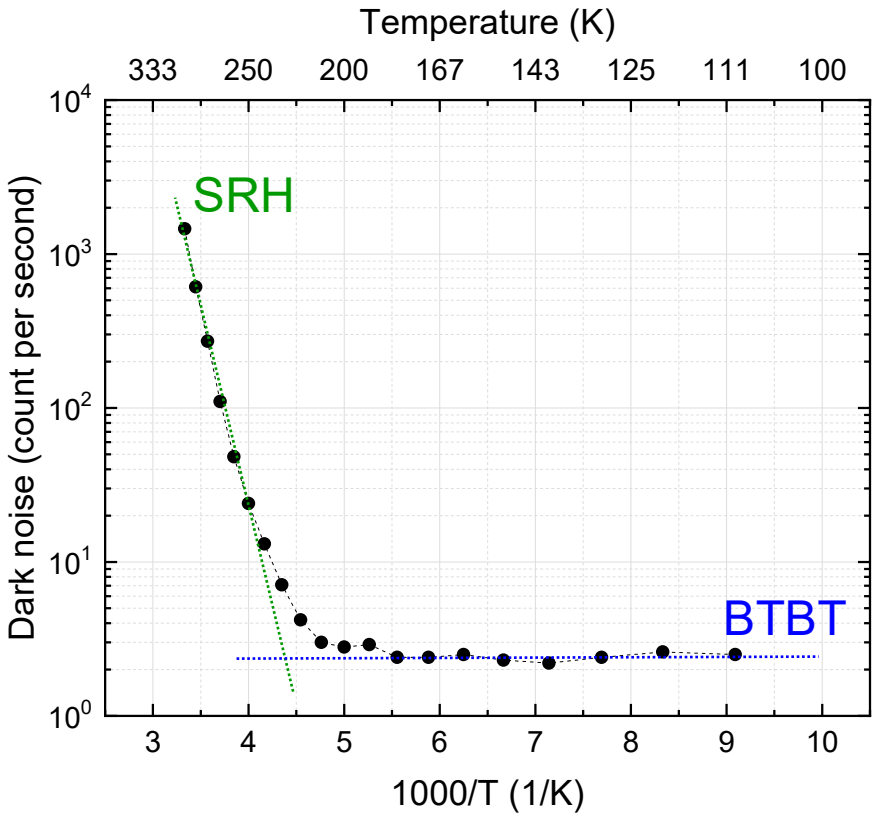

Parent, Samuel, et al. "Single photon avalanche diodes and vertical integration process for a 3D digital SiPM using industrial semiconductor technologies." *2018 IEEE Nuclear Science Symposium and Medical Imaging*

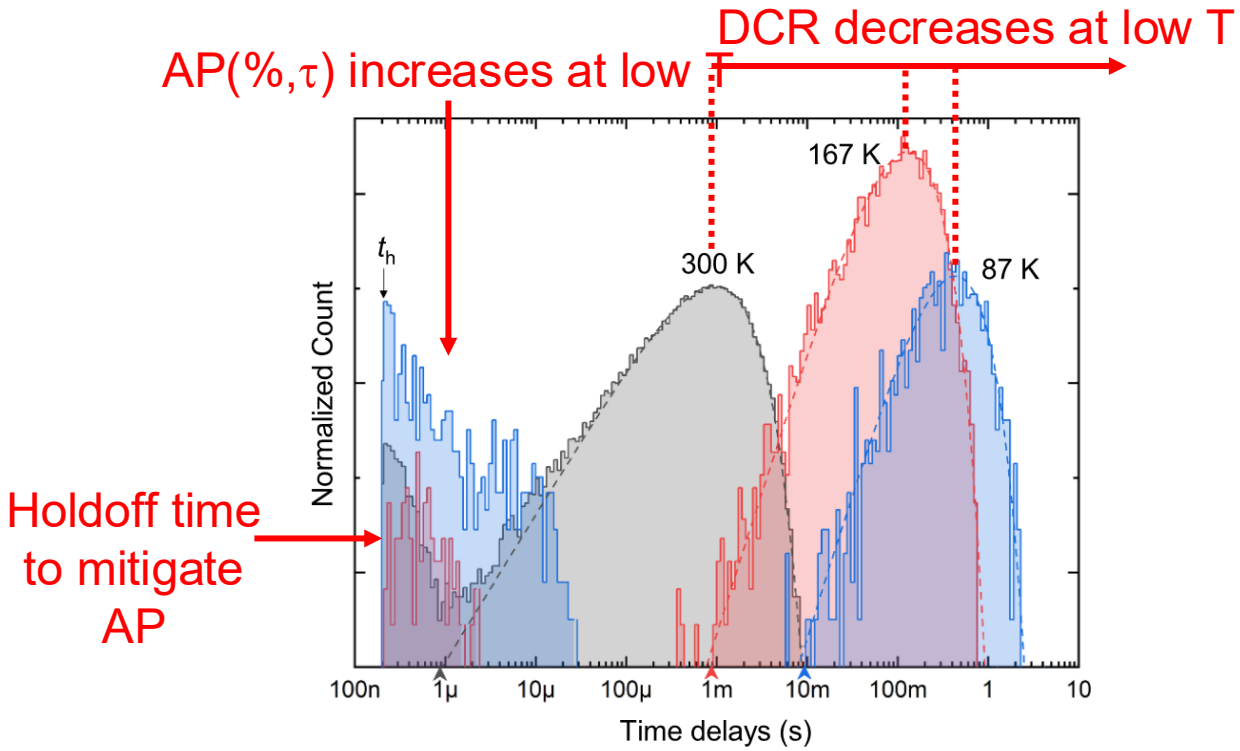

Vachon, Frédéric, et al. "Measuring count rates free from correlated noise in digital silicon photomultipliers." *Measurement Science and Technology* 32.2 (2020): 025105.

serge.charlebois@usherbrooke.ca

Crosstalk sources

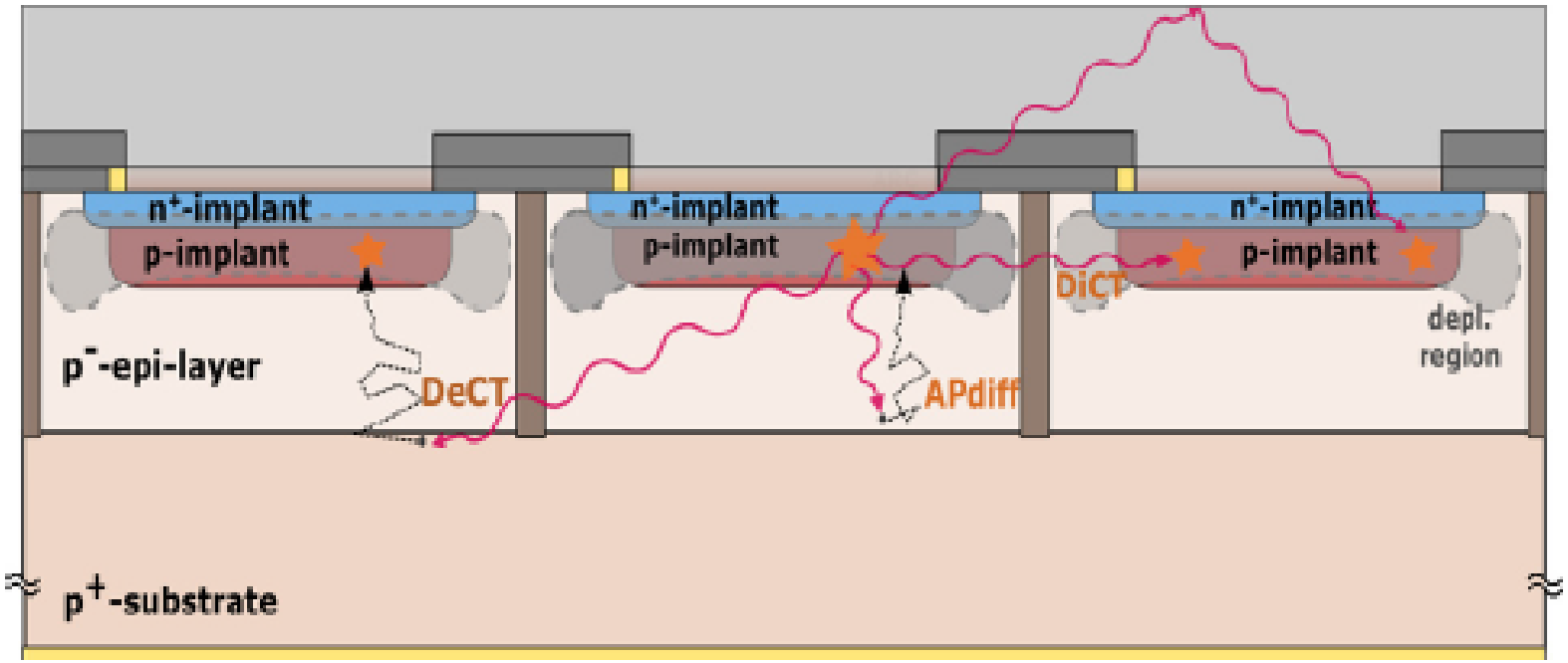

Fig. 10. Typical SiPM crossection with the different type of correlated noise represented: direct (or prompt) crosstalk (DiCT), delayed crosstalk (DeCT), afterpulsing optically induced (or diffused) (APdiff) and external crosstalk due to reflection on the top protective layer of the SiPM (this can as well generate either direct or delayed crosstalk events). Afterpulsing due to trapping in the high-field region in not represented.

In analog SiPMs

- Many information on the afterpulsing and crosstalk can be obtained from studying the signal stream in time
  - Specifically, the **height of the pulses**

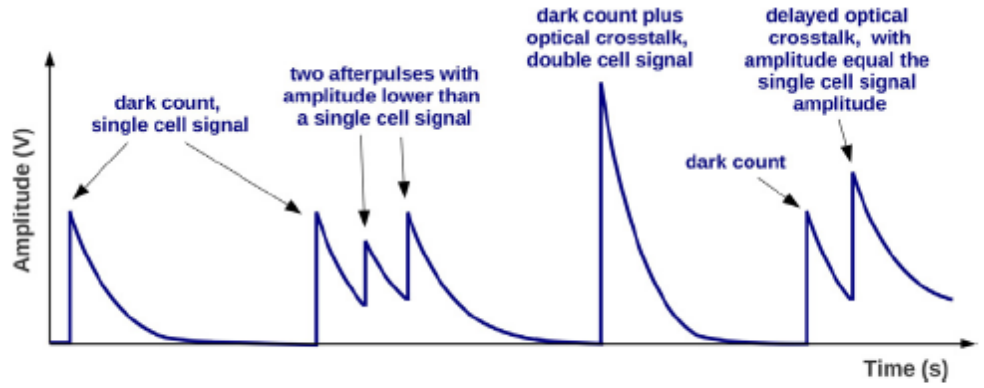

Fig. 11. Representation on the SiPM output signal of the different kinds of noise observable: primary events, prompt crosstalk, afterpulsing and delayed crosstalk events.

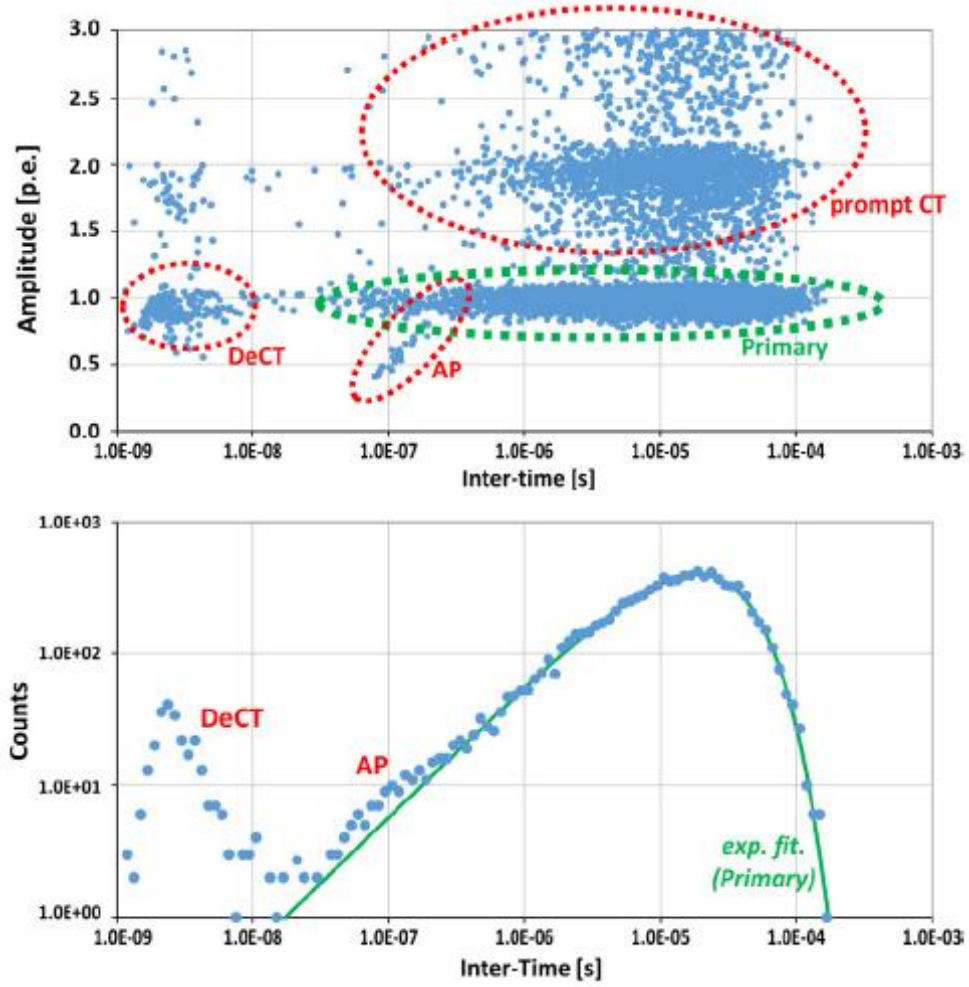

Another example

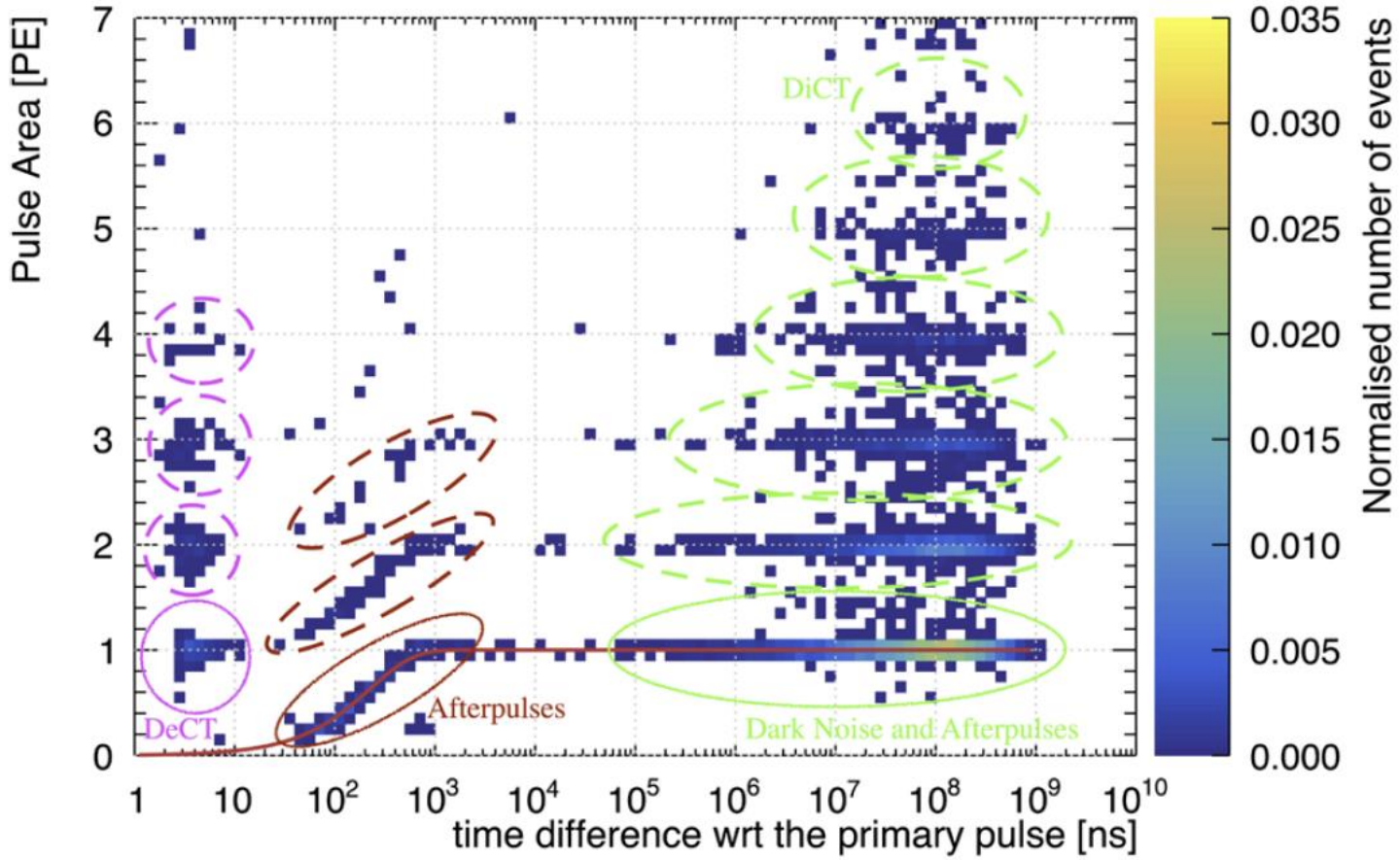

G. Gallina *et al*., 2022, doi: 10.1140/epjc/s10052-022-11072-8.

But in a digital SiPM…

- All pulses are identical at the SPAD level !

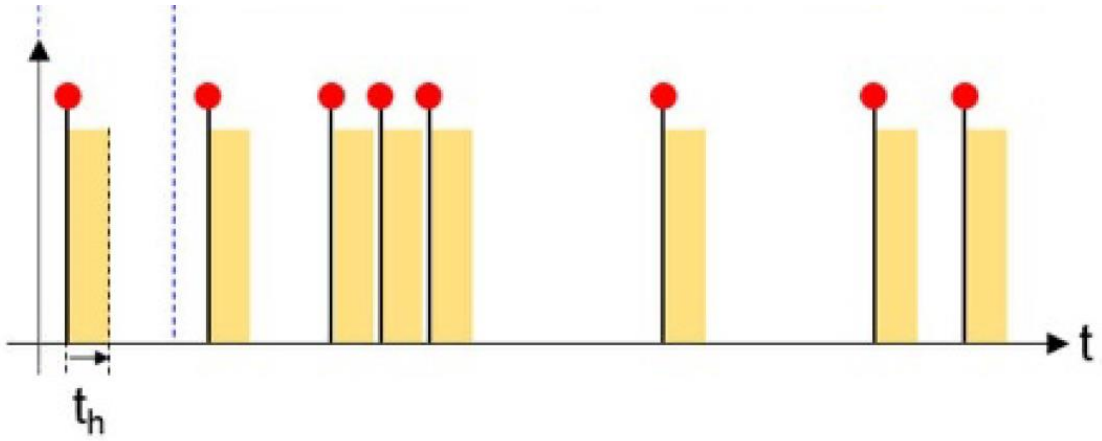

observable: primary events, prompt crosstalk, afterpulsing and delayed crosstalk events.

t_h : hold off delay

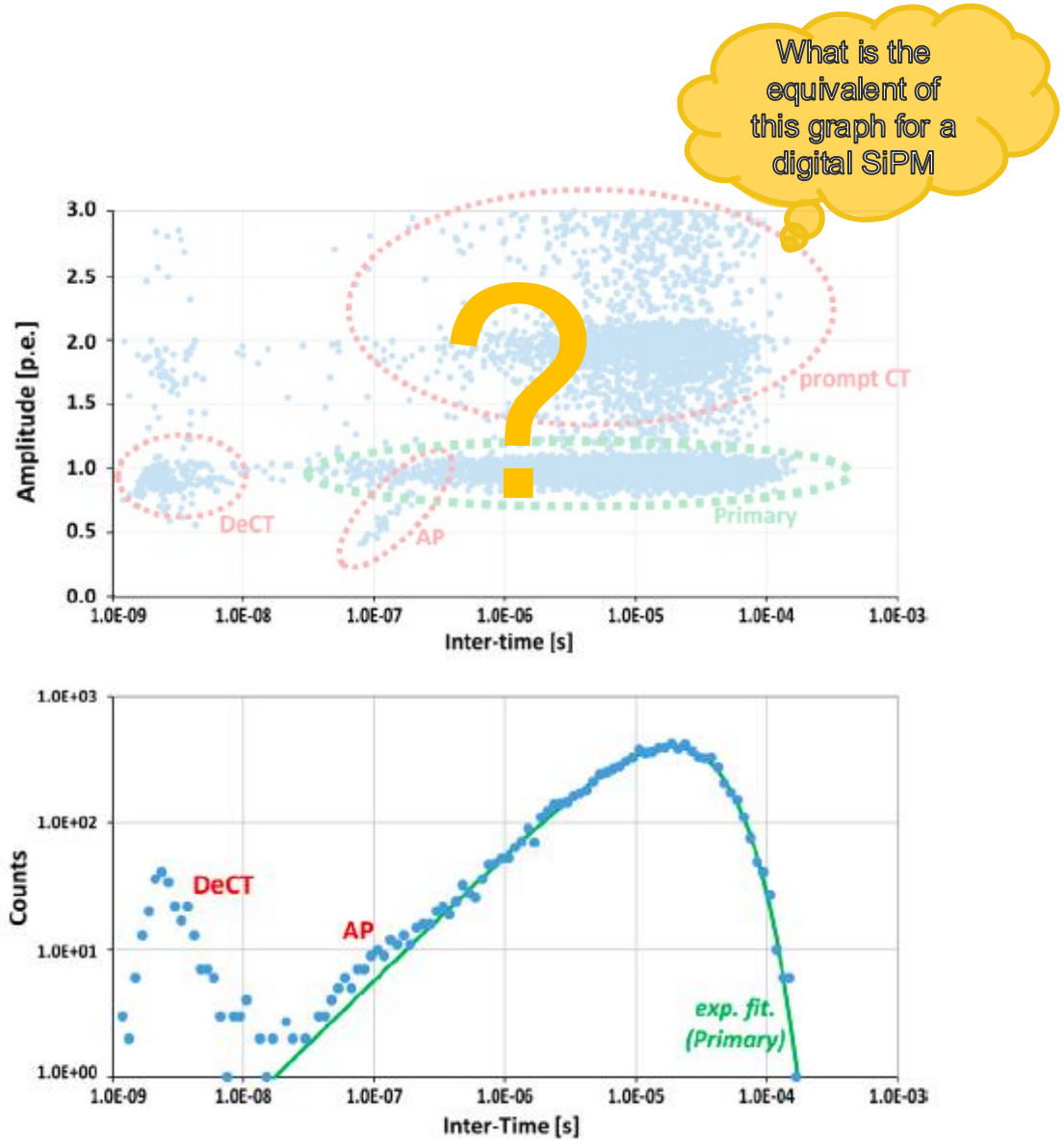

Reducing the impact of afterpulsing with extended hold-off delays

UDS

- Controling the hold-off delay is only possible with active control on SPADs

SPAD control sequence: held off below V_{BD}

Exponential time release of trapped carriers

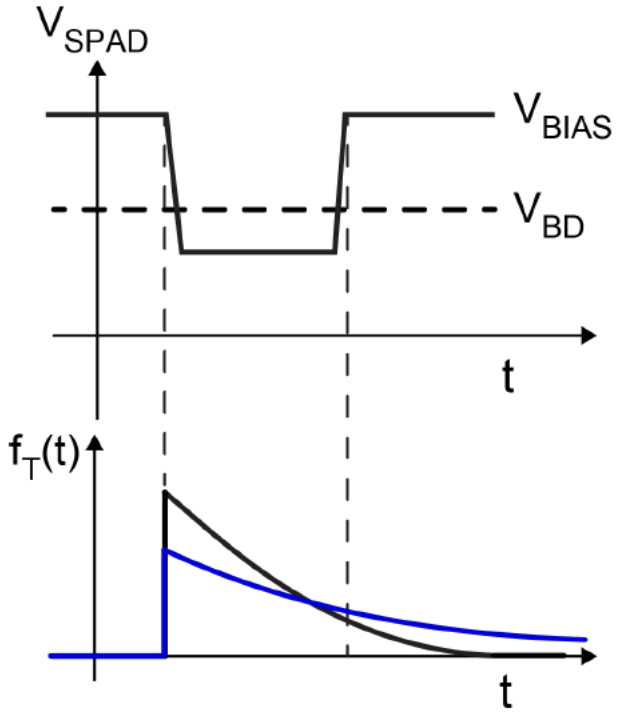

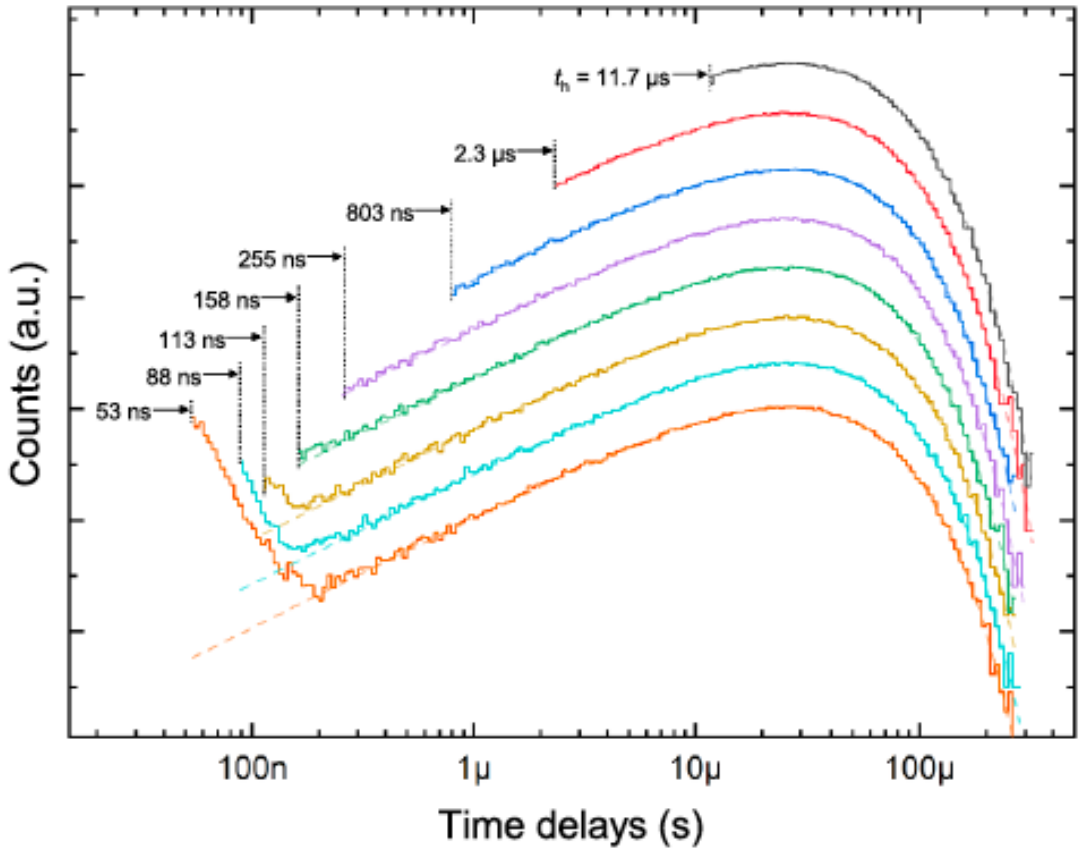

Figure 7. The capability of the digital SiPM to control the holdoff delay (t_h). The time delay distributions are offset to highlight the effect of the holdoff delay. Dashed lines correspond to the fit of uncorrelated events (equation (4)).

F. Vachon et al. *Measurement Science and Technology*, 2020, doi: 10.1088/1361-6501/abba4b.

Active quenching reduces afterpulsing

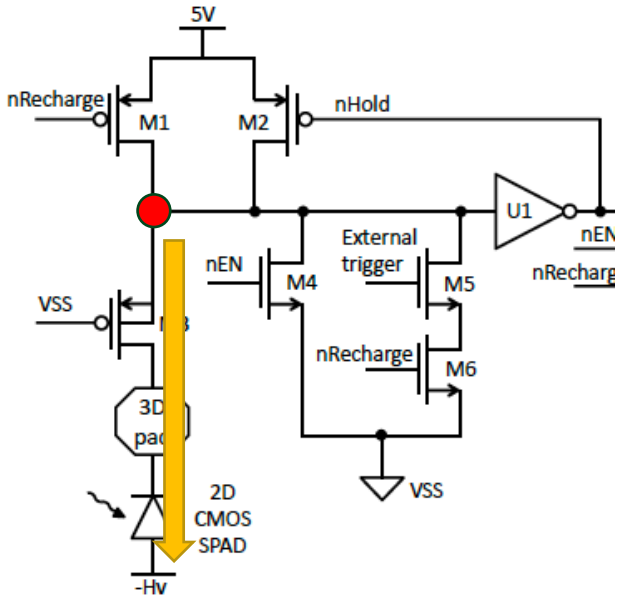

- Passive quenching
  - M1 plays the role of the quenching resistor
- All the charge on the reading node must flow through the SPAD
  - Increases the probability that a carrier gets trapped and released later – afterpulsing
  - Increases optical crosstalk

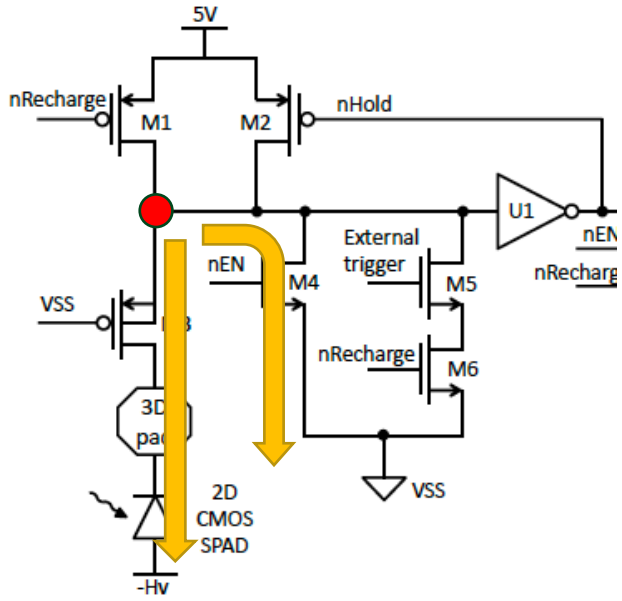

- Active quenching
  - Once an avalanche is detected…
  - M4 is used to provide another current path to discharge the reading node
- All the charge on the reading node must flow through the SPAD
  - Increases the probability that a carrier gets trapped and released later – afterpulsing
  - Increases optical crosstalk

Random telegraphic signal or noise

- Random telegraphic noise or signal
  - The dark count rate changes between « levels »
- Example: Radiation damage generates RTS noise in certain SPADs

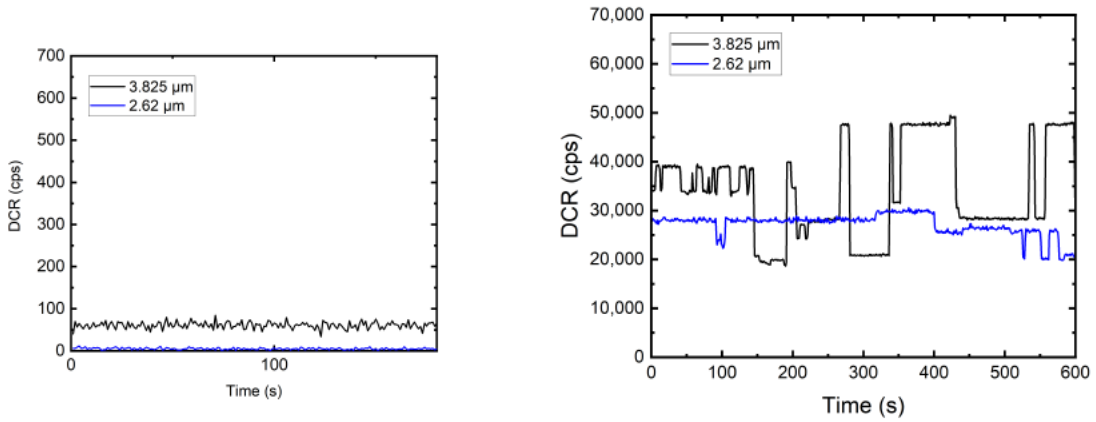

(a) Before irradiation (b) After irradiation

Figure 3.12: Two 55 nm SPADs, with active area radii of 3.825 and 2.62 µm, exhibiting DCR RTS at DDD of 80 TeV/g. The DCR rate in each second fluctuates randomly between several levels during a 600-second measurement.

- Dark count activation energy
  - Spectroscopy of defects, traps, dopants

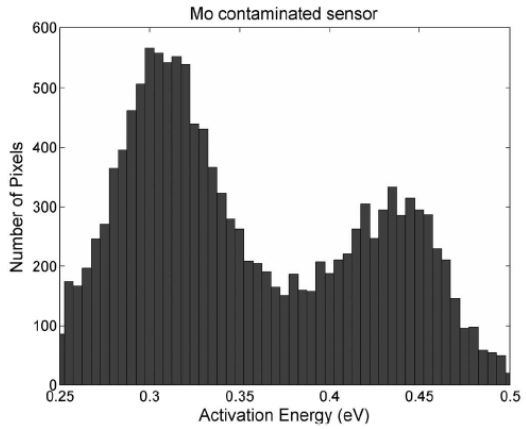

Fig. 2. Density of deep-level defect states for image sensor contaminated with molybdenum. The peak at ≈0.3 eV is attributed to molybdenum, and the ≈0.44-eV peak is attributed to the E-center (phosphorus-vacancy).

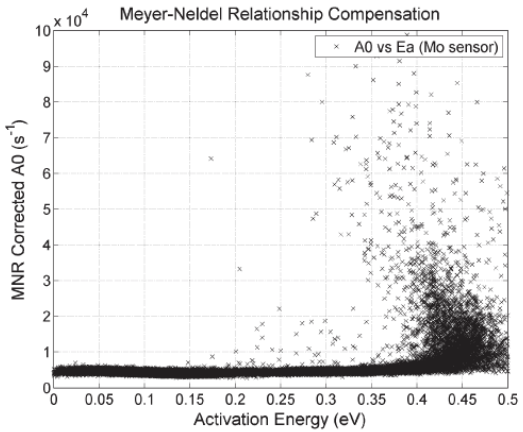

Fig. 6. Scatter plot of A_0 versus E_a corrected for the MNR using (4).

So… SPADs emit light during avalanche

UDS

- Many examples in the literature…

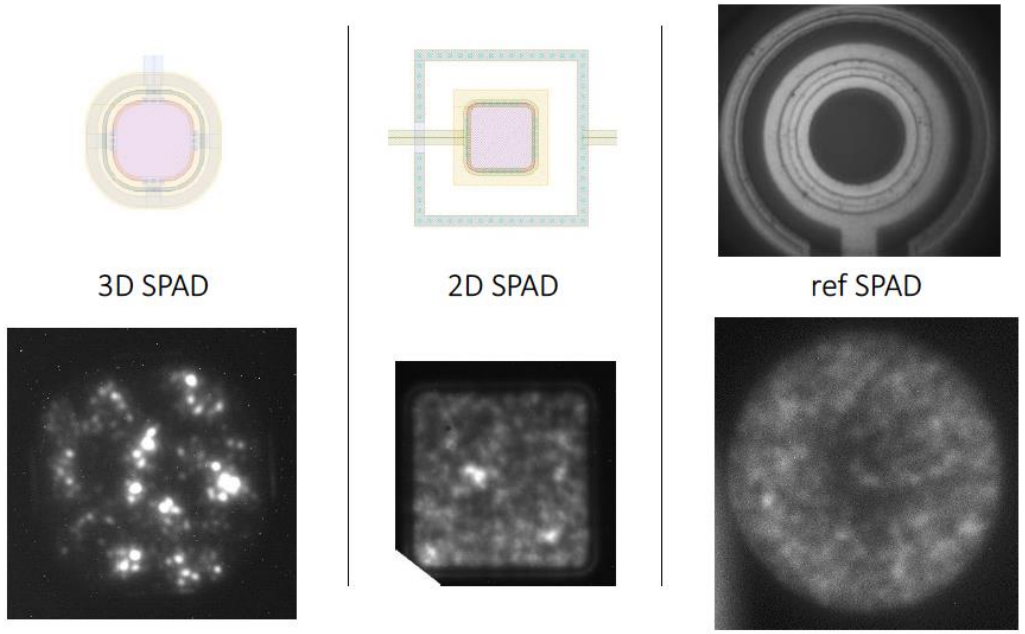

Figure 5.21 Light emission test performed on a typical 3D SPAD, compared to a typical 2D SPAD and to a reference commercial SPAD. The top row gives top-view layout drawings as a guide to inspect the bottom row light emission pattern observed on each SPADs. All the light emission images are acquired with the same camera (Qimaging exi-blue fluorescence camera) with the same setting (typically 30 s exposition at high gain).

S. Parent, 2022, thesis U. de Sherbrooke

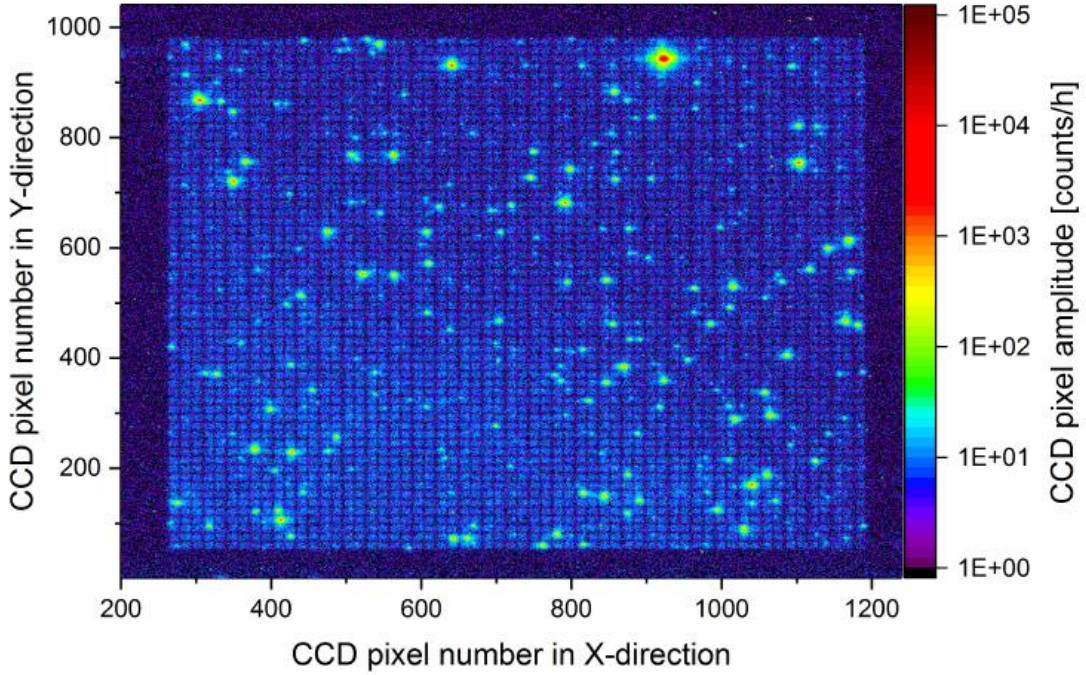

Fig. 19. Light emission image of the PM3350T MOD at $\Delta V = 5.4$ V and $t_{exp} = 1$ h.

E. Engelmann, 2018, doi: 10.1140/epjc/s10052-018-6454-0.

Stimulated Secondary Emission of Single Photon Avalanche Diodes

Measured light emission spectrum

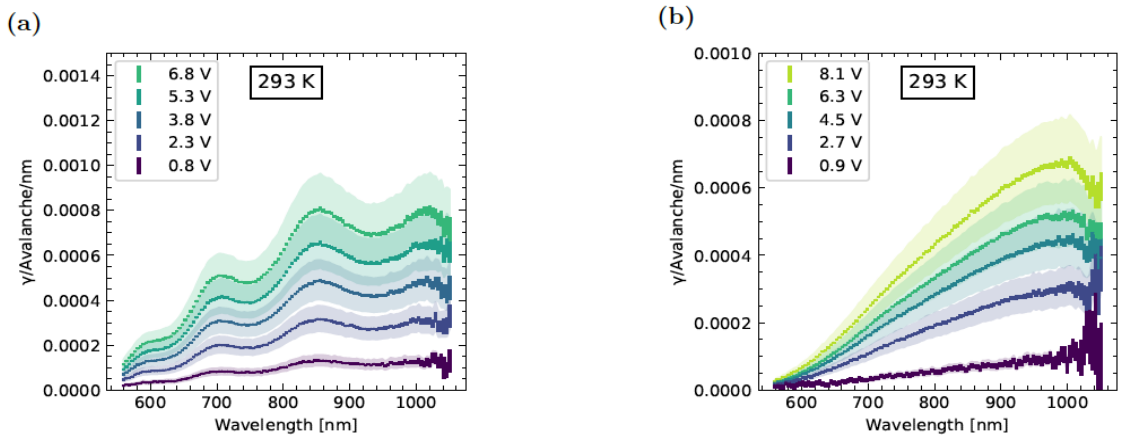

Figure 4: Emission from the HPK (left) and FBK (right) SiPM into a 0.45 NA objective at room temperature (top) and liquid xenon temperature (bottom). Systematic errors are shown as shaded error bands. Intermediate temperatures have been omitted for clarity.

Number of emitted photons

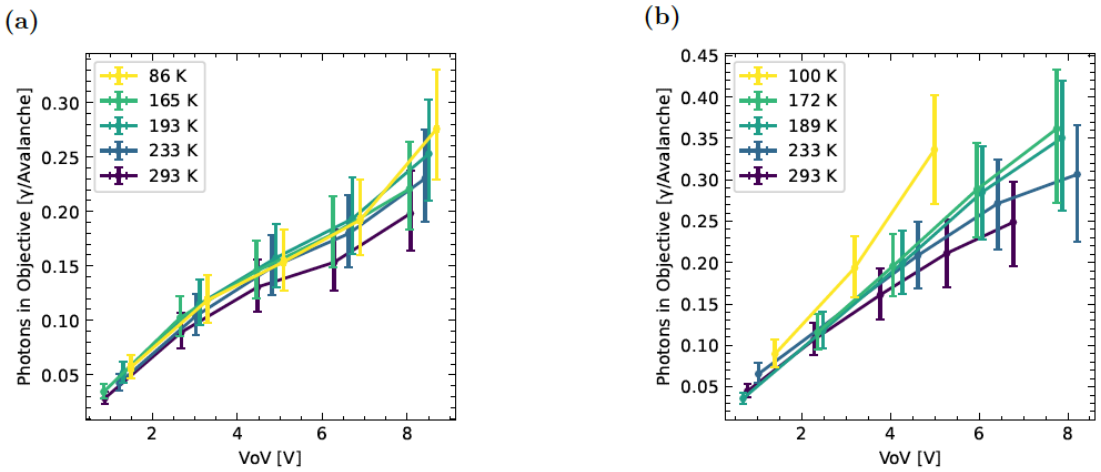

Figure 5: Photon yield integrated between 550 and 1000nm for the HPK (left) and FBK (right) SiPM into a 0.45 NA objective at different temperatures. Systematic errors are included. The spread of points in the FBK device at high over voltages is due to applying the N_{cda} correction from near LXe temperatures to other temperatures.

K. Raymond, 2024, doi.org/10.48550/arXiv.2402.09634

External crosstalk

- For example in noble liquid experiments where some detectors face others
  - Also possible in other scintillating medium
- Possible mitigation: reducing detector sensitivity at long wavelength

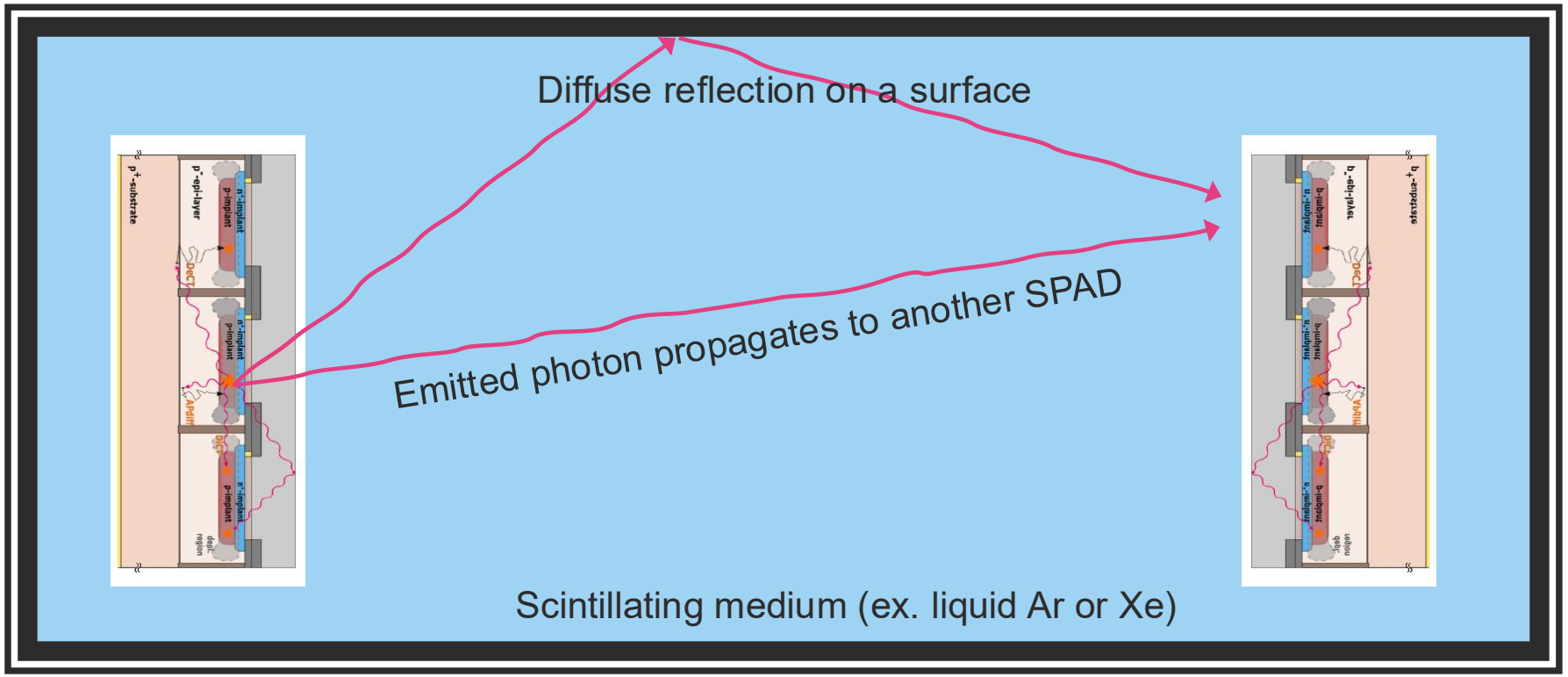

Some references to start from

New compendium from DRD4

- F. Acerbi and S. Gundacker, “Understanding and simulating SiPMs,” NIM-A, vol. 926, pp. 16–35, May 2019, doi: 10.1016/j.nima.2018.11.118.
- Cova, S., Ghioni, M., Lacaita, A., Samori, C., & Zappa, F. (1996). Avalanche photodiodes and quenching circuits for single-photon detection. Applied optics, 35(12), 1956-1976.
- A. N. Otte, D. Garcia, T. Nguyen et D. Purushotham, «Characterization of three high efficiency and blue sensitive silicon photomultipliers», Nuclear Instruments and Methods in Physics Research Section A : Accelerators, Spectrometers, Detectors and Associated Equipment, vol. 846, p. 106–125, 2017.
- W. J. Kindt, «Geiger mode avalanche photodiode arrays : For spatially resolved single photon counting», PhD Thesis, p. 471, 1999.

The spectrum detectable using silicon

The absorption/penetration depth chart of semiconductors

UDS

Semiconductors cover all the visible spectrum to infrared wavelength

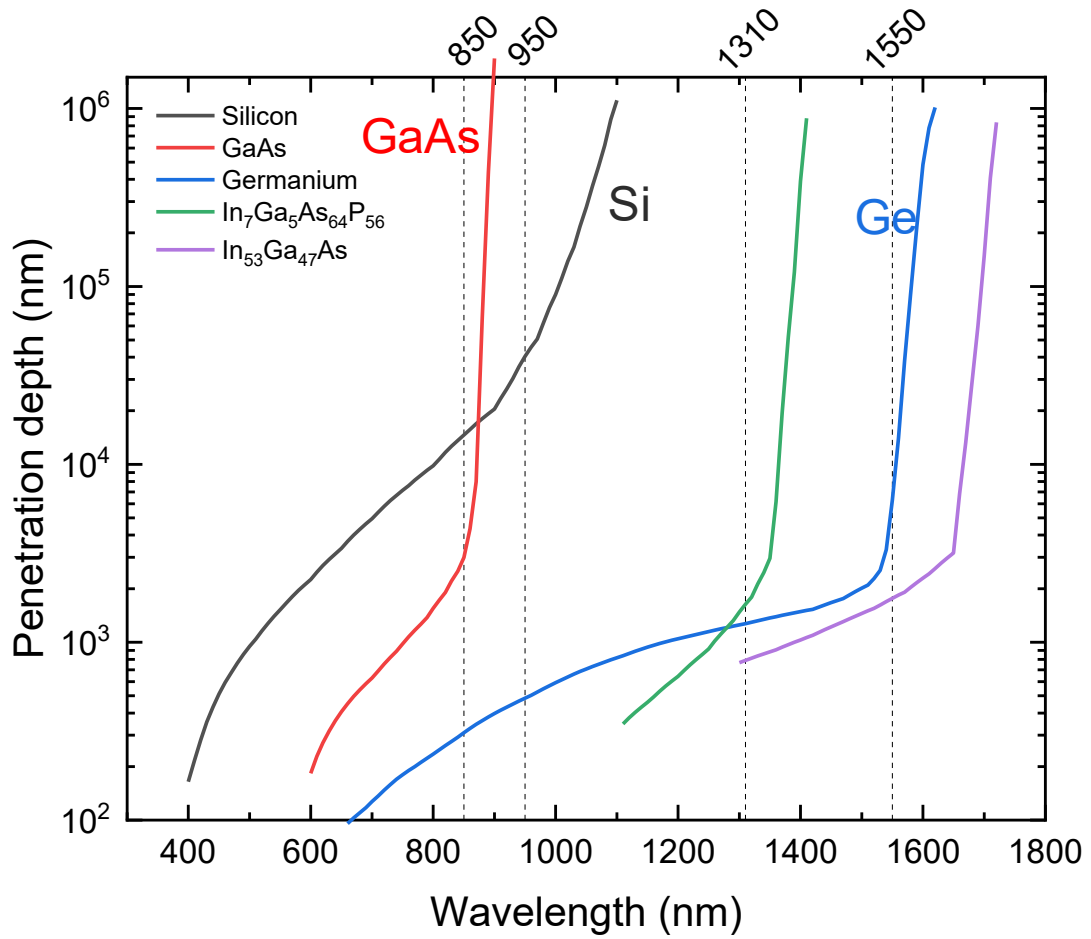

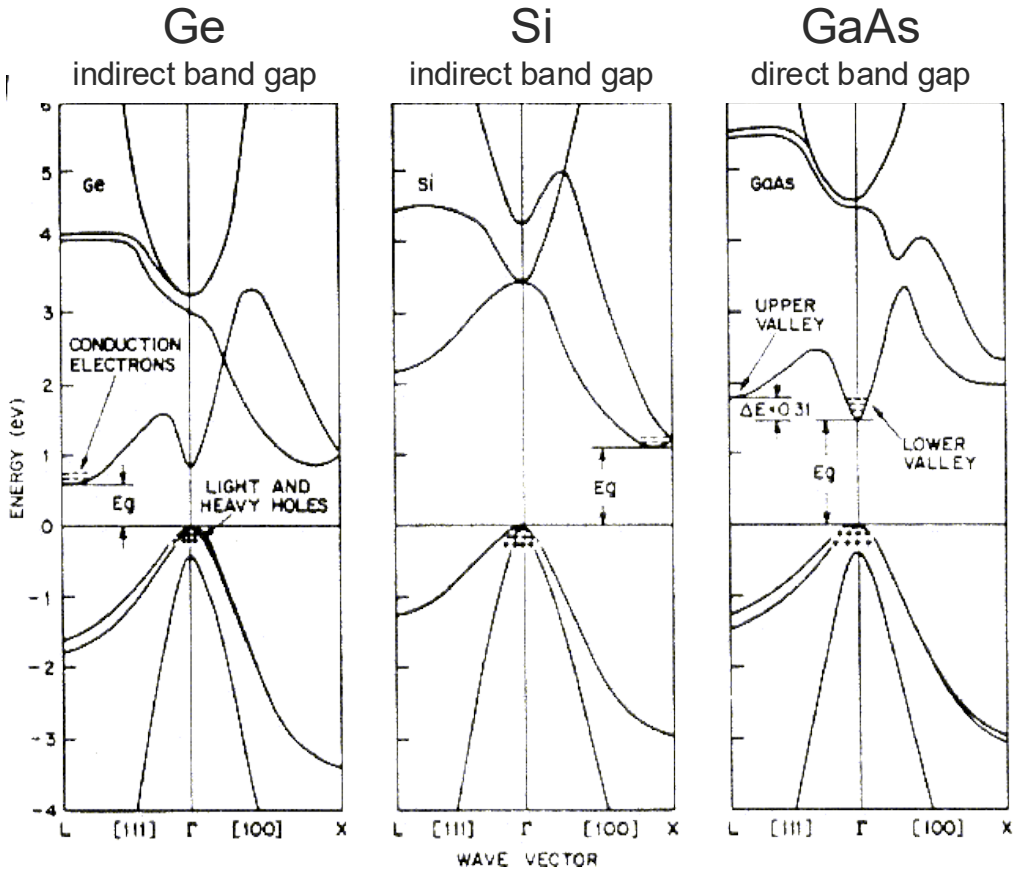

$E_g = E_L = 0.65$ eV
$\lambda = 1907$ nm
$E_{\Gamma 1} = 0.75$ eV

$E_g = E_X = 1.11$ eV
$\lambda = 1110$ nm
$E_{\Gamma 1} = 3.4$ eV

$E_g = E_{\Gamma 1} = 1.42$eV
$\lambda = 873$ nm

See also Tsai 2018 https://doi.org/10.1063/1.5028053

The absorption/penetration depth chart of semiconductors

UDS

What about the short wavelengths?

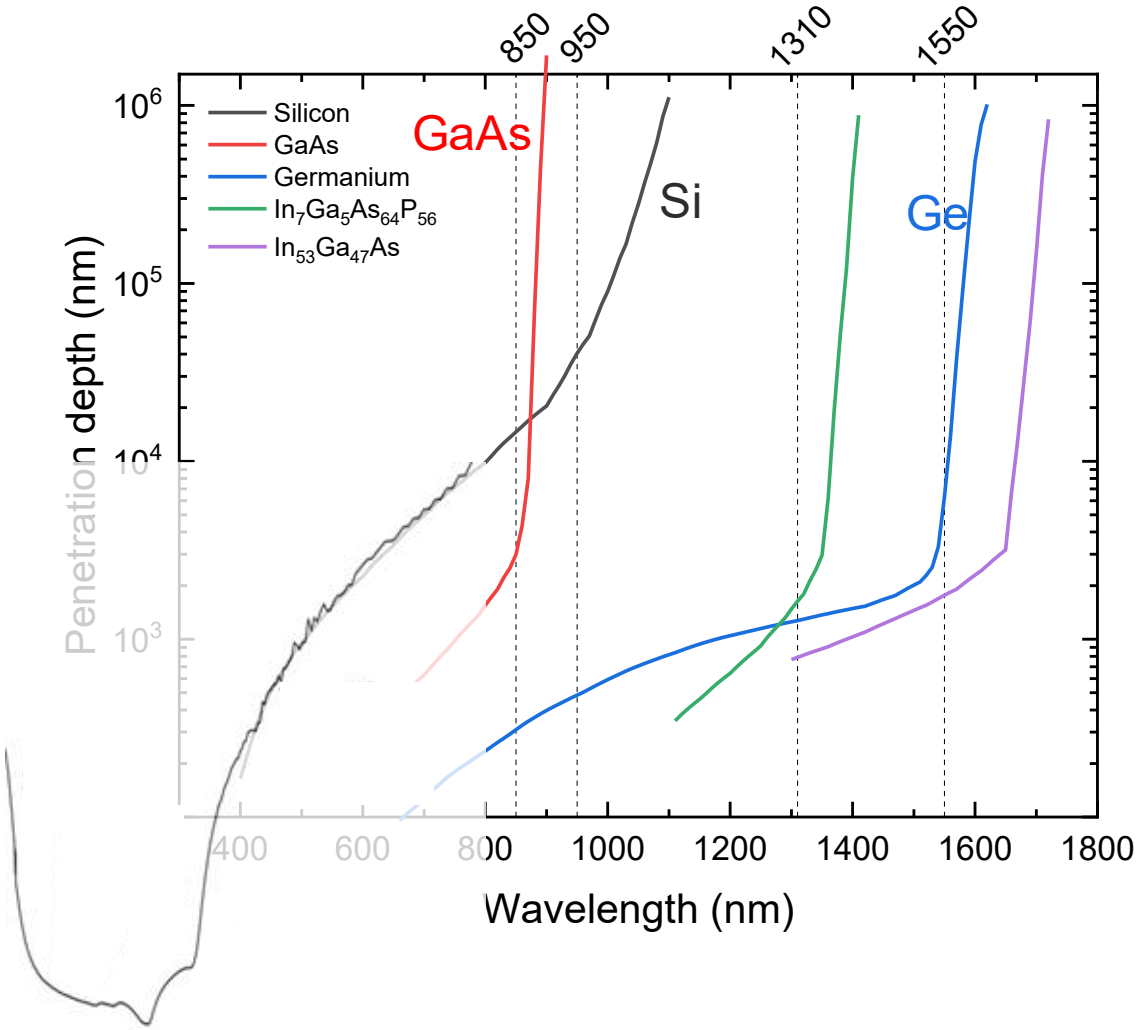

Photon penetration depth in silicon

Silicon stops to be a good detector…

- in the infrared because it gradually becomes transparent
  - Diverging penetration depth
  - Residual absorption through
    - In gap defect and impurity states
    - Free carrier absorption $\propto n_{eh}^2 m^{*-1}$
- but in the ultraviolet, penetration depth is certainly not a problem…

  (we'll come back to this later)

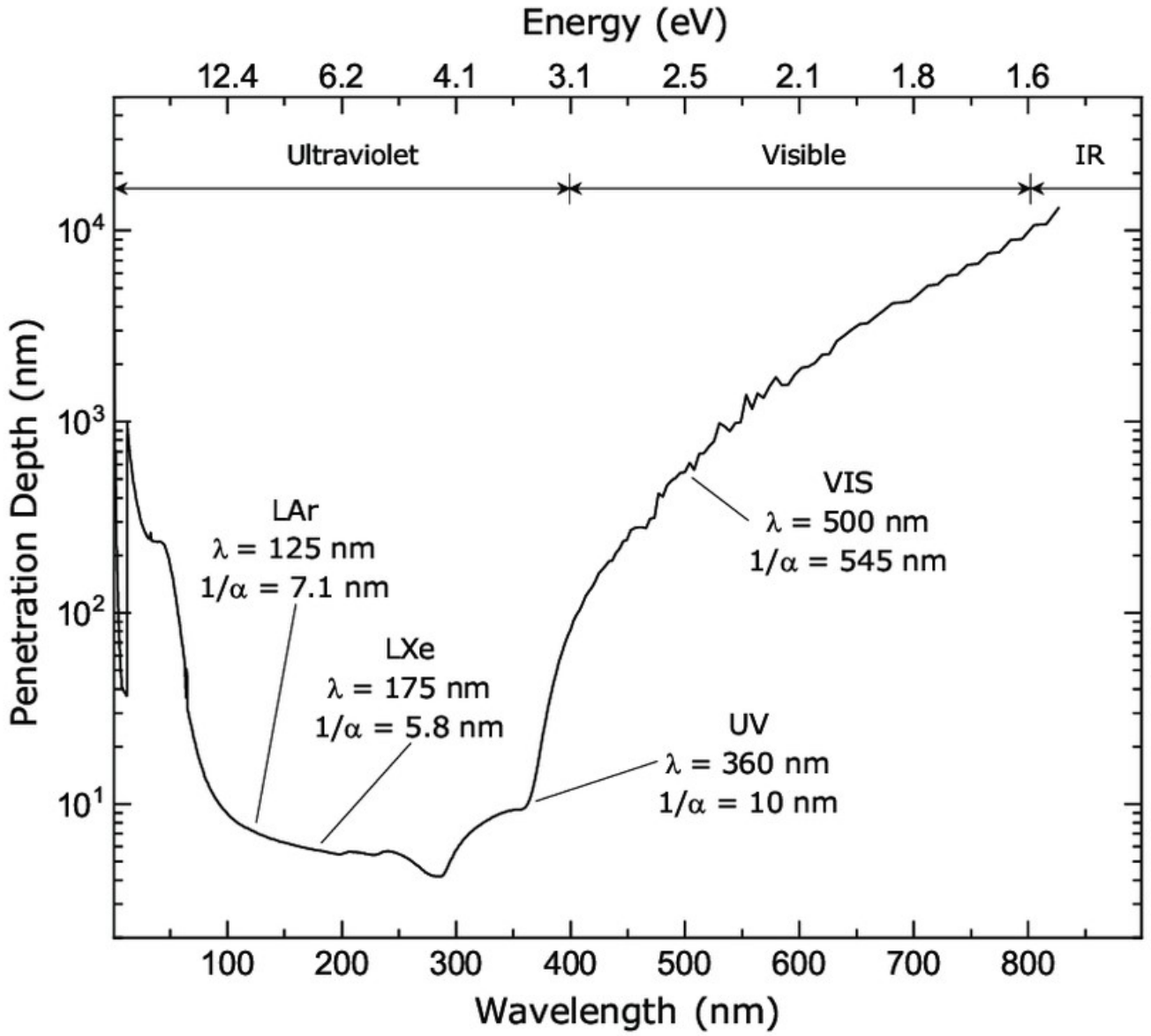

serge.charlebois@usherbrooke.ca

Pratte, JF. 3D Photon-To-Digital Converter for Radiation Instrumentation: Motivation and Future Works 2021

Detecting UV and VUV light

i.e. below 350 nm

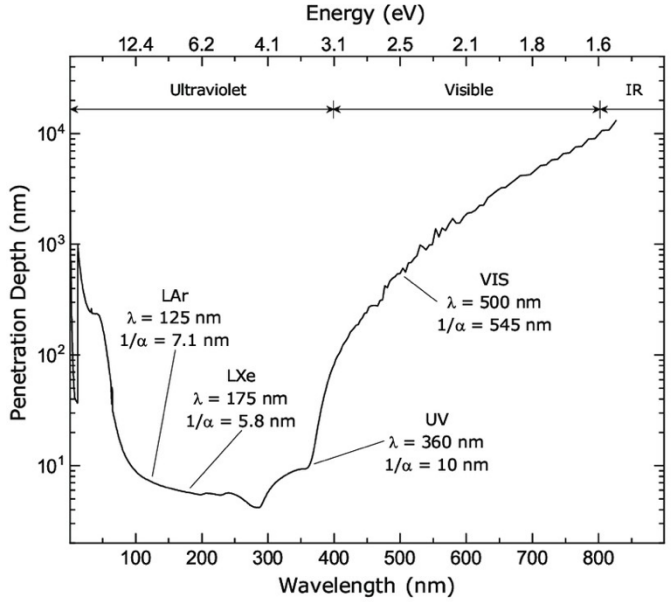

Photon penetration depth and the sensitivity problem in UV

- Photons are absorbed in the first few nanometer at the silicon surface
- And are trapped in a potential well at surface
  - due to surface/interface states that pin the fermi level at mid-gap
- Not neglecting the challenge of having a passivation material that does not absorb VUV photons

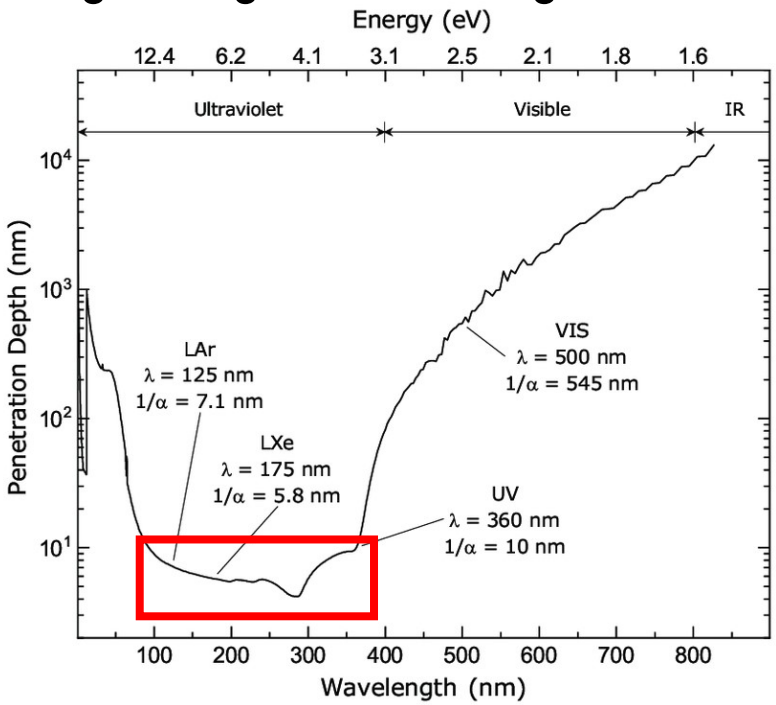

Pratte, JF. 3D Photon-To-Digital Converter for Radiation Instrumentation: Motivation and Future Works 2021

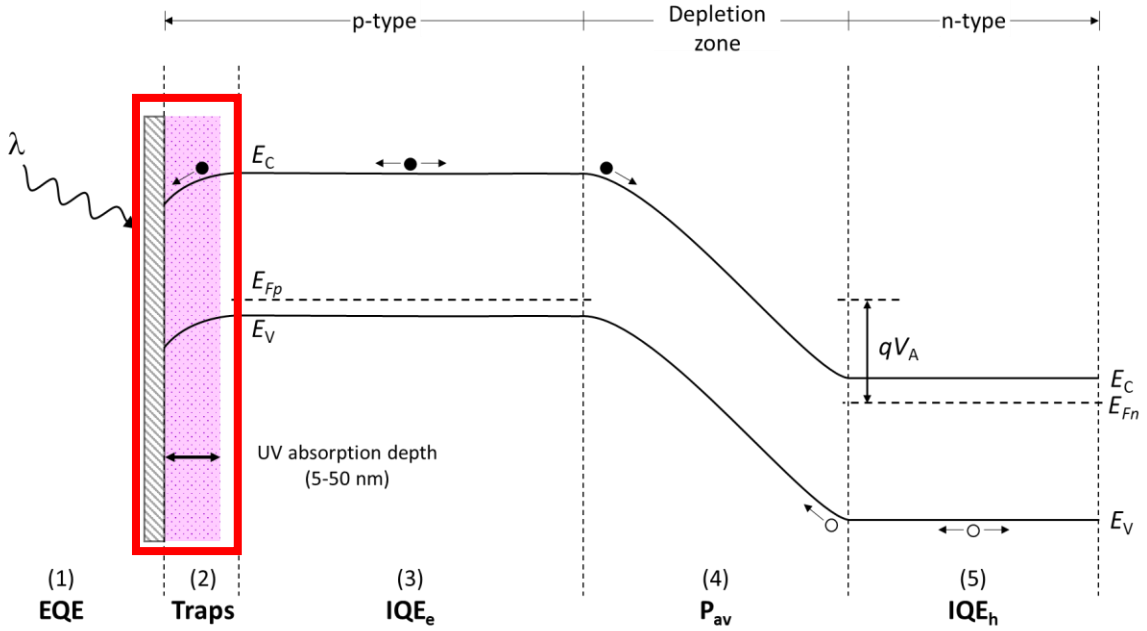

F.Vachon, Masters thesis, Université de Sherbrooke, 2021.

δ-doping

- Growing a thin (few nanometers) highly boron doped layer
  - By MBE on the p^+ surface, developed at JPL in the 1990's for CCDs
  - Effectively removes the potential well at surface
- Internal quantum efficiency ~ 1
  - Measurements follow the transmittance limited silicon response
  - Multi electron-hole pair yield is observed (red triangles)

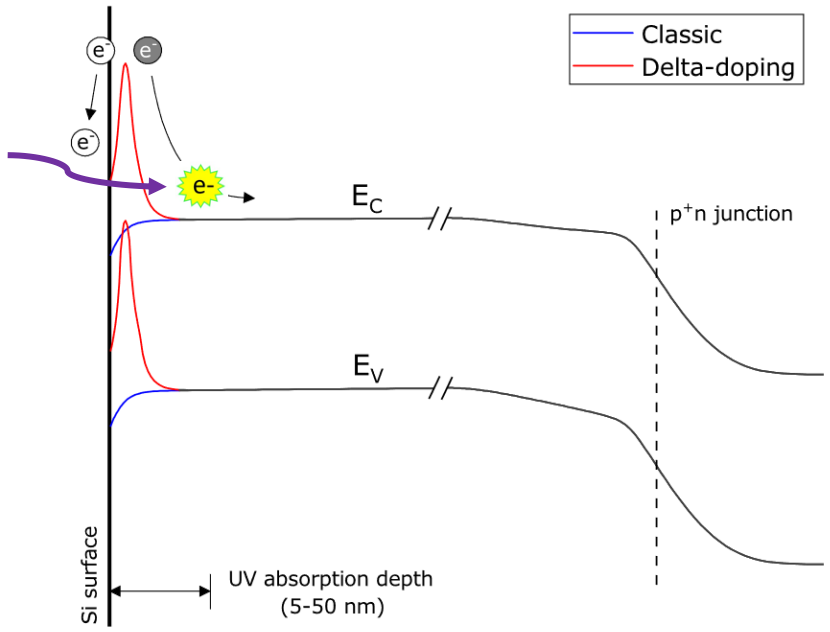

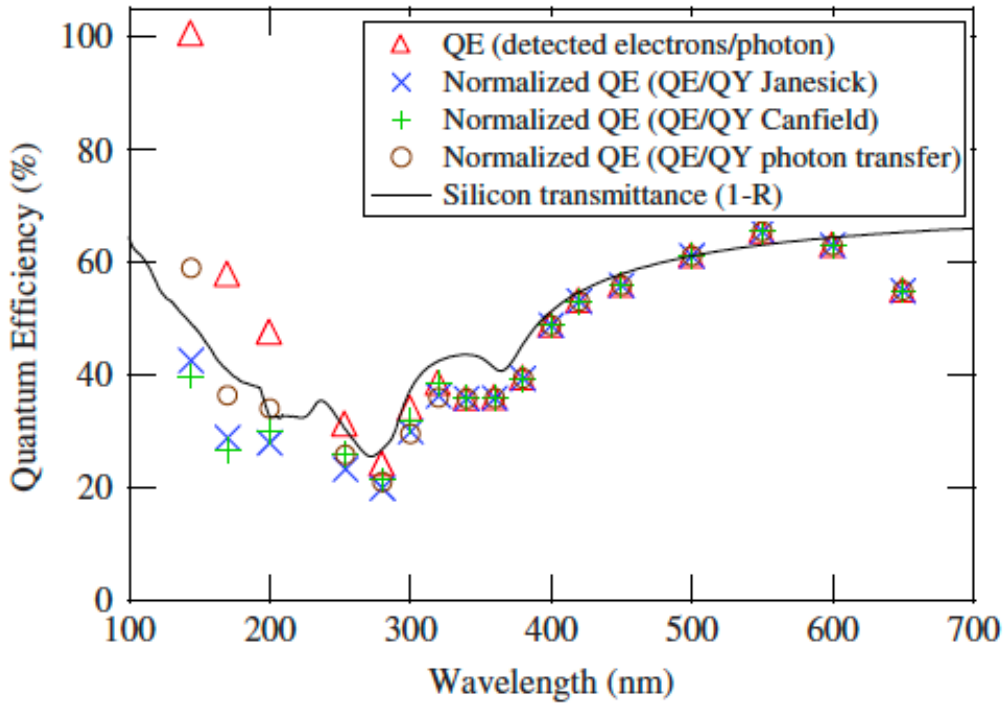

Nikzad etal. Appl. Opt. 51, 365-369 (2012)

The PureB technology

- Deposition and processing of a pure boron layer on the silicon surface
  - Few nanometer thick
  - Chemical vapor deposition (CVD)
  - Temperature/laser annealing
- Effectively suppresses the surface potential well
  - Similar to δ-doping
- Demonstrated sturdy to aging and further processing
  - Possible deposition of an antireflective coating

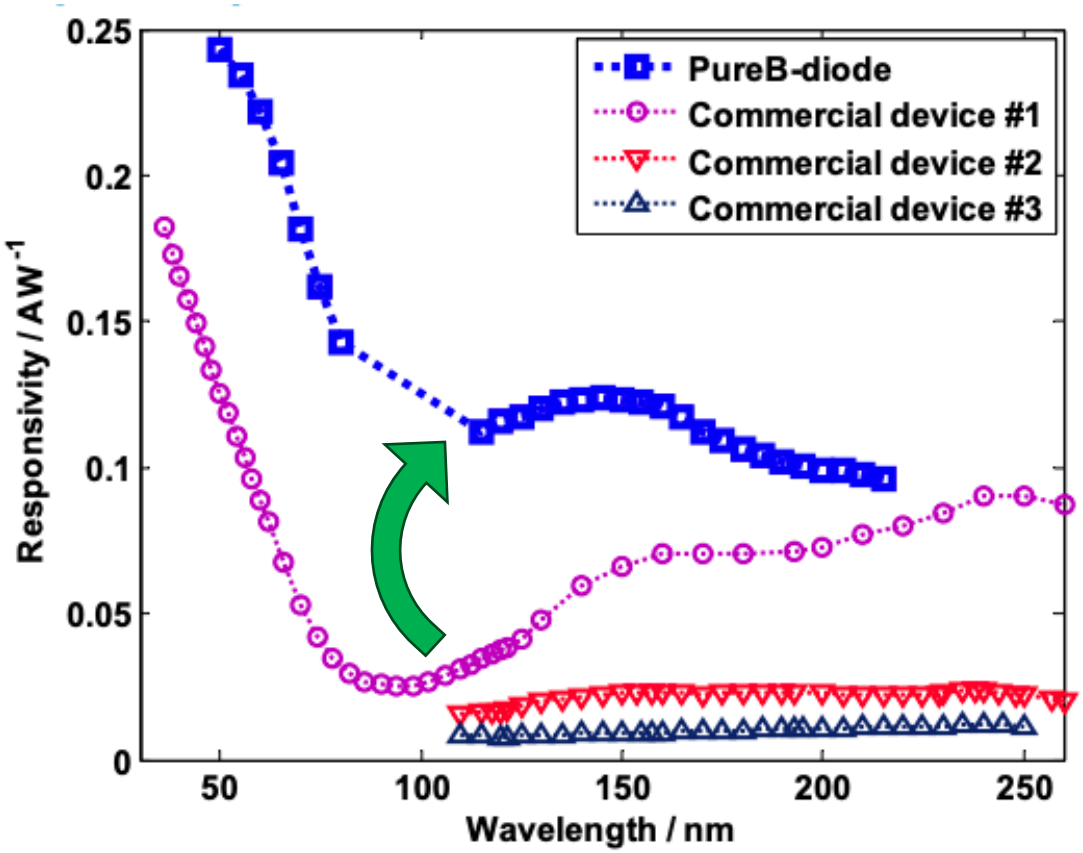

L. Shi 2011 DOI: 10.1117/12.891865

“Black silicon”

- Addresses both transmission through silicon interface and surface well

- Nanostructured surface
  - Randomizes the incidence angle of light
  - Effective smooth index transition

  Near zero reflections from VUV to IR

  The surface is pitch-black, hence the name

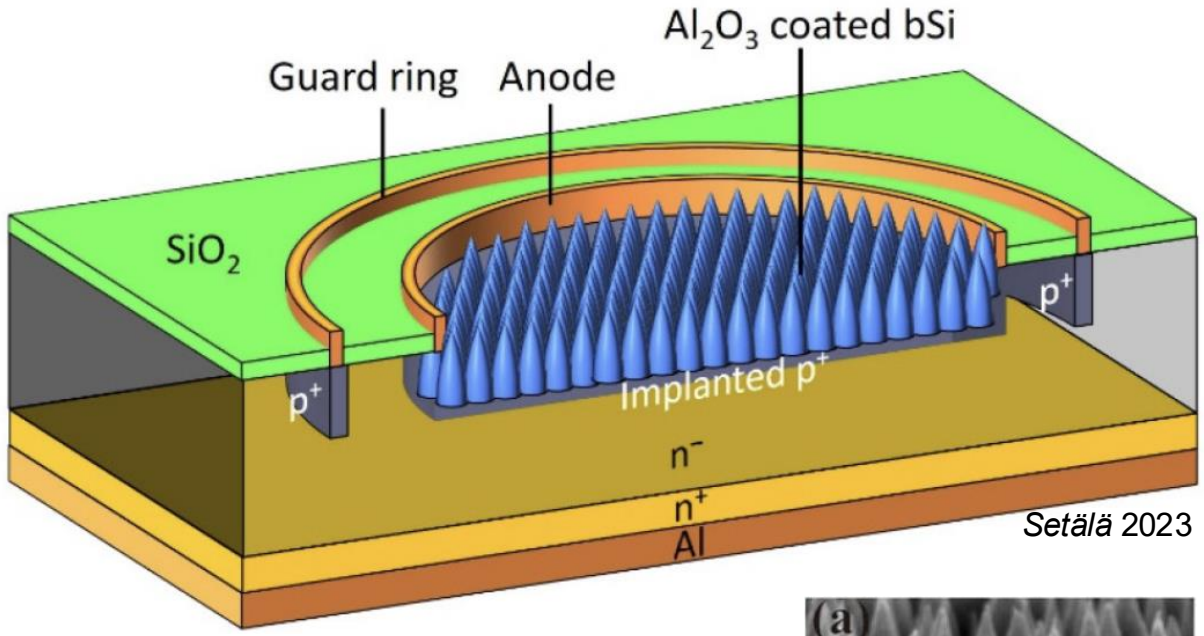

Setälä 2023

- Al_2O_3/Si interface
  - Negative charging of interface

  Removal of potential well at surface

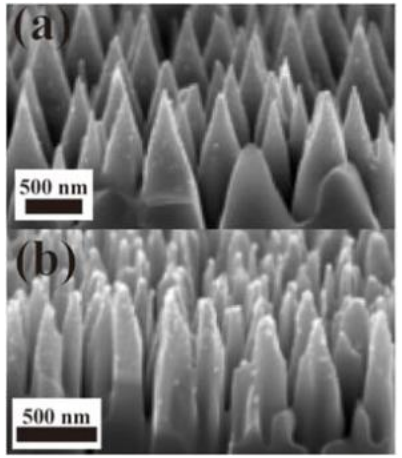

Tsang 2020

- See also a broad review by Z. Zhao https://doi.org/10.1063/5.0133770

“Black silicon”

- Quantum efficiency (QE)
  - Nears 100% for photons below ~4 eV (λ > 350 nm)
  - QE > 100% above 4 eV: more than one electron-hole pair is created per photon
- Responsivity
  - Reaches theoretical value $^{q\lambda}/_{hc}$

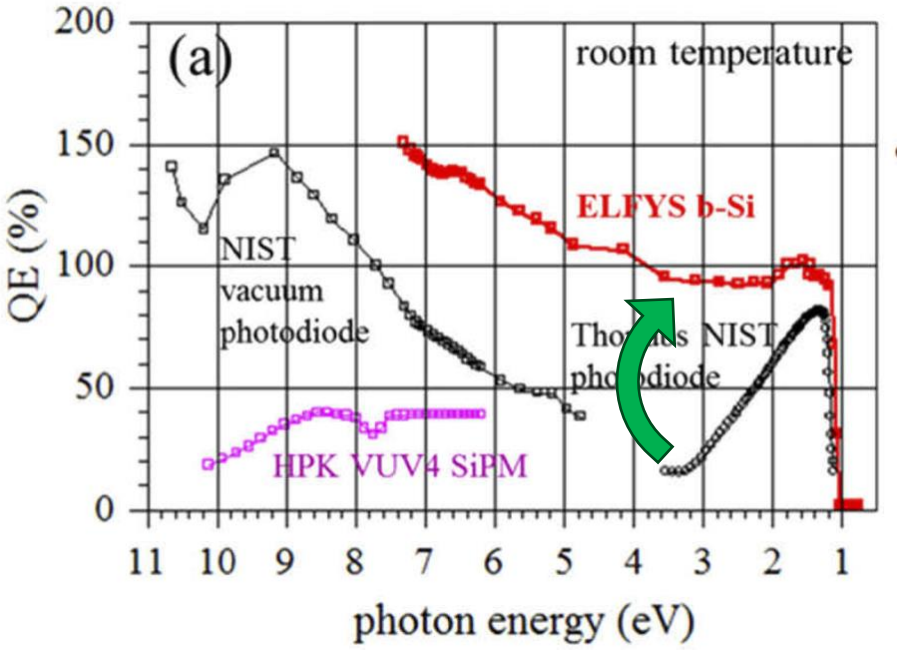

Tsang et al. Opt. Express 28, 13299-13309 (2020)

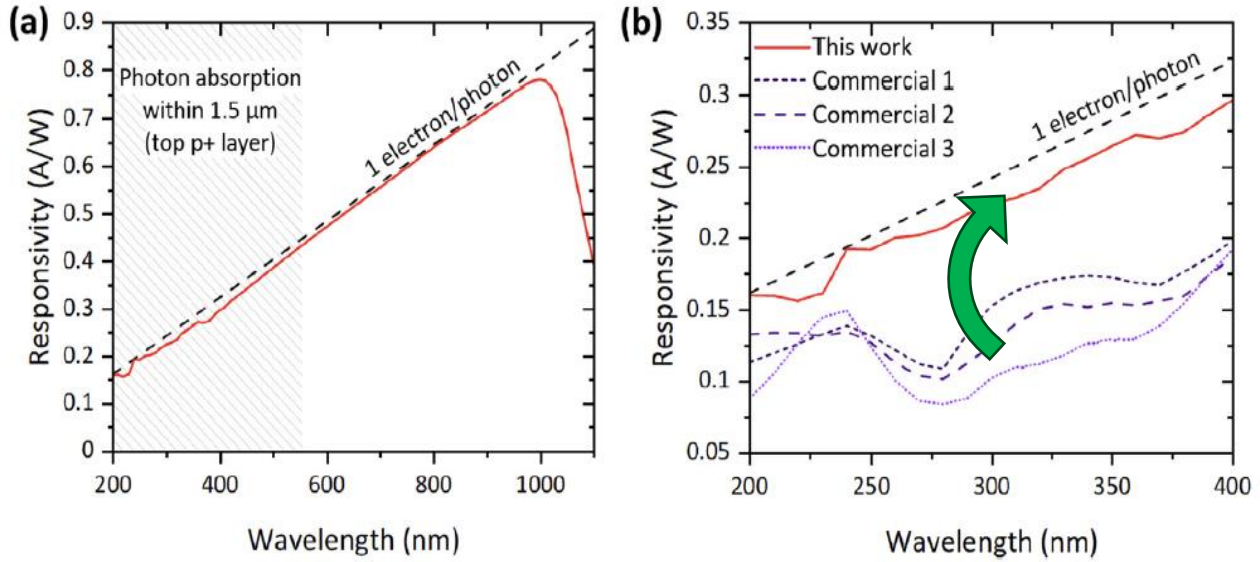

Figure 2. (a) Responsivity of a boron-implanted b-Si detector over a wide wavelength range measured at 0 V bias. Dashed line represents one collected electron per a photon. 1/e photon absorption limit for 1.5 μm junction is highlighted. (b) UV responsivity of market leader diffused Si UV photodiodes[23–25] compared to this work.

Setälä et al. ACS Photonics 2023, 10, 6, 1735–1741

Number of electron-hole pairs yielded by one UV photons

- In a linear detector (e.g., APD, CCD), the pair yield acts as an extra gain on the current
  - Need to be calibrated out to properly represent the photon flux
- In a SPAD, the number of pair does not change the Boolean response: still 0 or 1
  - But there is a greater probability of triggering an avalanche because more pairs attempt to do it

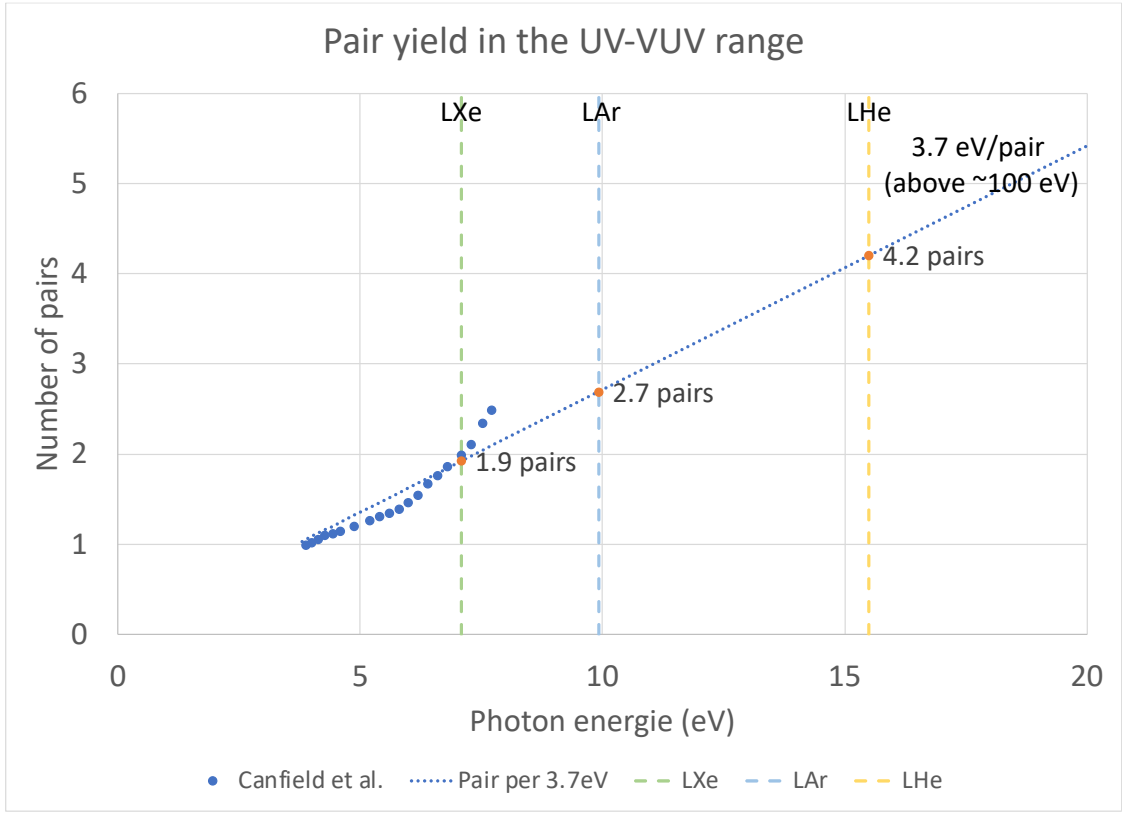

Dotted line: extrapolated pair yield from the high energy value for silicon W~3.7 eV/pair

L. Canfield, Metrologia, vol. 35, no. 4, p. 329, 1998

In summary for the VUV wavelenghts

UdS

- PureB since ~2010
  - Demonstrated in SPAD
  - Frontside and backside illuminated
- δ-doping since 1990's
  - Demonstrated on avalanche photodiodes and EMCCD
  - Backside implementation
  - Not yet demonstrated on frontside in SPADs
- Black silicon since ~2018 (for UV light, 1995 otherwise)
  - Demonstrated on avalanche photodiodes
  - Frontside
  - This year : N-31-02 N-01-023 (BNL)
- And maybe using other materials than silicon
  - A review: M. Razeghi & A. Rogalski J. Appl. Phys. 79, 7433–7473 (1996) https://doi.org/10.1063/1.362677
  - Facing the same challenge for industrialization and array integration as for IR detectors

Section final comments

UDS

- Silicon is hard to beat for dark count rate and sensitivity range
  - Particularly for the short wavelengths (UV)
- Other semiconductors
  - Can be operated in Geiger mode
  - Can extend sensitivity in the IR at the cost of much device engineering
    - Yet dark count remains a challenge
- Would/could benefit from integration in a digital SiPM
  - Another nice engineering challenge!

Geiger operation

Exploiting enormous intrinsic gain

SPAD (Geiger mode)
Gain = 10^4-10^6
$V_{BR} < V_{bias}$
metastable

Avalanche Photodiode
Gain = 10-1000
$V_{APD} < V_{bias} < V_{BR}$

Photodiode
Gain = 1
$V_{bias} < V_{APD}$

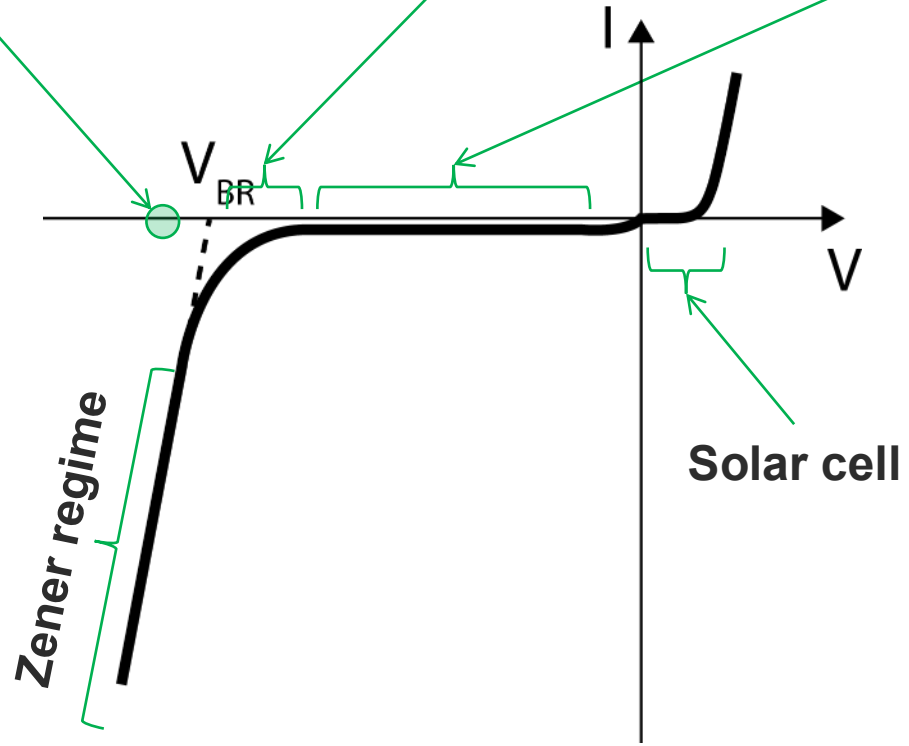

The saturation current (Shockley's equation)

$$I_S = qA\left(\frac{D_p}{L_p}p_n + \frac{D_n}{L_n}n_p\right) = q\left(\frac{AL_p p_n}{\tau_p} + \frac{AL_n n_p}{\tau_n}\right)$$
$$\approx 6 \times 10^{-19} A \approx 4 \text{ carriers per second}$$
$$\approx 300\ ms \text{ between carriers!}$$

Diode parameter:
A = 20 µm diameter
$N_a = 10^{19}$ cm^{-3} $\tau_n = 10^{-6}$ s
$N_d = 10^{16}$ cm^{-3} $\tau_p = 10^{-4}$ s

The depletion zone contribution through thermal generation

$$I_{DepZone} = q\frac{AW_{dep}n_i}{\tau_{gen}}$$
$$\approx 2 \times 10^{-15} A \approx 10^4 \text{ carriers per second}$$
$$\approx 100\ \mu s \text{ between carriers!}$$

The reverse current is in reality a stream of electrons with "long pauses" between each.

Other contributions omitted to simplify the arguments: Shockley–Read–Hall, field enhanced SRH, tunneling …

Single photon avalanche diode (SPAD)

UDS

SPAD cross-section

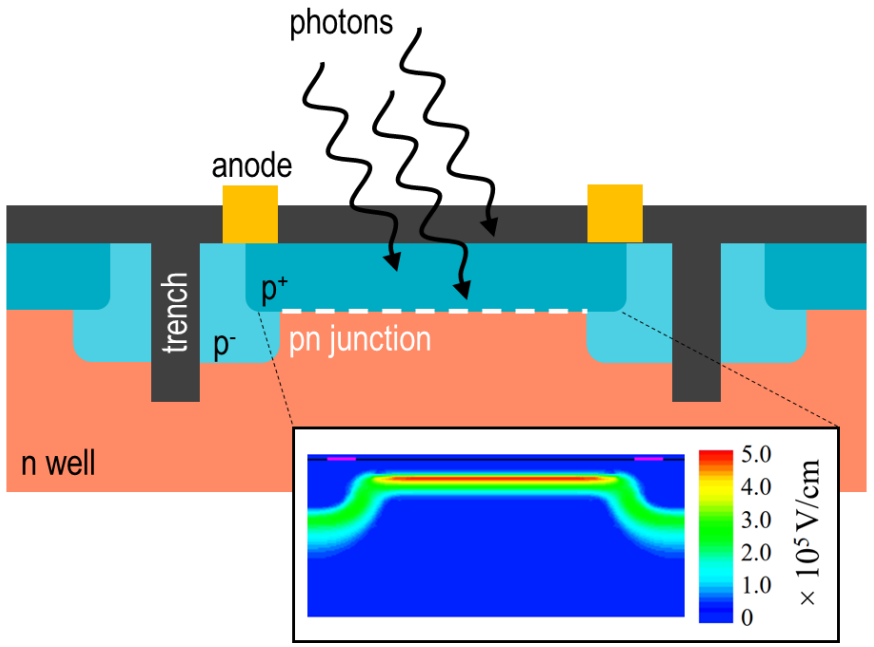

Schematic circuit

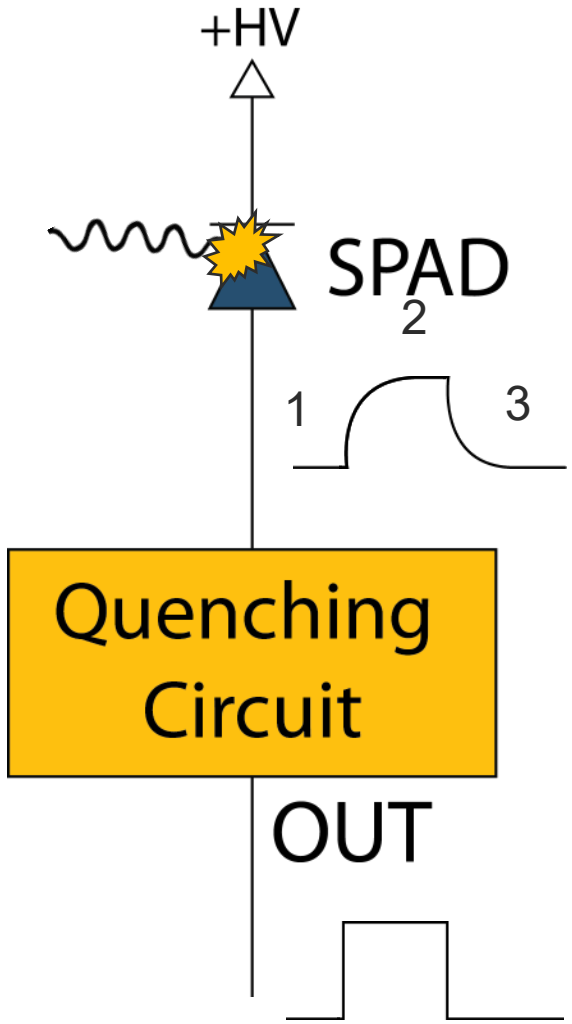

SPAD I-V curve

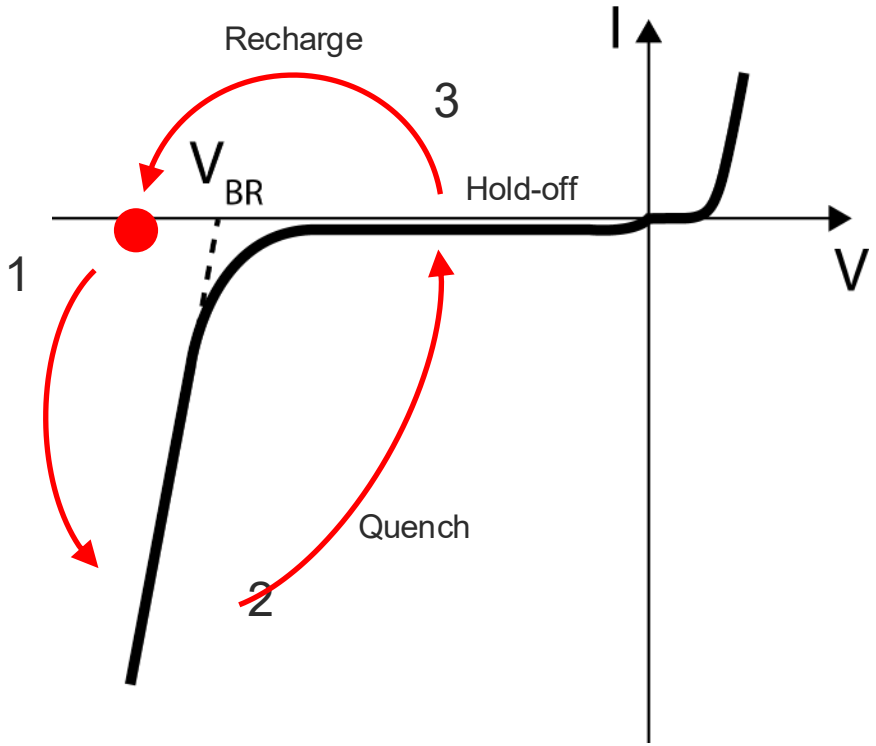

The response of the SPAD is Boolean: either **idle** or **triggered**

serge.charlebois@usherbrooke.ca

The present trend : SiPM – Silicon PhotoMultiplier

UDS

- Array of SPADs in parallel quenched passively

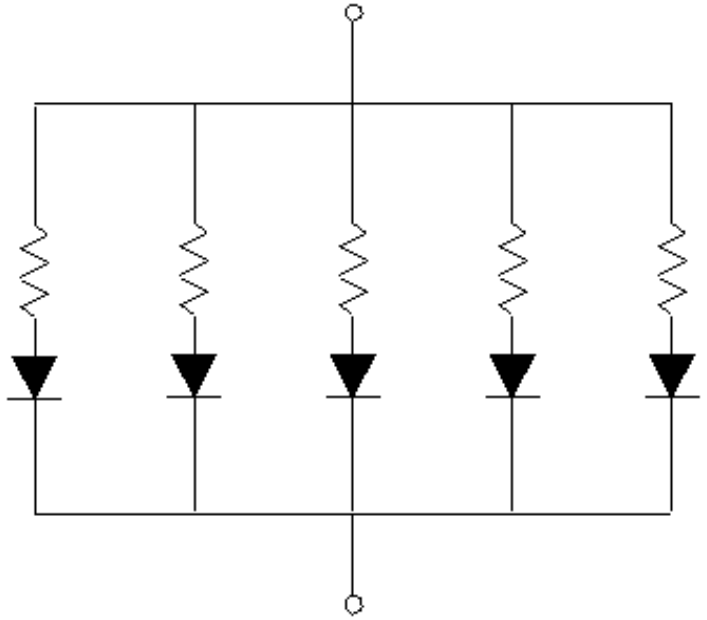

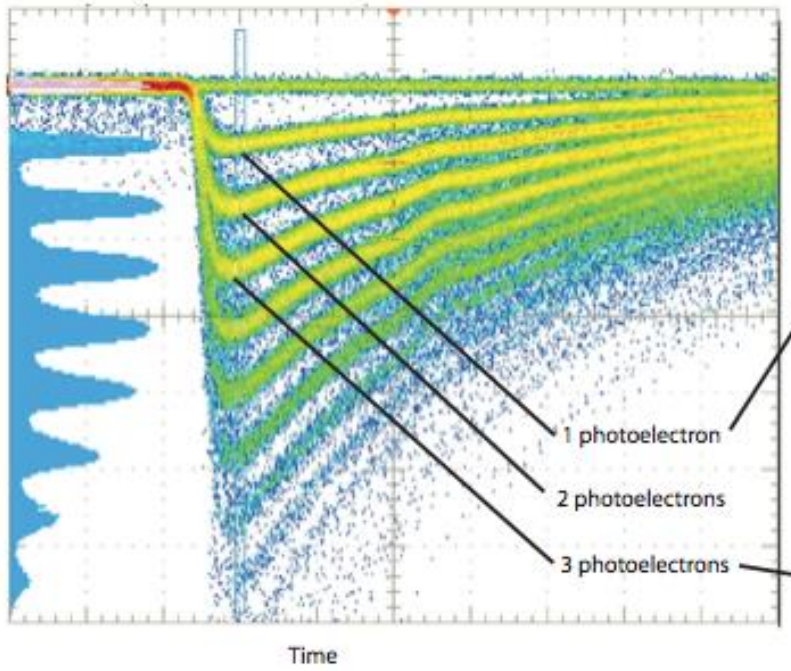

Persistence trace on an oscilloscope

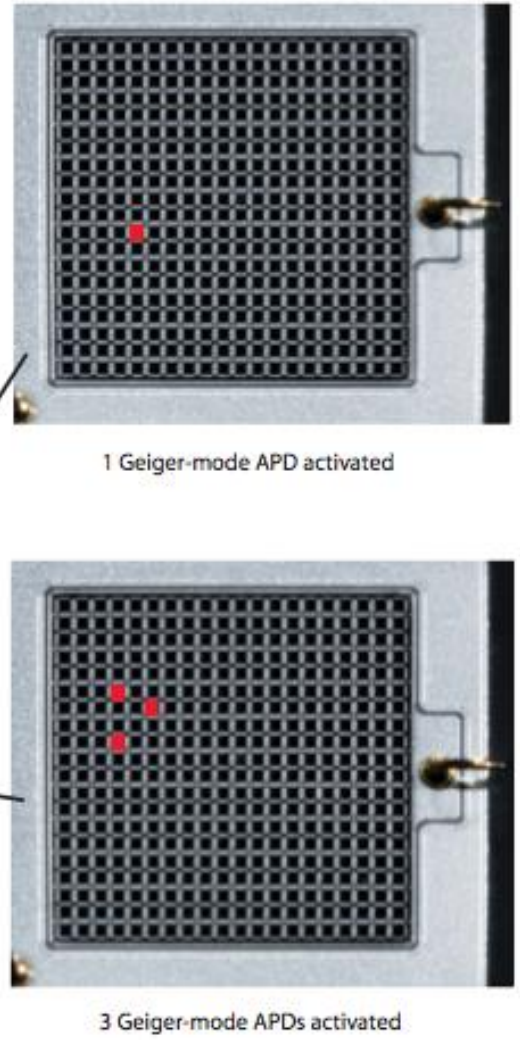

Source: Hamamatsu

SiPM – Silicon Photo Multiplier: an array of SPADs

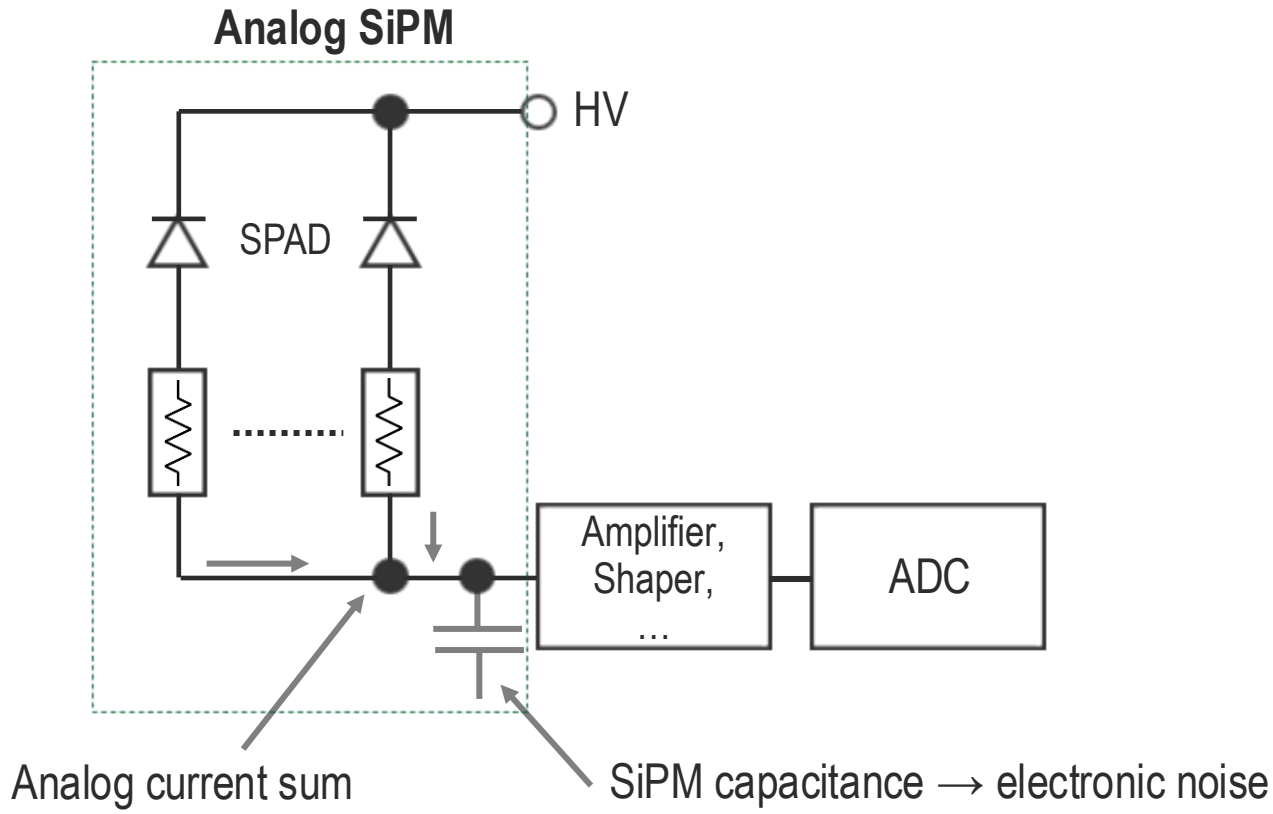

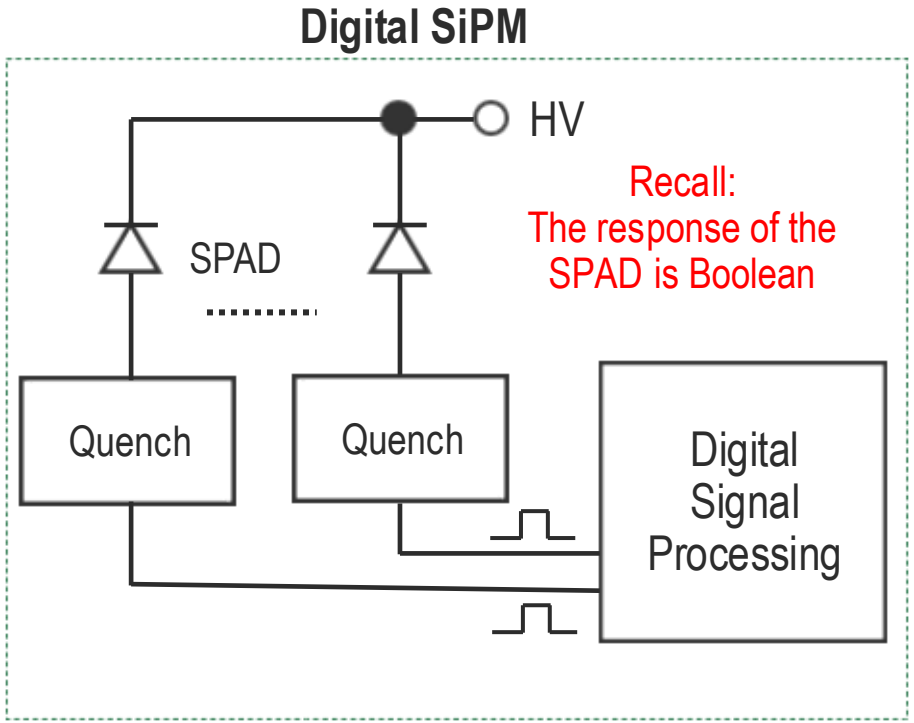

The amplifier transforms charge into voltage and then BACK to digital.

Individual SPAD readout, no D/A+A/D conversion. Everything stays digital.

Analog SiPM output

- Typical ”finger plot” from an analog SiPM

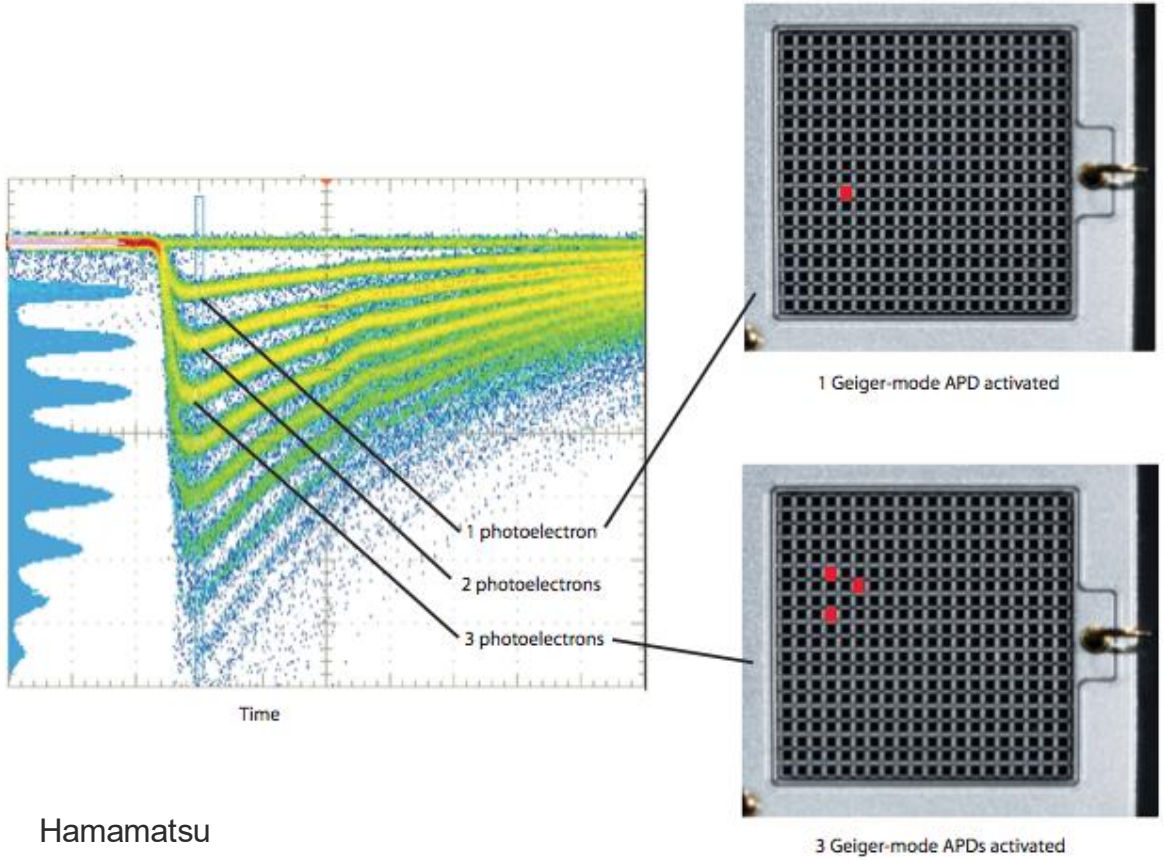

Hamamatsu

Analog monitor output

- The high uniformity of the CMOS current sources reduce dispersion and increases dynamic range even in if readout with an analog chain

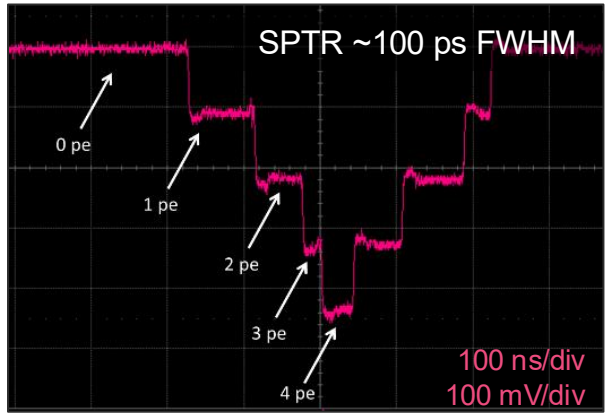

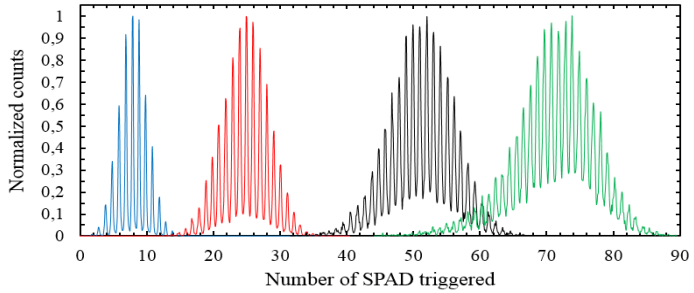

The challenge of creating large area photon counting systems

The following is a (absolutely biased) selection of approaches to building large area photon counting detection systems

My purpose is to illustrate significant trends, not to provide an exhaustive review.

Analog SiPM based

- Segmented SiPMs / mini-SiPMs / µSiPMs
  - DIGILOG
  - PET Vision
- Many groups develop good systems with COTS available SiPM and readout technologies
  - I chose not to include these

Fully digital SPAD detectors

- in **2D** with CMOS and SPAD in the same technology
  - U. Heidelberg – Peter Fischer
  - EPFL
  - I chose not to cover Philips' PDPC no longer available
- in **3D** with distinct SPAD and CMOS layers
  - EPFL
  - Photon-to-Digital Converter – U. Sherbrooke

Approach

- Less complexity in 3D-integration than fully digital
- Simple analog/digital interface
- Higher signal amplitude and good SPTR due to segmentation of the (large) SiPM chip

- Segmented SiPM with vias by FBK
- Readout of comparable size as the SiPM array
- Multi-threshold discriminator (~ADC)
- Aiming at using the prompt photons → 10 ps

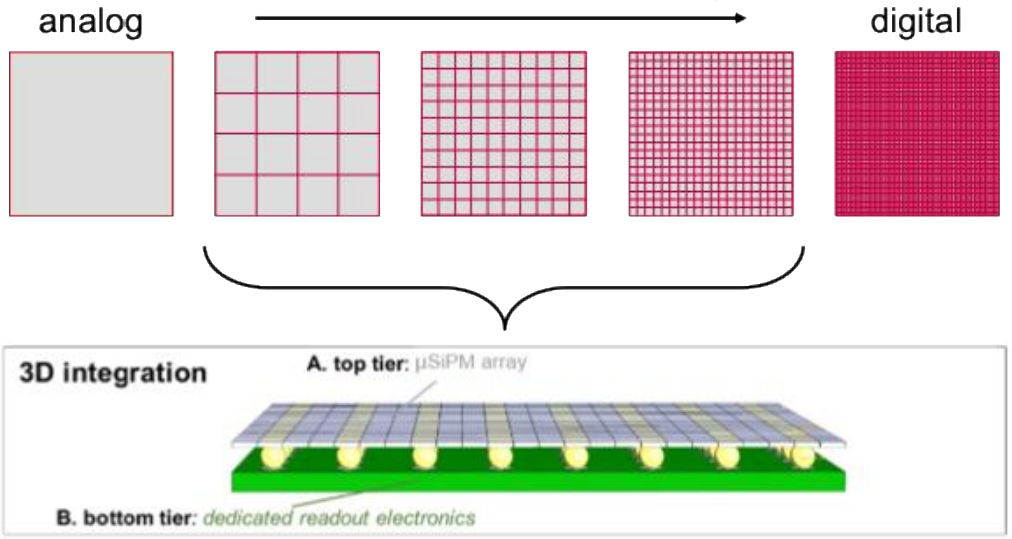

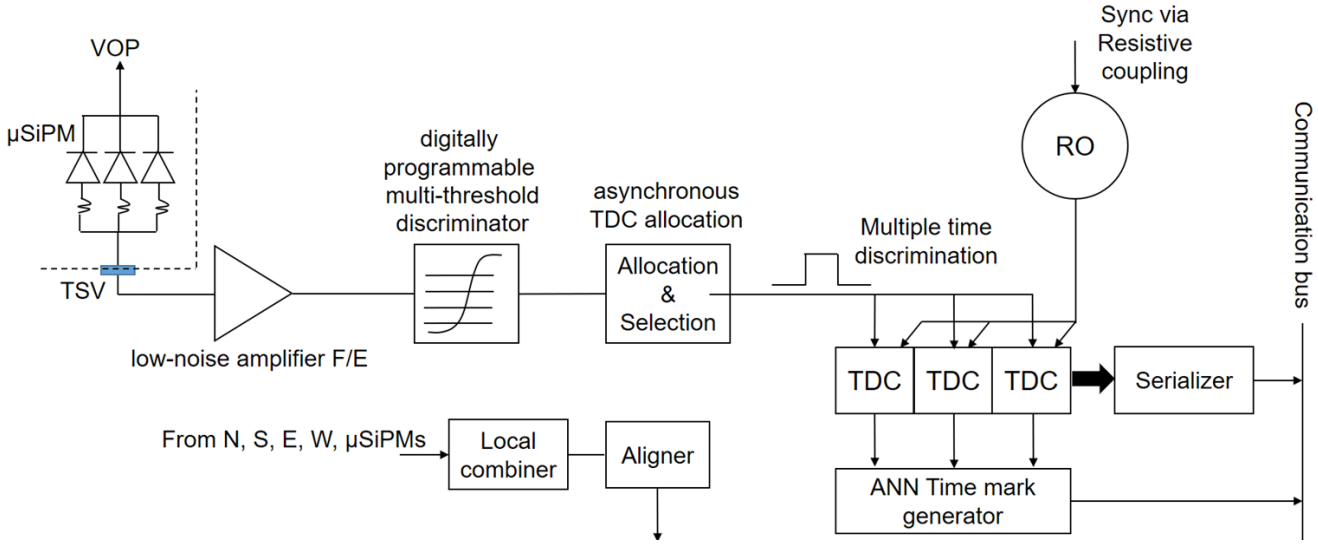

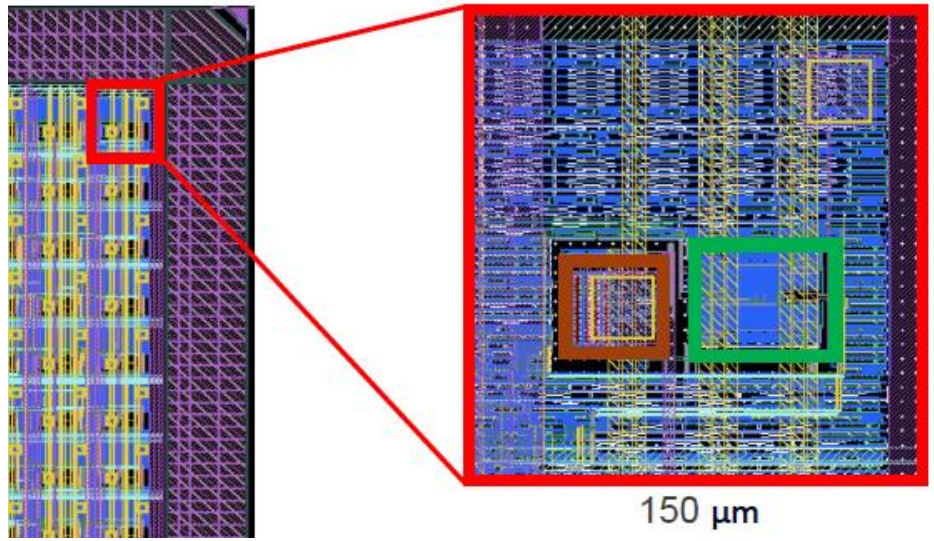

PET Vision – Barcelona / Ljubljana / MRI TUM / FBK / i3M / ONCO Vision / CERN / Yale

- Goal: Develop modules to enable a partial coverage PET scanner
- Requires exquisite timing resolution
  - At SPAD level
  - At system level also !
- 2.5D integration: small readout chip under interposer
- FastIC+ (32ch, 97 ps FWHM) with 3×3 mm^2 SiPM (50 um cell)

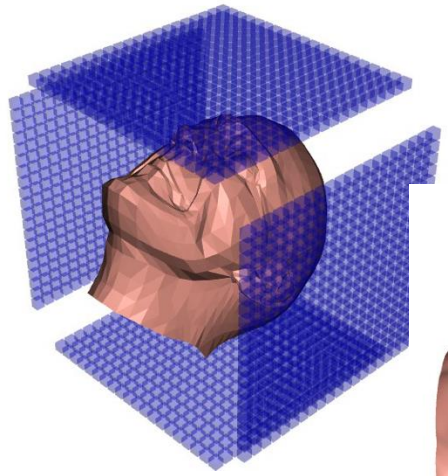

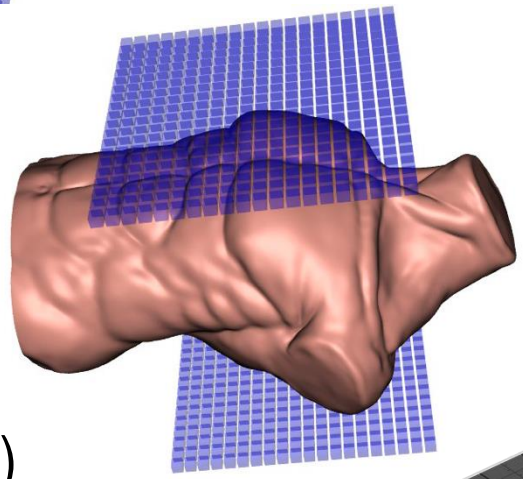

PET VISION

European nnovation Council
Funded by the European Union

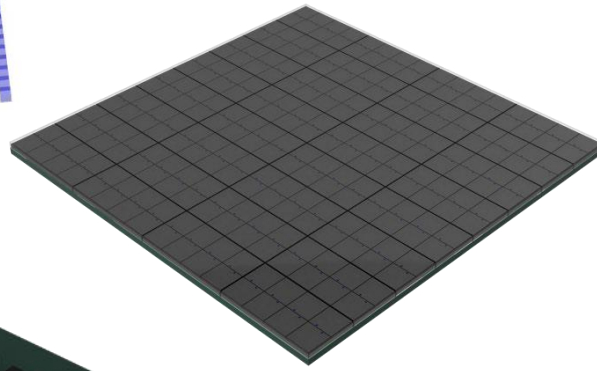

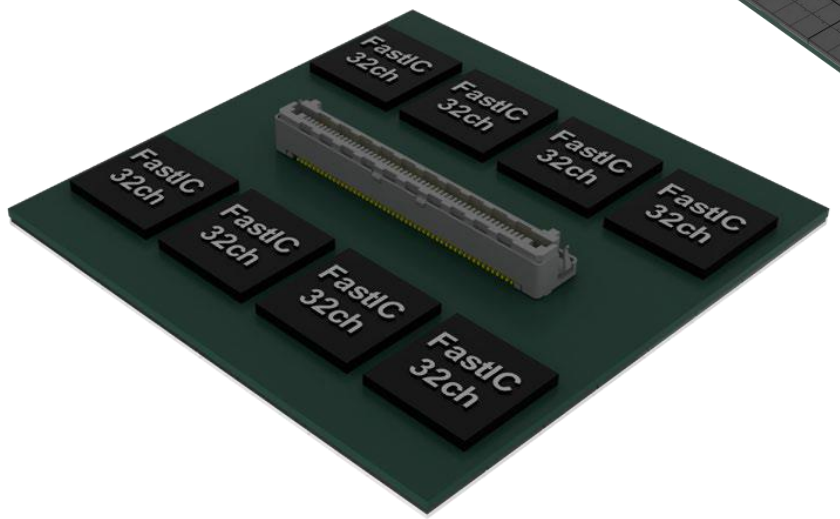

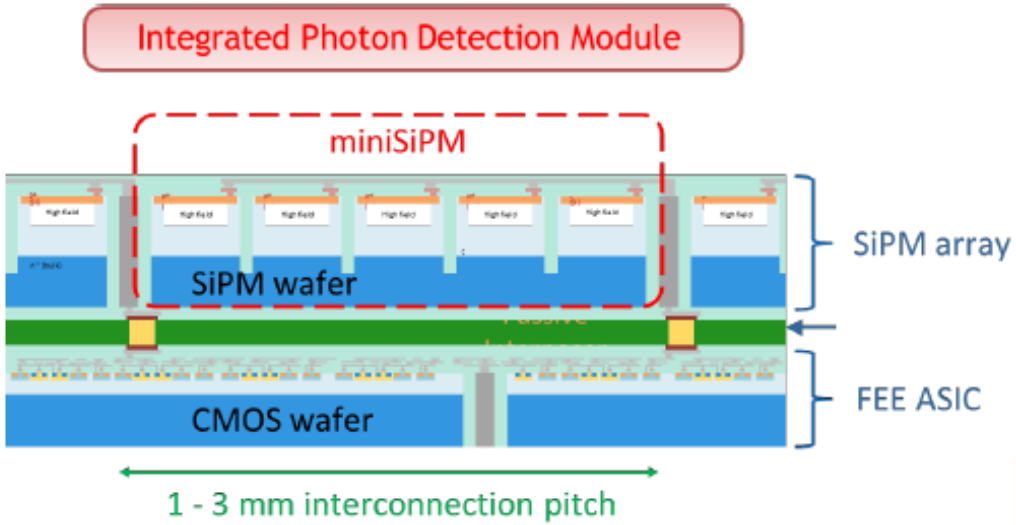

serge.charlebois@USherbrooke.ca

Fondazione Bruno Kessler – FBK

- Roadmap towards the next generation of 2.5D and 3D integrated SiPMs (2025/11)
  - Emphasizes the advantages of separated sensing and readout layers
  - Leverages a new clean-room facility for 3D integration: wafer thinning, bonding, µ-TSV

microSiPM – Segmented

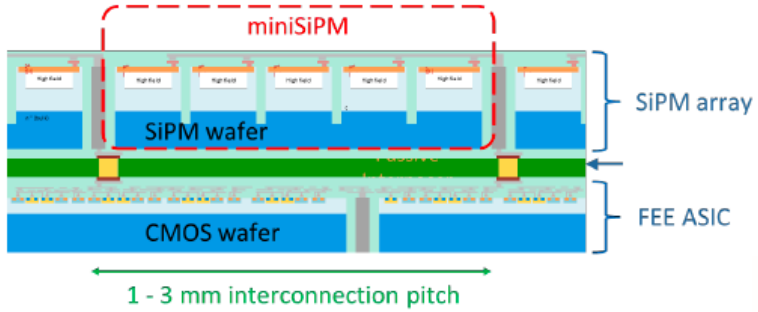

- High-density integration of small pixels (100's µm pitch)
- With 1 TSV per segment to maximize sensitive area

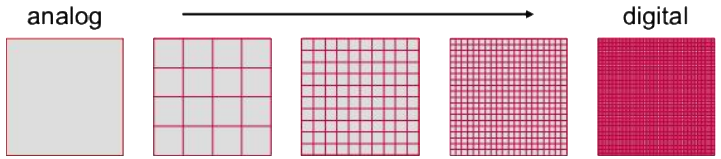

Hybrid SiPM – 3D with µ-TSV

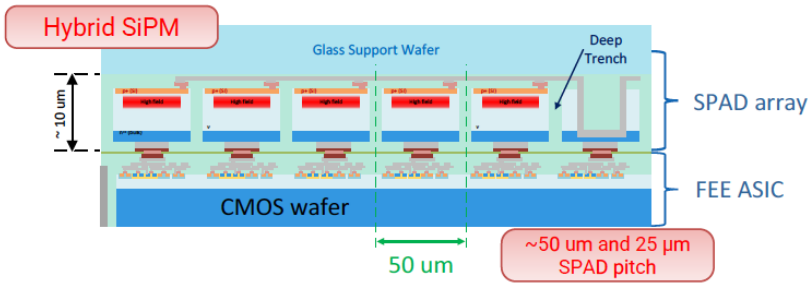

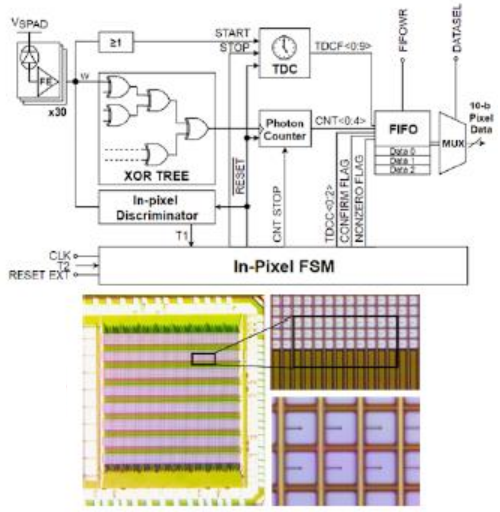

Example of dSiPM architecture developed at FBK (SBAM project)

Next-generation: BSI SiPMs

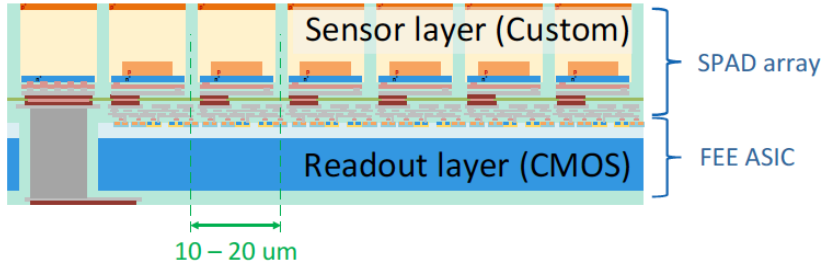

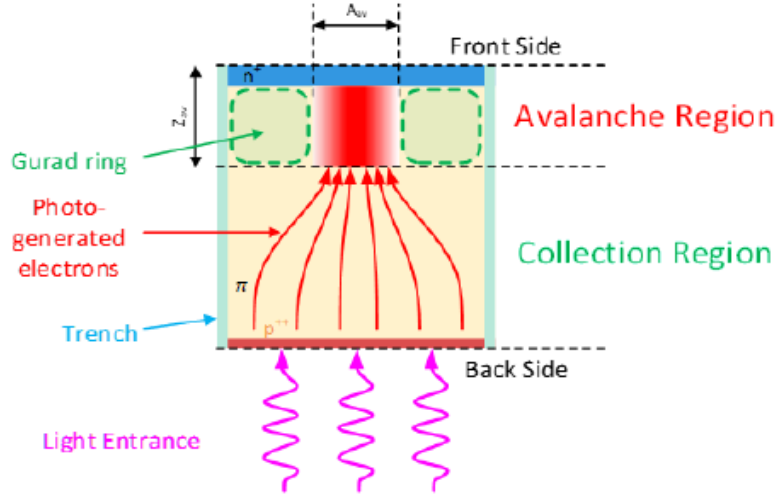

A large family of 2D Digital SiPMs – P. Fischer, U. Heidelberg

RUPRECHT-KARLS-
UNIVERSITÄT
HEIDELBERG

- Based on IMS (Duisburg) SPAD and CMOS
- Also did imagers (2015), time-of-flight camera…

Readout large scintillating fiber arrays

- For a Scintillating Fibre Tracker of LHCb
- Programmatically groups SPADs into channels
- Eases fiber alignment constraints for large systems
- Manageable integration density outside the tracker

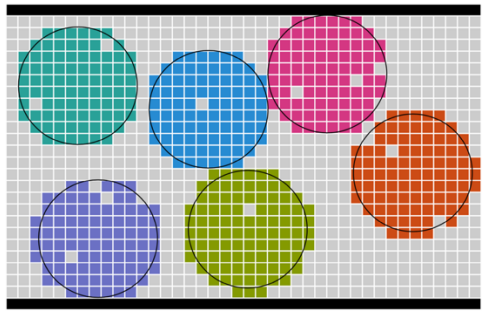

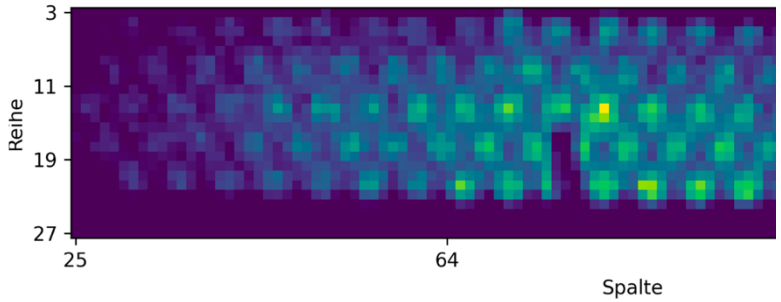

DARWIN – Dark Matter using LXe

- ~ 8×9 mm2, 32×30 pixels of 9 SPADs
- Fill factor ~72%
- Only 4 logical signals
- Daisy chain readout for modules

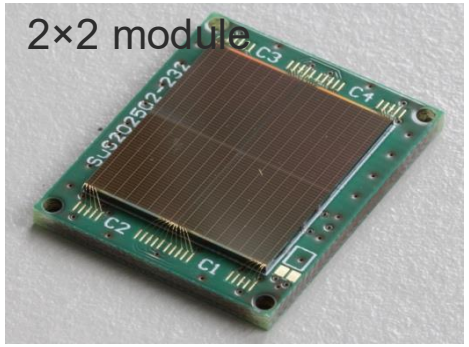

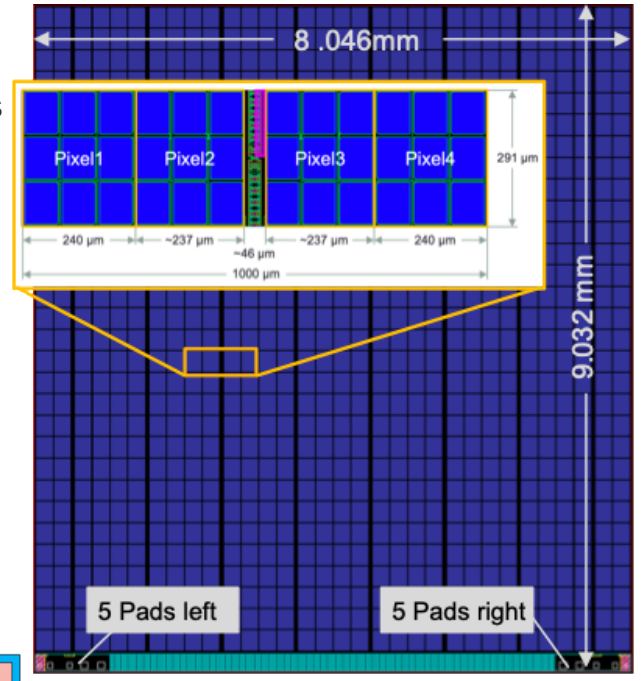

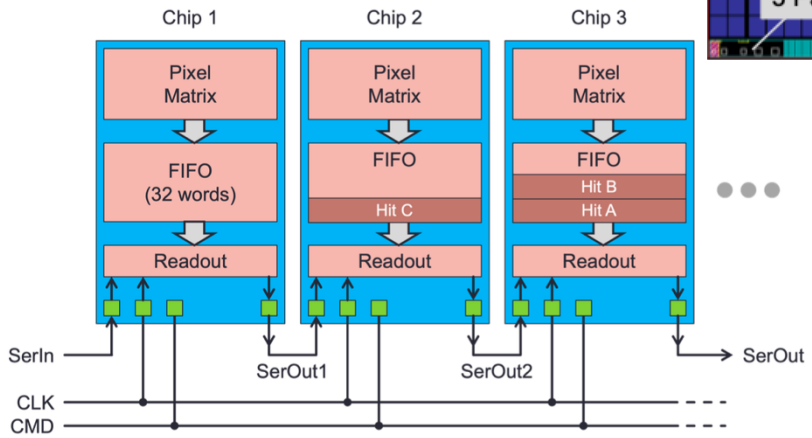

3D-stacked frontside-illuminated (FSI) multi-channel digital silicon photomultipliers (MD-SiPM) at EPFL

- Top- and bottom-tier in 0.18 µm CMOS technology
- 3D integration: Through-silicon vias (TSVs) and bump-bonds

- Top-tier: FSI SPADs
  - 50 µm pitch, 67% fill factor
  - 2x arrays 64x64 SPADs (8x8 cluster of 64 pixels)
  - Vbr: 22 V
  - peak PDP: 55% at 500 nm at Vov = 6 V

- Bottom-tier: readout electronics
  - SPAD address tree
  - photon counters
  - time-to-digital converters + calibration
  - data distribution
  - readout scheduler

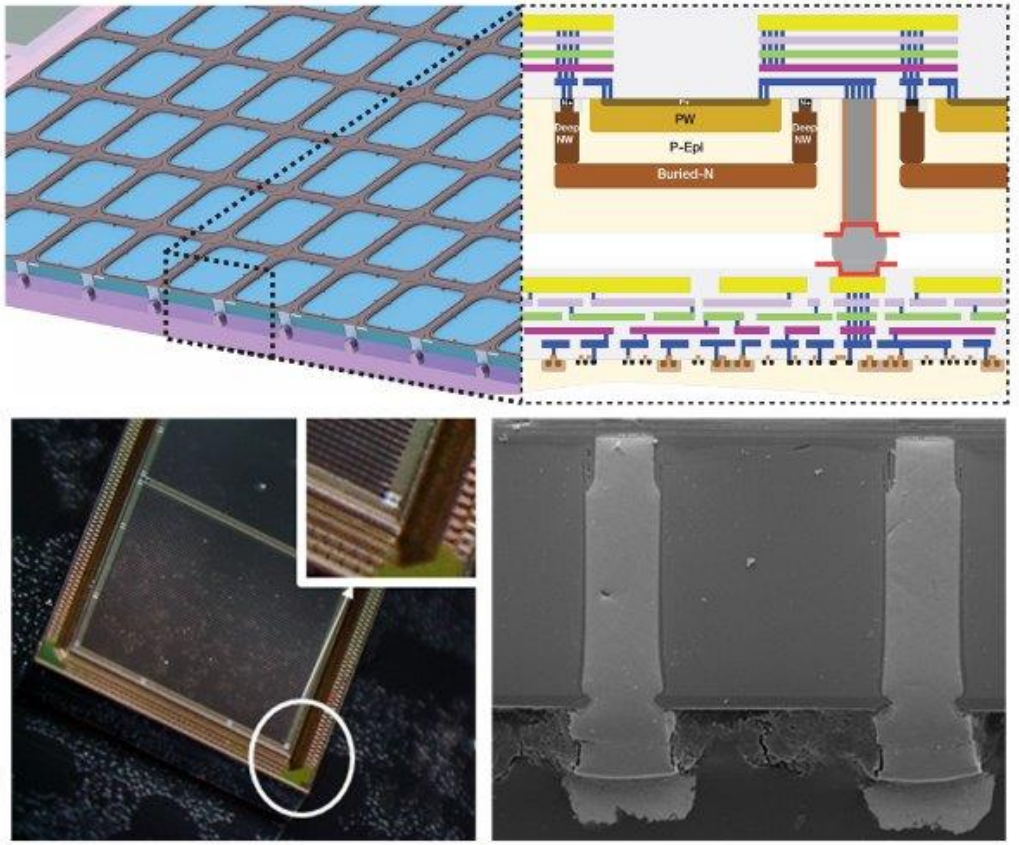

Fig. 1. *Top:* the top tier houses square SPADs with rounded corners and is 3D-stacked to the bottom-tier chip (*left*). The bonding with the bottom-tier chip is ensured through TSVs and micro-bump connections (*right*). *Bottom:* Optical microscope image of the final implementation *(left);* SEM image of the cross section (*right*).

[14] Gramuglia, Francesco, et al. "CMOS 3D-Stacked FSI Multi-Channel Digital SiPM for Time-of-Flight Vision Applications." 2021 International Image Sensor Workshop (IISW). No. CONF. International Image Sensors Society, 2021.

# of power consumption

- An **analog readout chain** consumption increases with SiPM capacity (area), timing resolution needed
  - Can power scaling laws guide us
- A **fully digital chain** already includes ADC, TDC, and data transmission

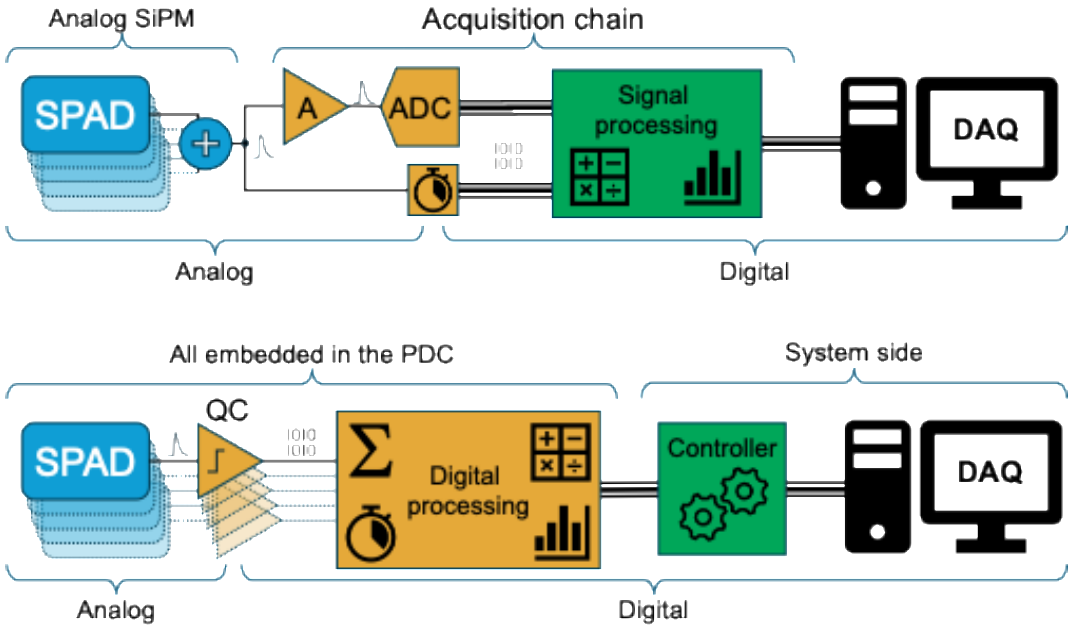

# of fabrication cost

- Interesting scaling of cost analysis by FBK (2024)
- Base simple and reasonable assumptions
- In need of data

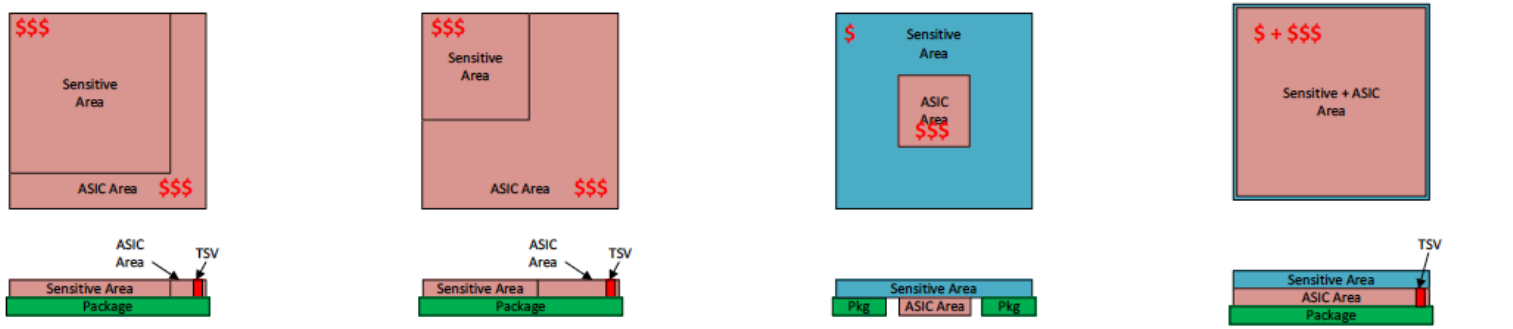

Fully CMOS – large pitch:
- Only CMOS
- TSV needed

Fully CMOS – small pitch:
- Only CMOS
- TSV needed.

Hybrid – large pitch:
- Custom sensor
- CMOS readout ASIC
- Chip-to-wafer bonding

Hybrid – full 3D – small pitch:
- Custom sensor
- CMOS readout ASIC
- Wafer to wafer bonding

FONDAZIONE BRUNO KESSLER
FUTURE BUILT ON KNOWLEDGE

Cost Estimation
Very preliminary comparison of different approaches

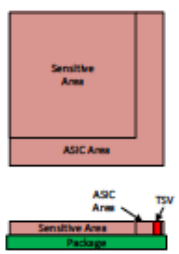

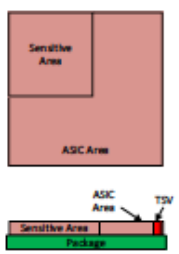

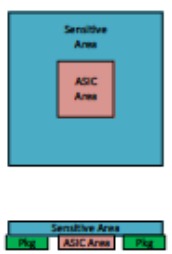

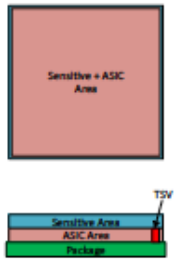

\	CMOS – large pitch	CMOS – small pitch	Hybrid – large pitch	Hybrid – small pitch
Detection Efficiency	Medium	Low	High	High
Pitch	Large	Small	Large	Small
Silicon Cost	$C_T = C_{CMOS}$	$C_T = C_{CMOS}$	$C_T = 0.35\ C_{CMOS}$	$C_T = 1.25\ C_{CMOS}$
TSV	Yes	Yes	No	Yes
3D Integration cost	0	0	TBD (chip to wafer)	TBD (wafer level) Depends on pitch
Packaging	Normal	Normal	More complex	Normal
Notes	Poor performance? Radiation hardness?	Poor performance? Radiation hardness?	Signal integrity? Package complexity?	Highest performance? Need for single cell?

Probably, a more detailed study is needed to select the best option based on the experiment specifications.

https://agenda.infn.it/event/47073/contributions/273095/

Optimization of power consumption – A trivial scaling model

- Power of a TIA scales with the SiPM capacitance

$$P \propto [C_{SiPM} + C_{in}]^2$$

where C_{in} is TIA input capacitance

- By segmenting power can be reduced

$$P(N_{seg}) \propto N_{seg} \left[\frac{C_{SiPM}}{N_{seg}} + C_{in}\right]^2$$

- We should add : ADC × N_{seg}

Where is the minimum located…?

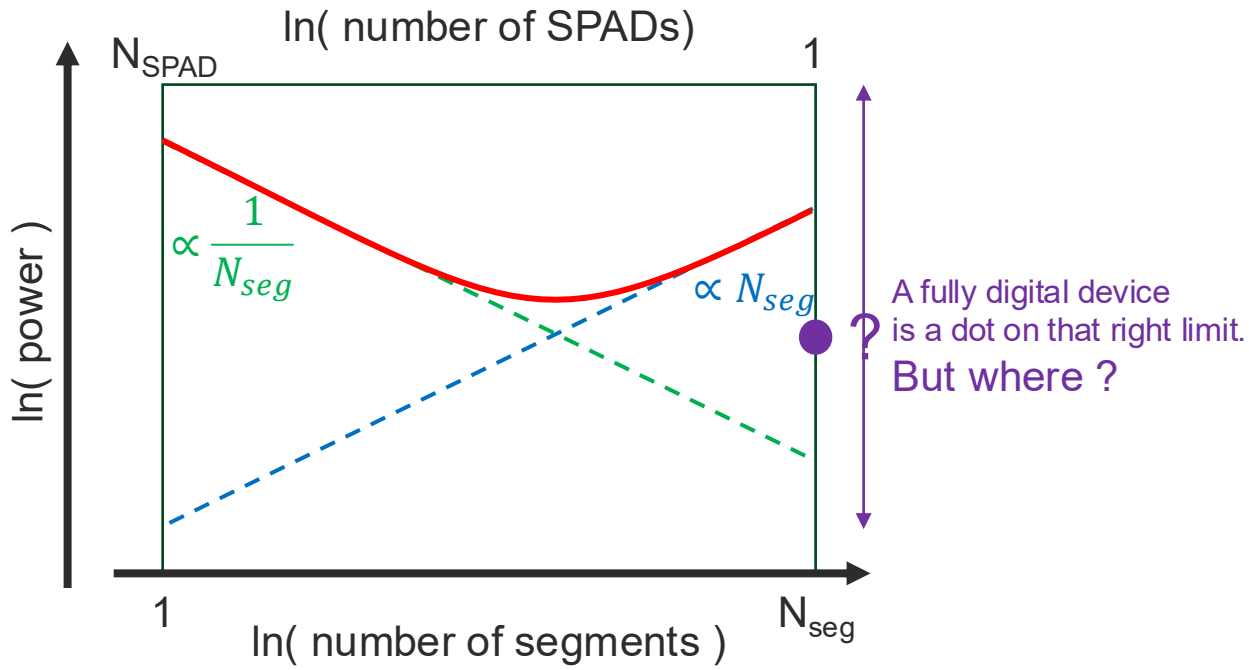

- It assumes the readout architecture will be kept the same as the SiPM segment reduces
  - Designers will find clever ways to optimize the design
    - Ex. ADC resolution can be reduced with the size of the segment (less SPADs!)

So why not start at the single SPAD to readout coupling with maximal information quality ?

Custom SPAD array fabricated by Teledyne

- 64 × 64 SPADs – 78 × 78 µm^2
- Active area 5 × 5 mm^2
- 26% fill-factor

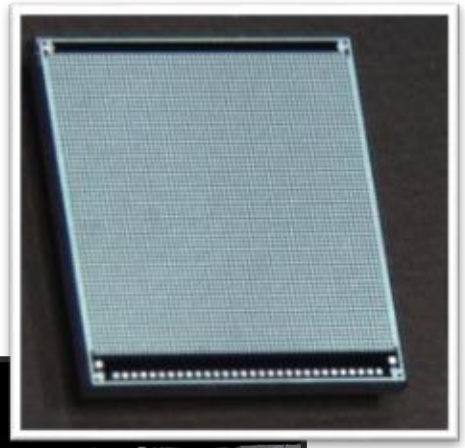

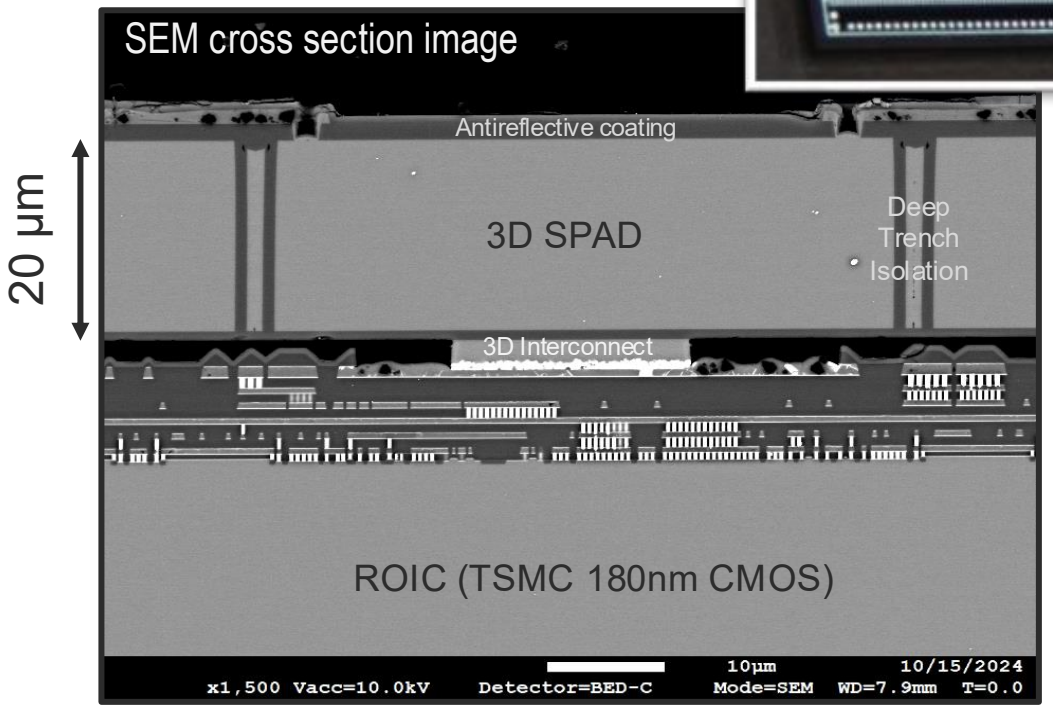

3D integrated over two readout flavors

- Low power for large area systems
  - Digital sum of 5 × 5 mm^2 pixel
  - Timing precision <200 ps FWHM on 1st photon

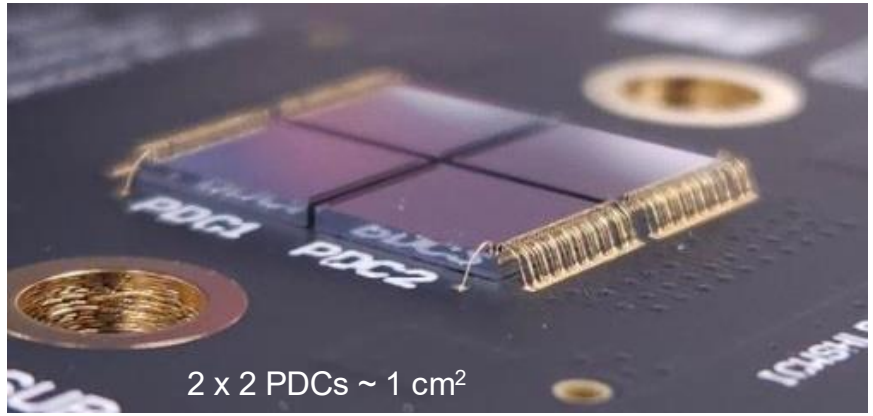

- Timing-optimized (TSMC 65nm)
  - Time stamping of each photon
  - Advanced embedded processing within 16 sectors
    - on timestamps
    - on photon count

serge.charlebois@USherbrooke.ca

Photon-to-Digital Converters - 3D versus 2D

2D

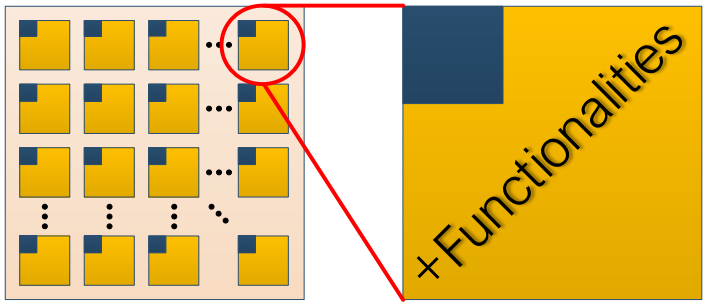

or

= SPAD layer

= CMOS electronics layer

The solution:

3D vertical integration

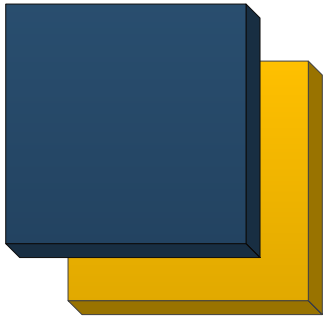

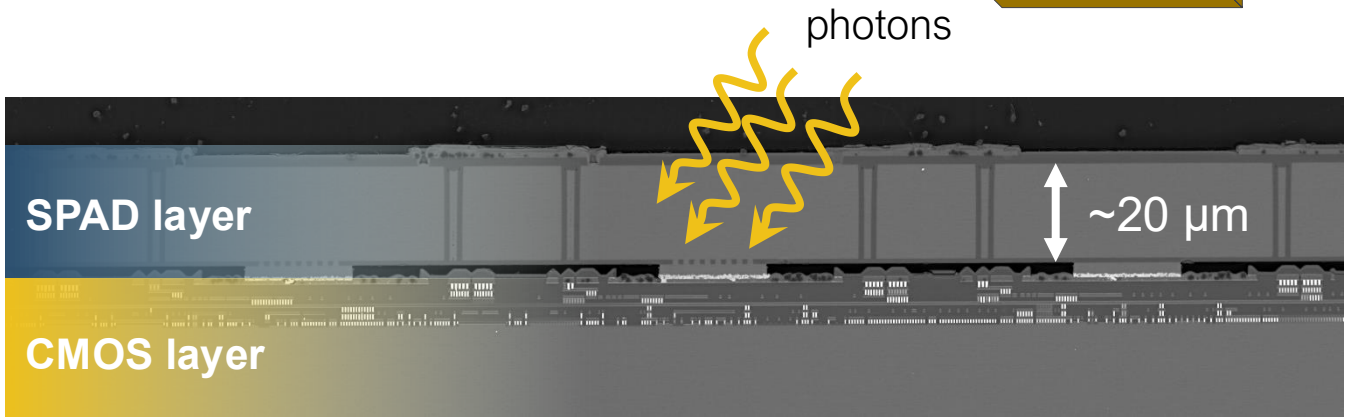

- Enables high photosensitive fill factor
  with
- Advanced digital processing
- Choice of SPAD optimal technology
  with
- Choice of CMOS optimal technology for application specific functions

Pratte JF et al. "3D Photon-to-Digital Converter for Radiation Instrumentation: Motivation and Future Works" (2021) Sensors;21(2):598. 10.3390/s21020598

3D PDC – SPAD array specifications and properties

- 64 × 64 SPADs
  - Active area 5 × 5 mm^2 (chip 5.35 × 5.85 mm^2)
  - 78 µm pitch
  - 26% fill-factor → to ~60% soon
- PDP ~50% @ 410 nm (PDE 13%)
- Single Photon Timing Resolution ~160 ps @ 410 nm
- Dark count rate ~30 cps/SPAD, <0.03 cps/$µm^2$
- Correlated noise
  - Hold off configurable (typical ~ 200 ns per SPAD)
  - Afterpulsing < 10% above 150 ns (90% array)
  - Crosstalk ~ 10%

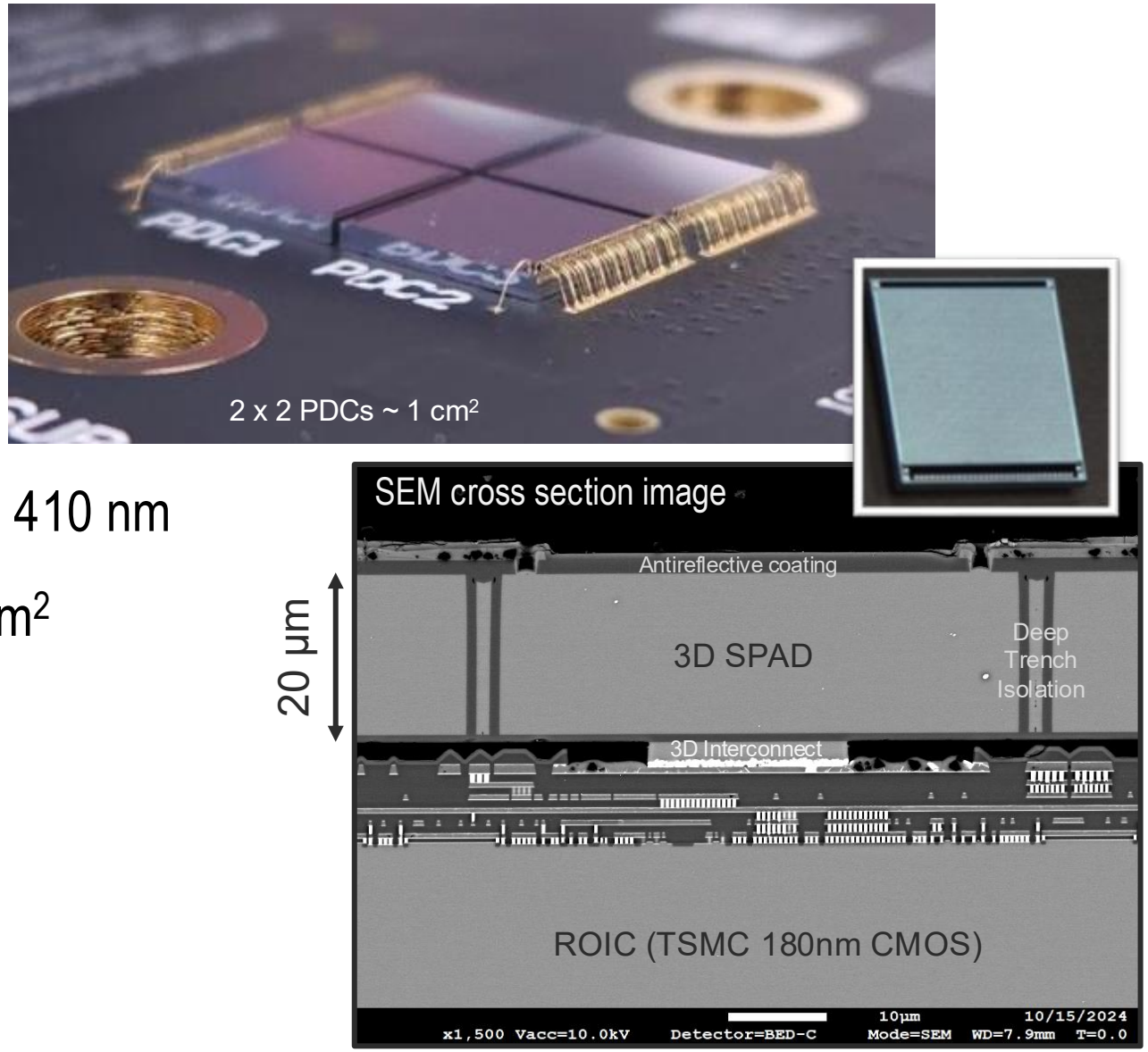

Photon-to-Digital Converter: Architecture

New article submitted

UDS

Flag output

- Pulsed output (adjustable 2 ns to 60 ns).
- From a global OR-tree.
- Flag timing jitter (<100 ps RMS)

Digital Sum

- Digital count of triggered SPADs inside a time bin (dynamic range of 4096 SPADs).
- Adjustable bin width (10 ns to µs)
- Internal FIFO of 128 bins.

Analog Monitor

- Current proportional to the number of triggered SPADs.

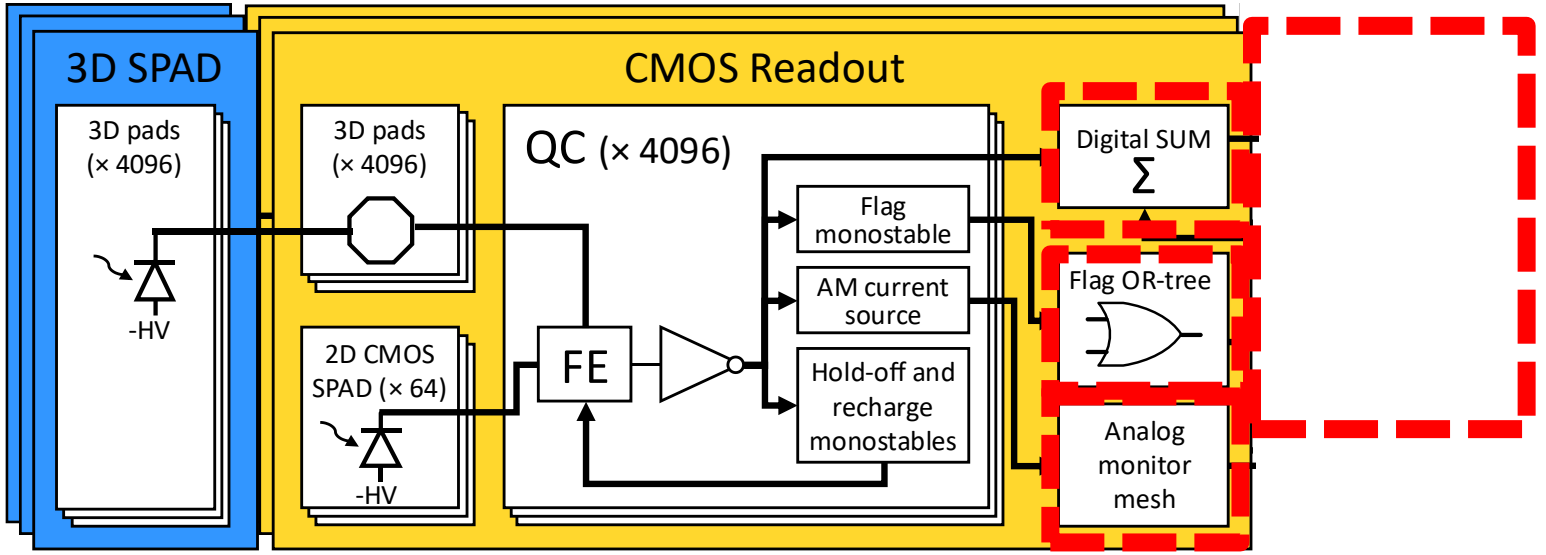

×64 PDCs/Controller

Controller (1 for 64 PDCs)

- Start PDC acquisition, based on the number of flag received to discriminate dark count.
- Bank of TDCs for timing measurements on flags.
- Receives data from PDCs and includes post-processing.
- Communicate with an external computer.

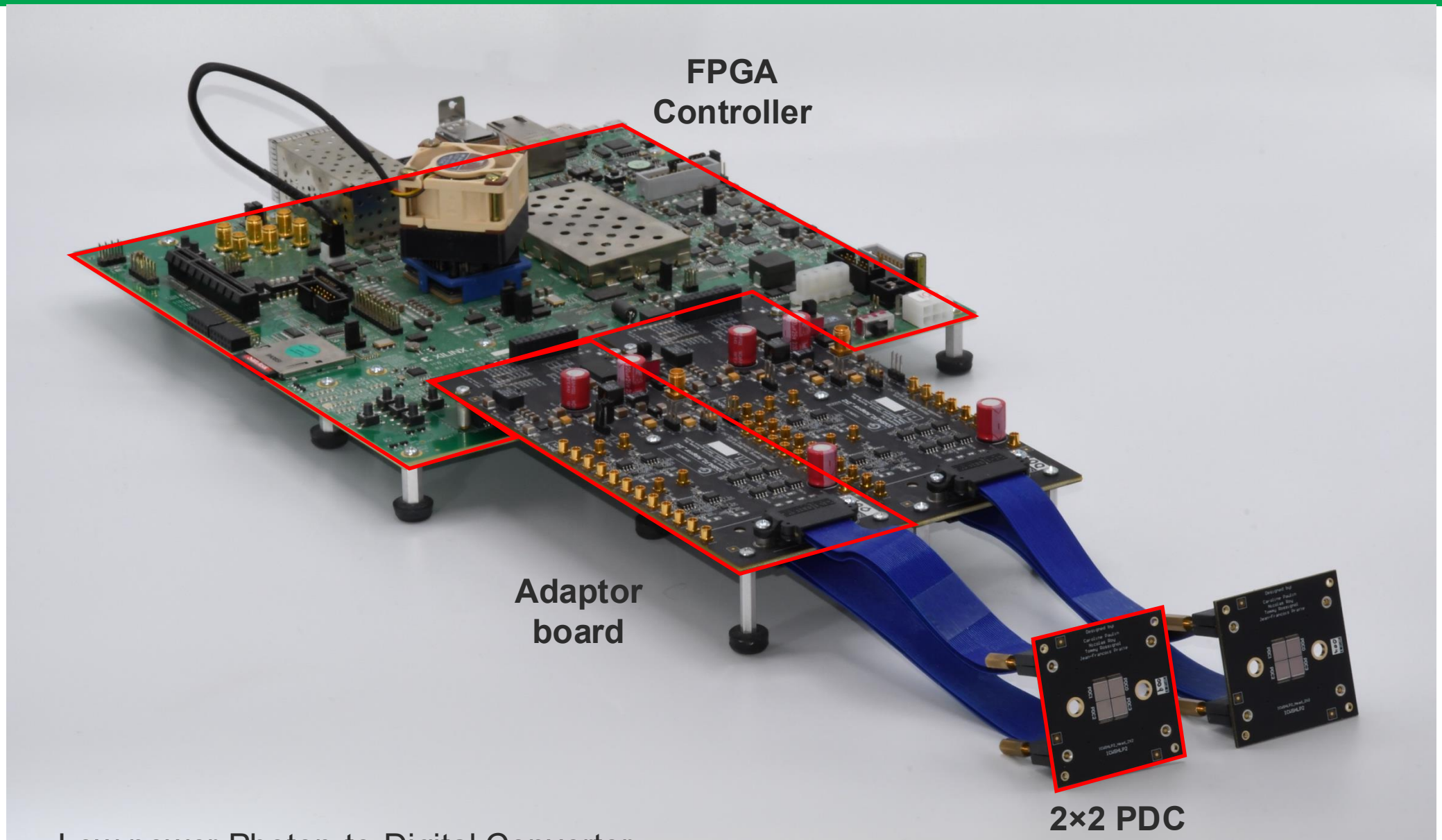

Low power Photon-to-Digital Converter

For details, see T. Rossignol et al., J. Inst., vol. 19, no. 09, p. P09017, Sep. 2024
https://doi.org/10.1088/1748-0221/19/09/P09017

serge.charlebois@USherbrooke.ca

Large PDC Tile Development

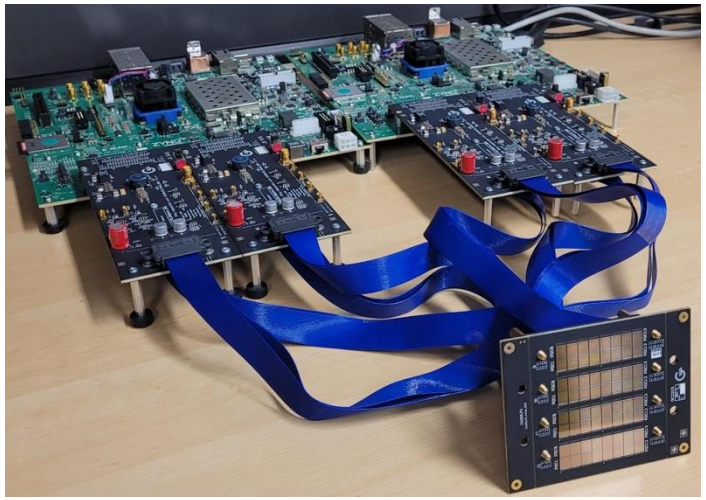

Present setup

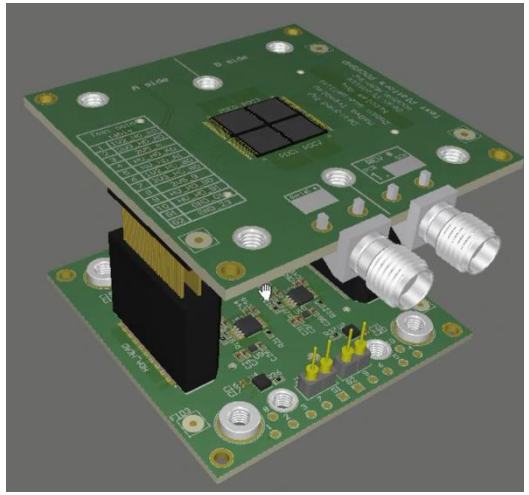

Next phase

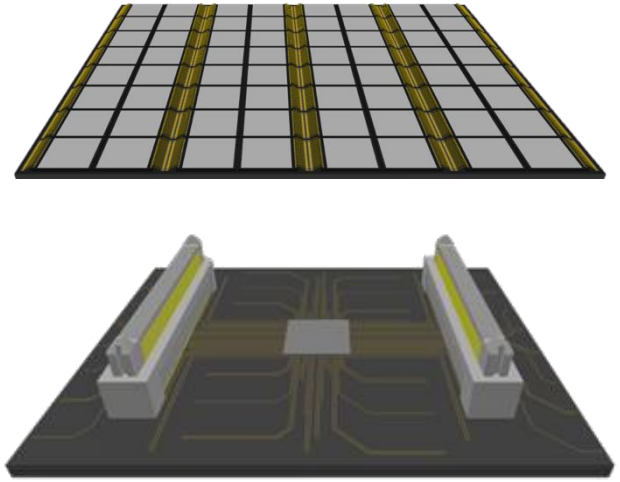

ASIC controller

- Developed mainly using CMOS only PDCs
  - Provide exactly the same signals (but with less SPADs and light sensitivity)
  - Cost effective for assembly learning curve
  - Swapping for PDC is straightforward
- Designing a dedicated more compact FPGA platform
- First step toward an ASIC controller

Supported by

OAK RIDGE National Laboratory

serge.charlebois@USherbrooke.ca

Energy reconstruction of PDC – Future Improvement

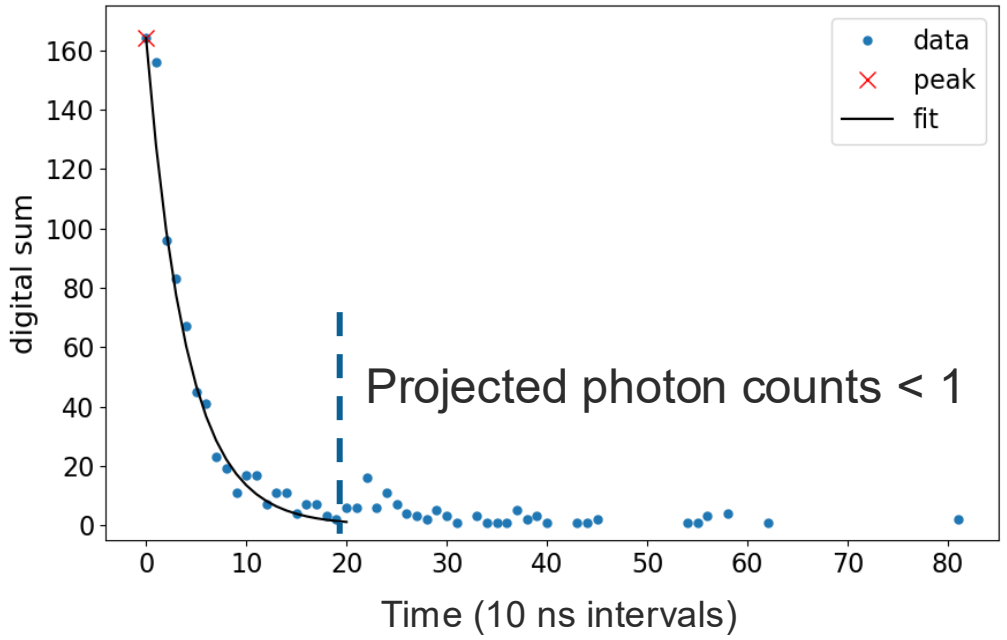

New article coming comparing measurements between PDC and SiPM

Energy Calculation per Event:
Could fit the projected decay of LYSO (40 ns) => Digital Shaping?

Can optimize parameters to choose proper summation range.

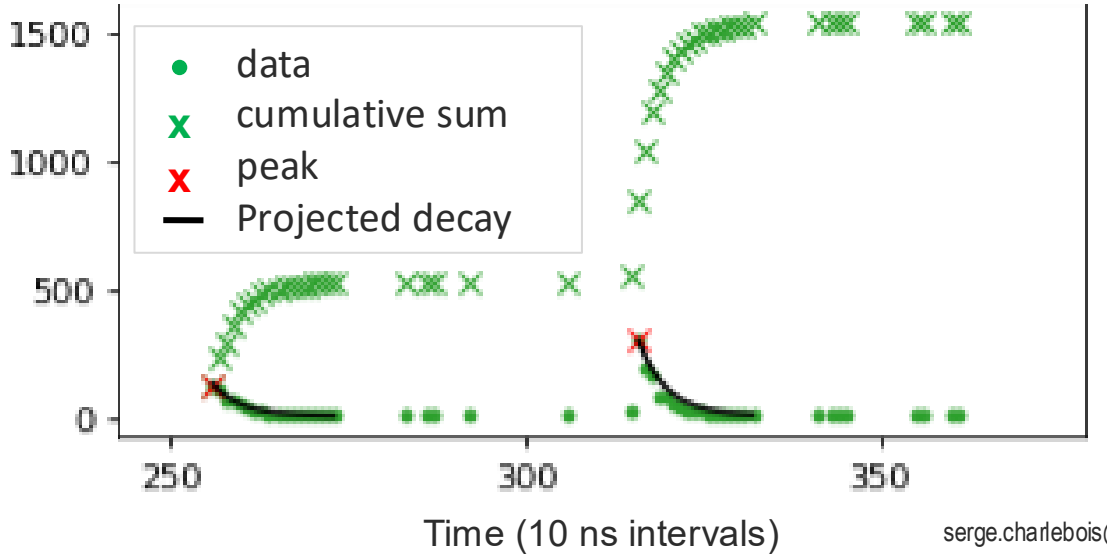

Helps separating pile-ups (2 events in same acquisition).
Easier processing than in the the analog domain, accessible early in the readout chain.

Data reduction from 0 suppression in the digital sum.

Distinguishing between close decay rates

- Phoswich assembly
  - Two LGSO 3×3×3 mm^3 cristal scintillators
  - Coupled with optical epoxy (NOA-83-H)
  - Emission wavelength: 420 – 480 nm
- Radiation source: Ge68, positron emitter → 511 keV peak

LYSO cristals	Fast – Top	Slow - Bottom
Decay time (ns)	32	45
Light Yield (ph.e/MeV)	35 000	40 000

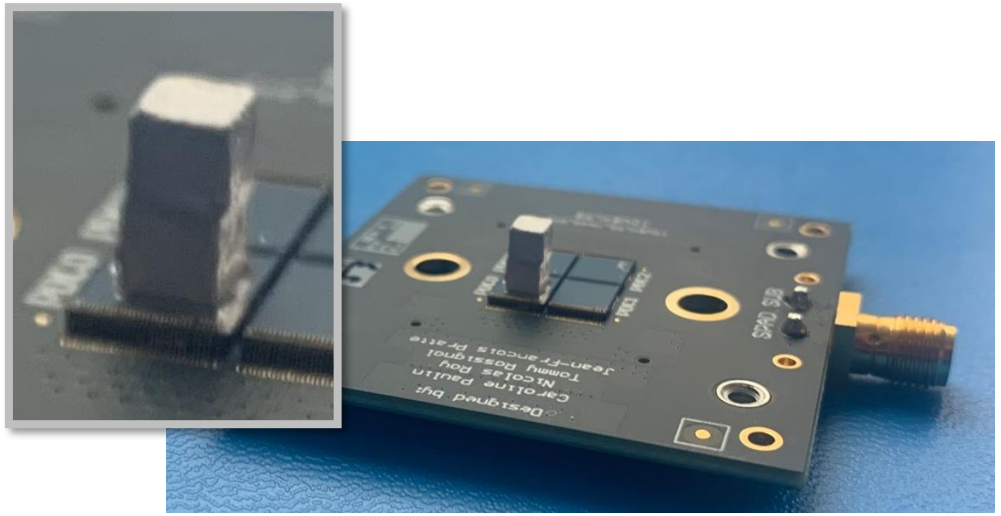

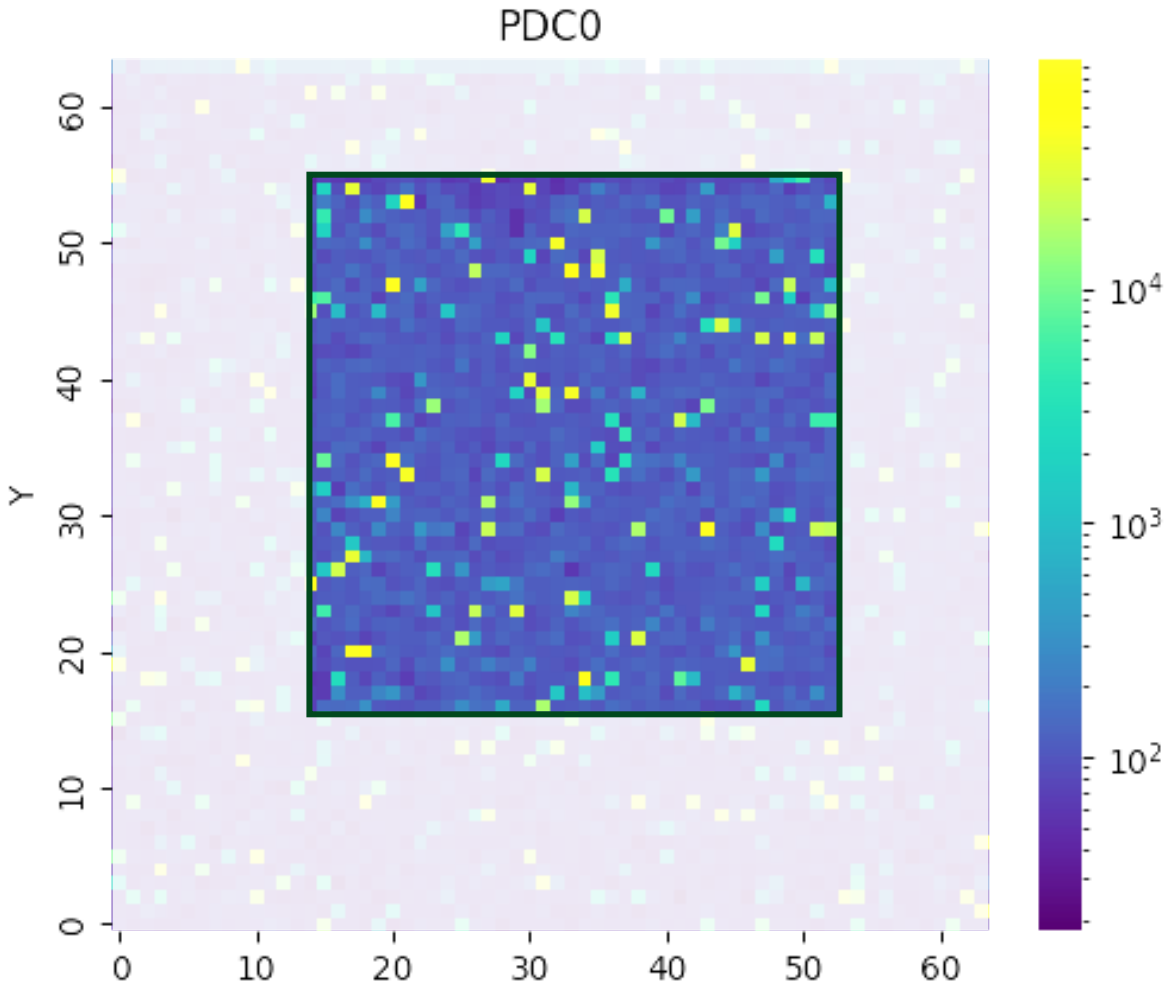

SPAD count rate with radiation source revealing the footprint of the scintillator.

SPADs around the cristal are turned off for measurements.

serge.charlebois@USherbrooke.ca

Energy and Pulse Shape Spectra with Ge68

- Pulse Shape Discrimination ratio
  - Proxy for the decay rate measurement
  - Ratio of early photon count (3 bins around peak) over the total photons count of an event

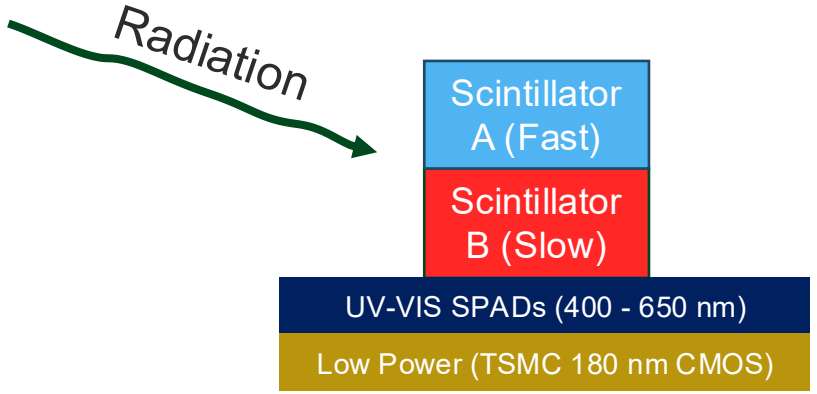

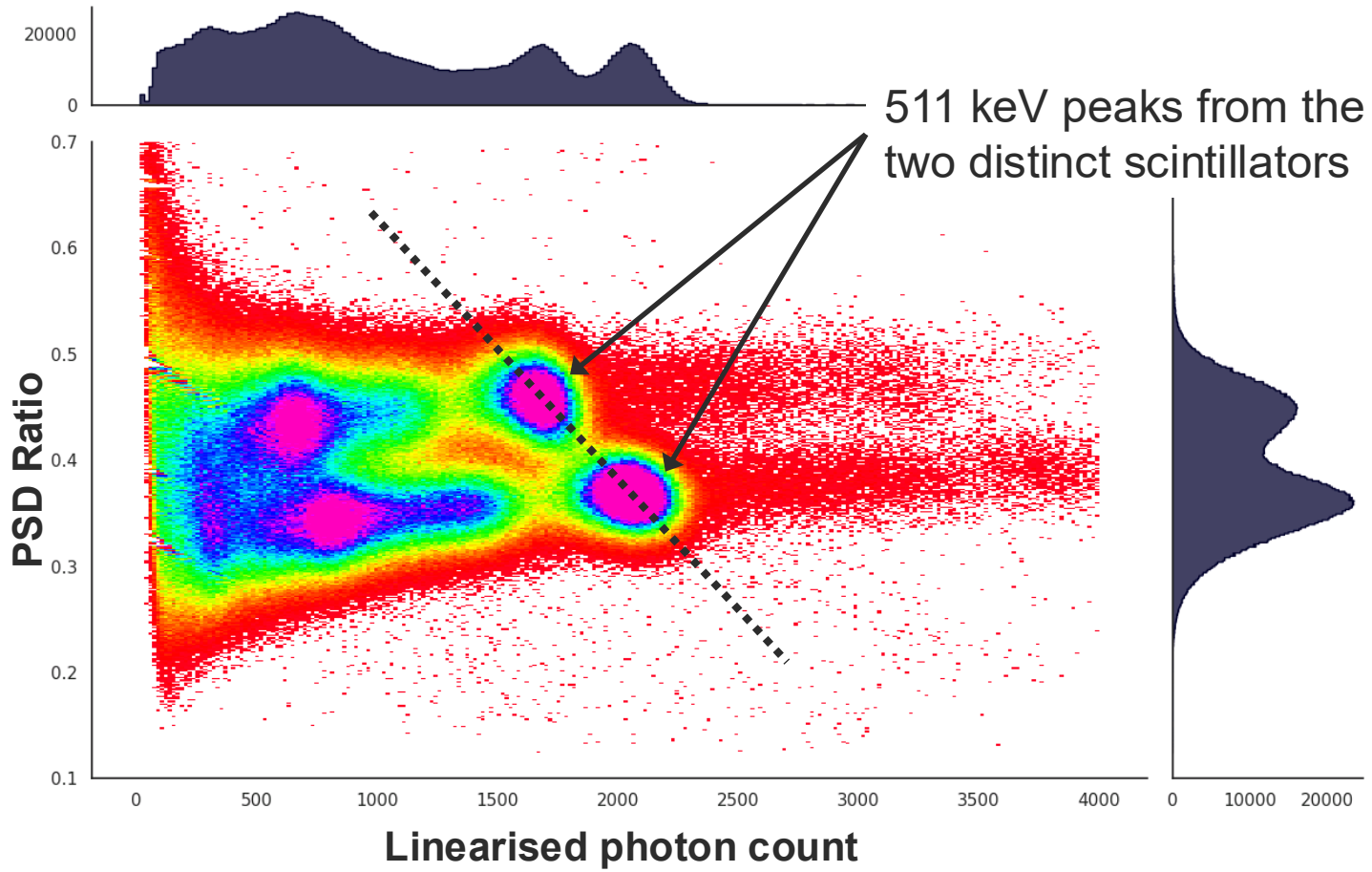

A basis change through the photopeaks allows for good classification

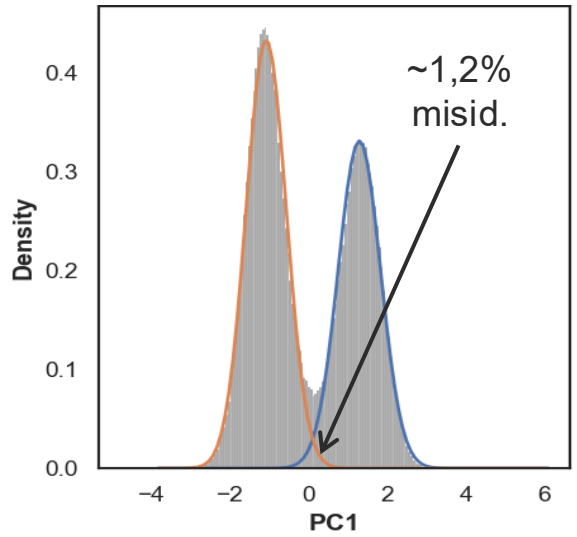

Detecting particles

How many electron-hole pairs can particles create?

- Below 5 eV photons produce: it seems to be 1 pair/photon
- Above 5 eV photons: clearly > 1 pair/photon
  - Even seems to follow approximately the 3.7 eV/pair scaling
- 3.6-3.7 eV/pair for silicon

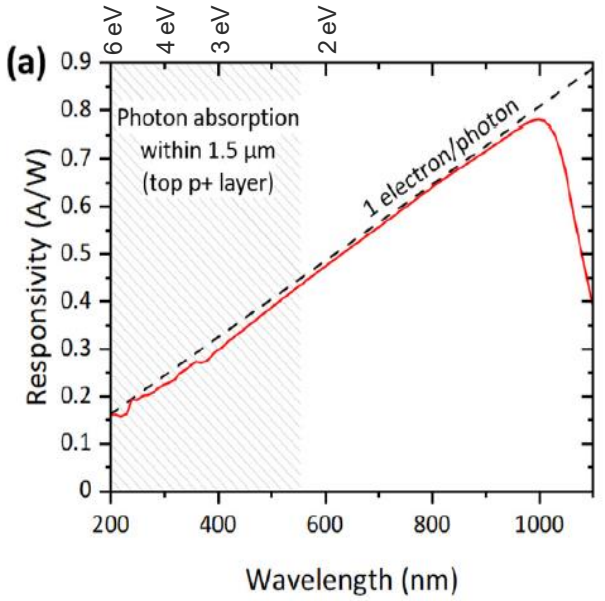

Setälä et al. ACS Photonics 2023, 10, 6, 1735–1741

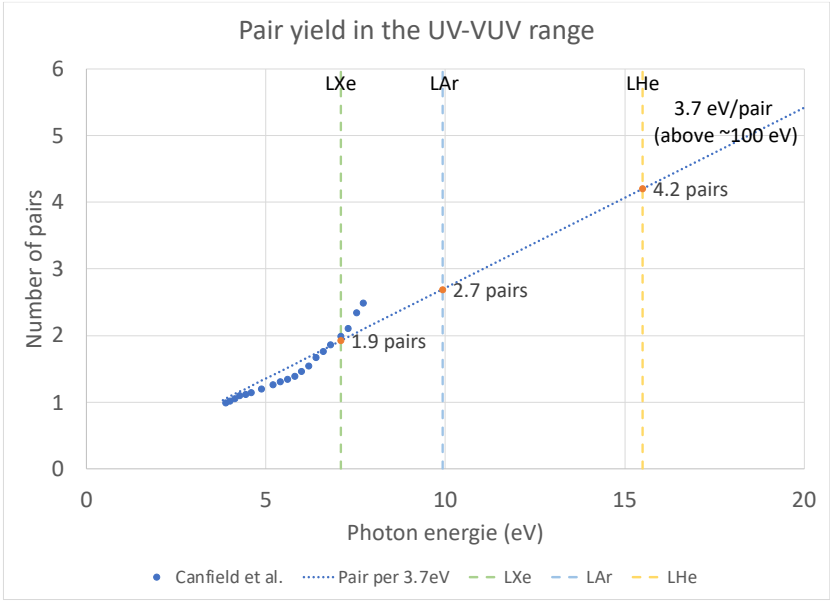

Data from L. Canfield, Metrologia, vol. 35, no. 4, p. 329, 1998

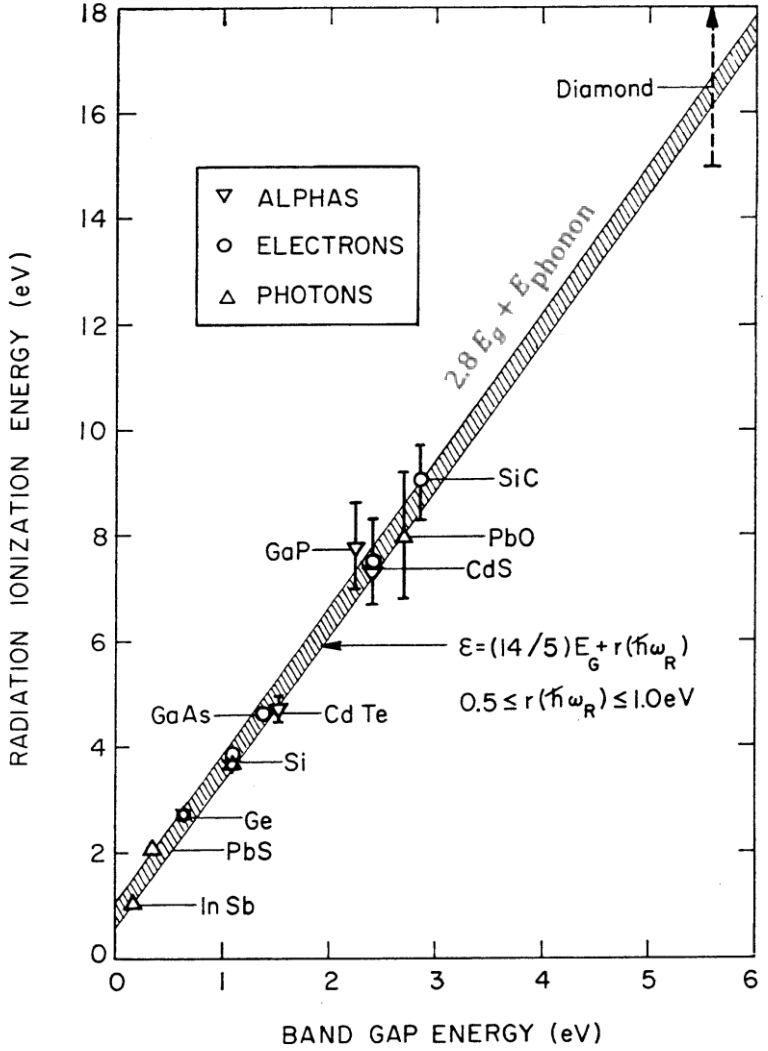

C.A. Klein, J. Applied Physics 39 (1968) 2029

Low Gain Avalanche Diodes – LGAD

UDS

- Charge multiplication
  - Gain ~ 10
  - Improved signal-to-noise w/r linear operation
- Uniform drift field
- The low gain in a small volume promises
  - Less charges involved, less crosstalk (not much relevant), less power, etc.
  - Better timing resolution
- R&D efforts
  - Increase spatial resolution
  - Include readout (LGAD-MAPS)

LGAD basic structure

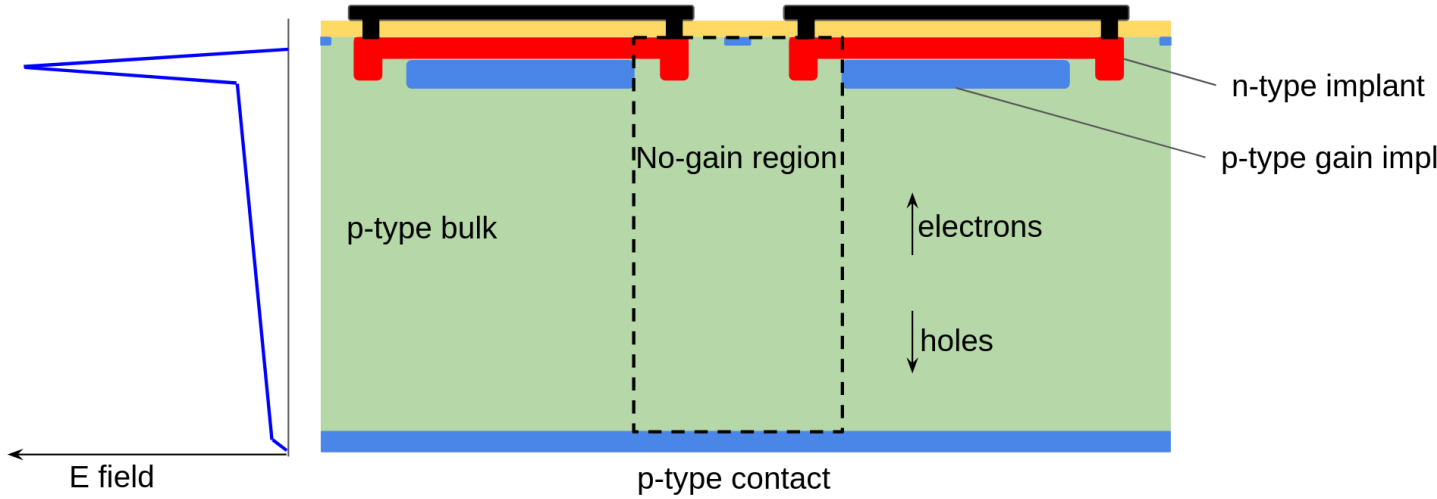

Trench Isolated LGAD: removes guard ring, smaller pitch

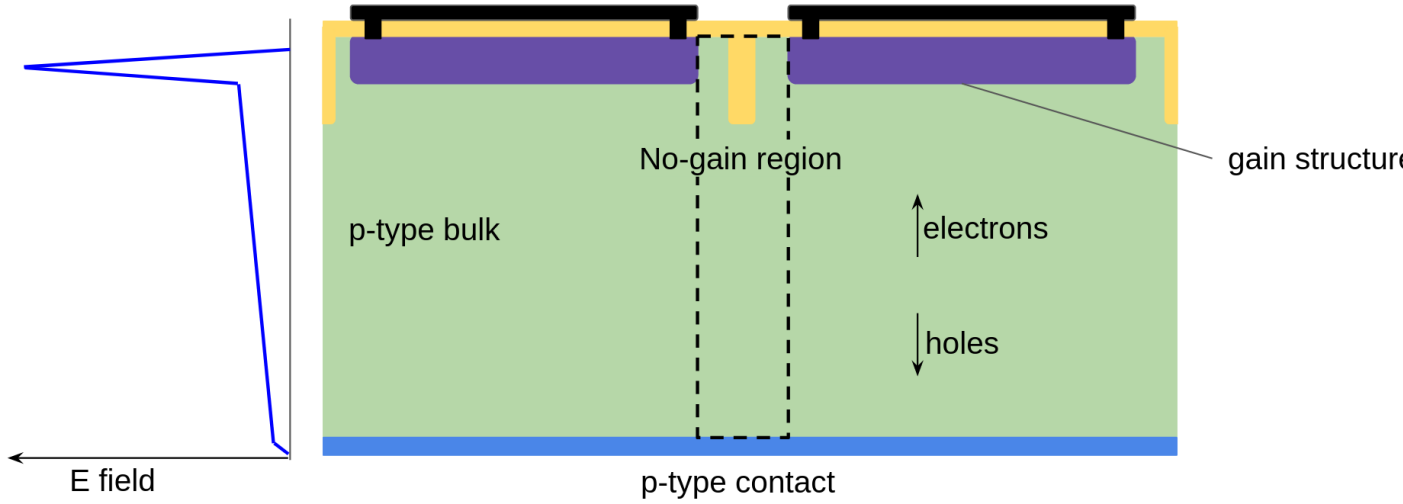

serge.charlebois@usherbrooke.ca

From Vignali et al, FBK 2025

Low Gain Avalanche Diodes – LGAD

UDS

- Various designs and optimizations exist

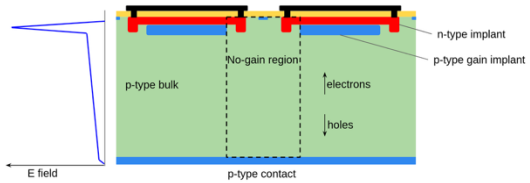

Trench Isolated LGAD

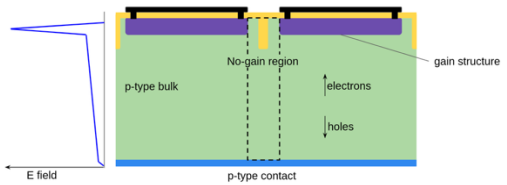

AC coupled LGAD

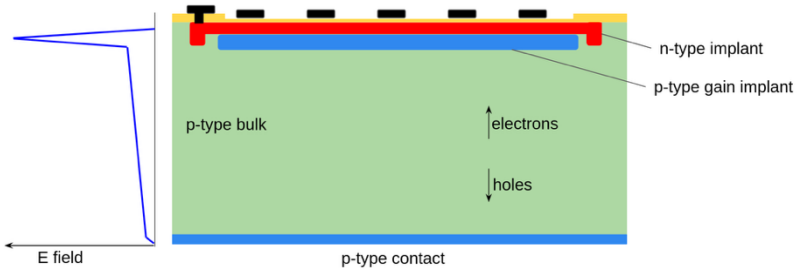

DC coupled LGAD

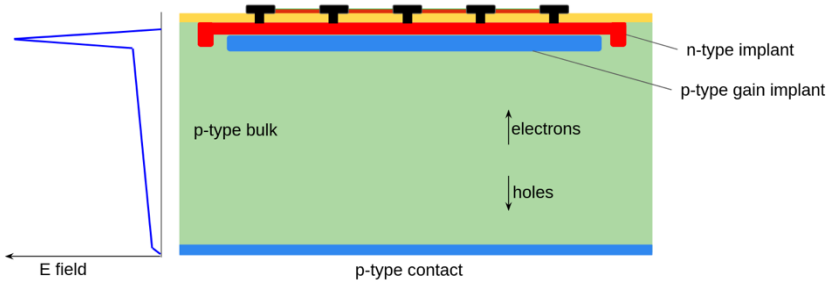

Double Junction LGAD

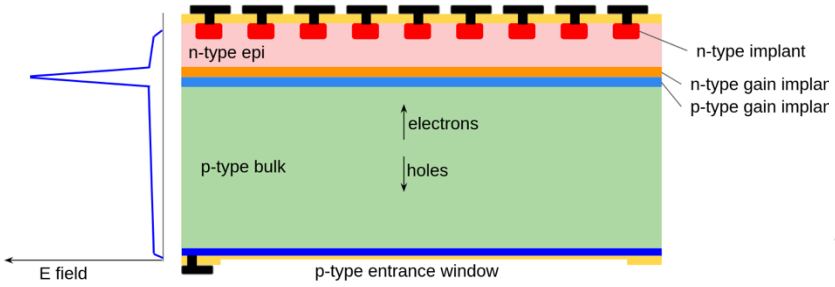

Double sided (inverted) LGAD

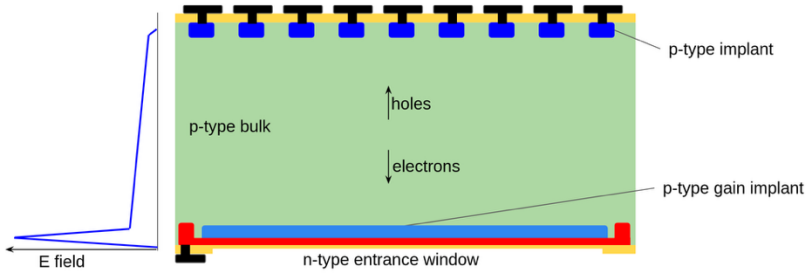

n-type LGAD

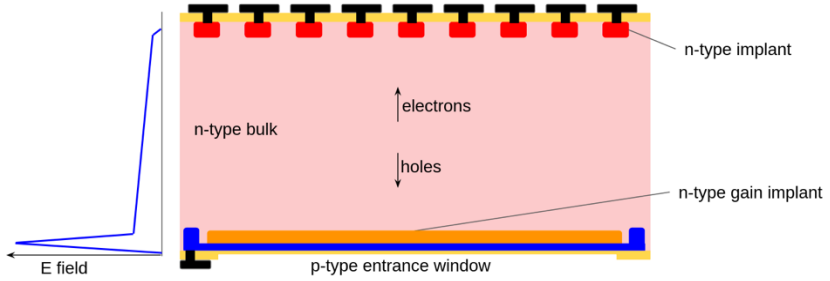

- A linear mode operated diode
- With embedded electronic readout
- A lot of variants and ongoing R&D:
  - Improving the charge collection volume, collection uniformity, timing jitter, etc.

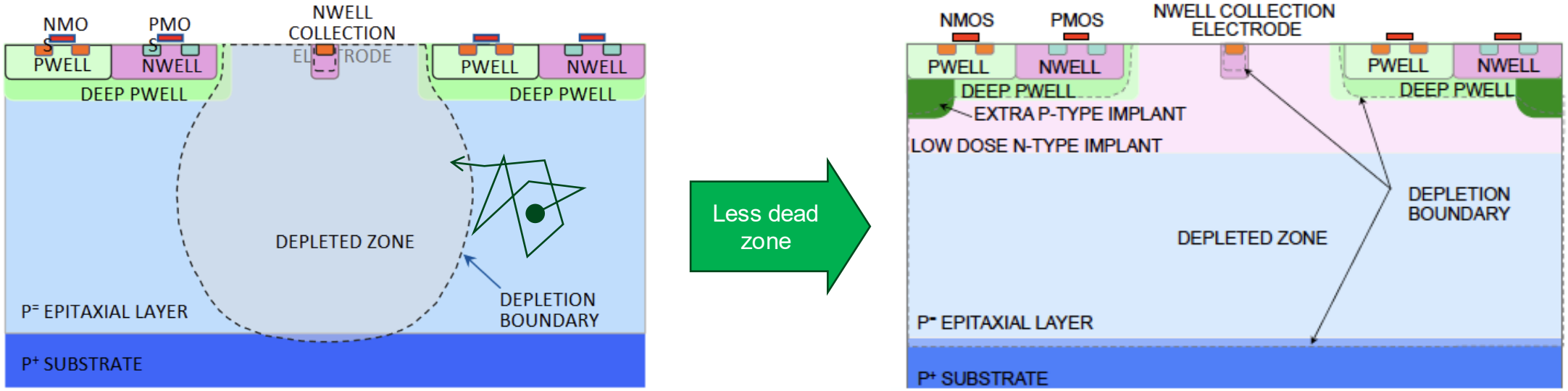

serge.charlebois@usherbrooke.ca

Extras

Extracting count rate and afterpulsing from data

Fitting an exponential distribution – many ways!

Exponential distribution in Lin-Lin representation

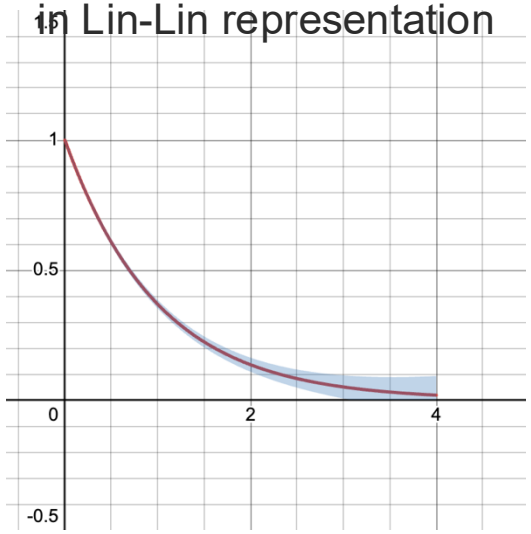

Log Y representation

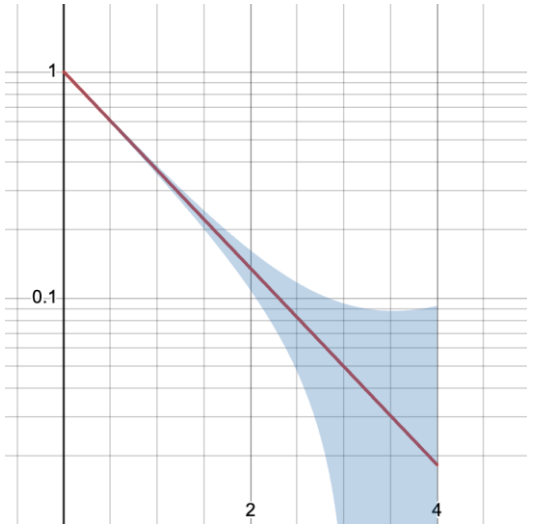

Log Y - Log X representation

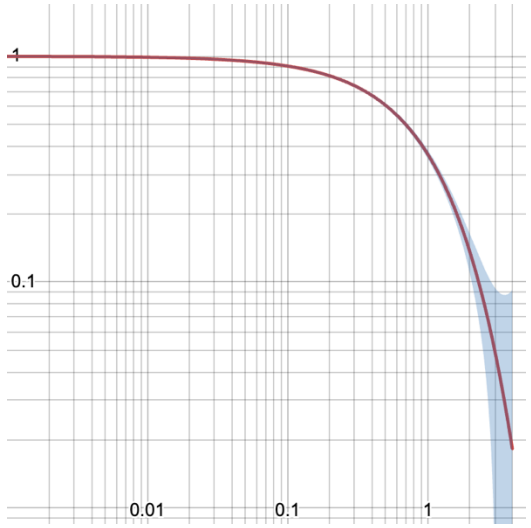

Log Y - Log binned X representation space

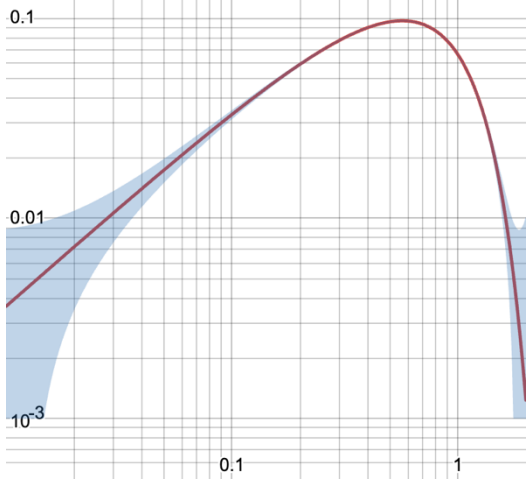

Lin Y - Log binned X fitting space

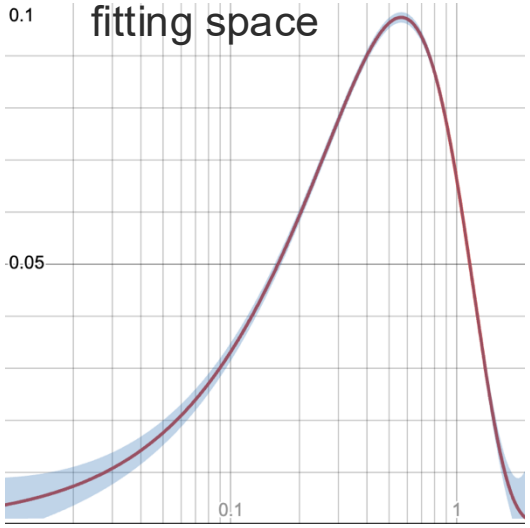

serge.charlebois@usherbrooke.ca

In a digital SiPM

- No need for pulse finding
- But no information on afterpulsing (partial charge peek)

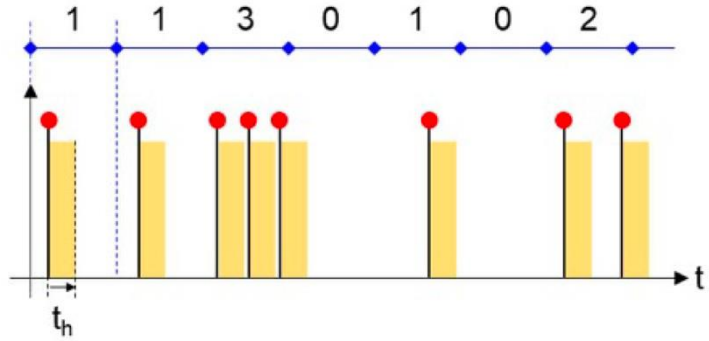

- Fitting a time delay histogram with abscissa logarithmically binned

$$f(t) \propto \frac{N_\Sigma}{1 - f_{AP}} \cdot t \cdot \lambda e^{-\lambda(t - t_h)}$$

  - Known parameters
    - t_h : hold off delay
    - N_Σ : total number of events in the histogram
  - To find
    - λ : the count rate
    - f_{AP}: the afterpulsing fraction

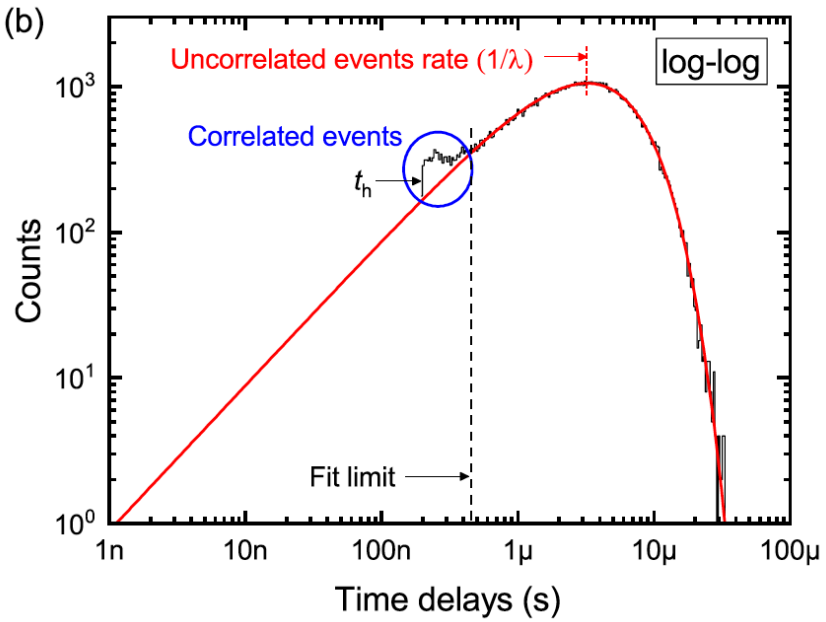

F. Vachon, 2020, doi: 10.1088/1361-6501/abba4b.

Detecting infrared using other materials than silicon

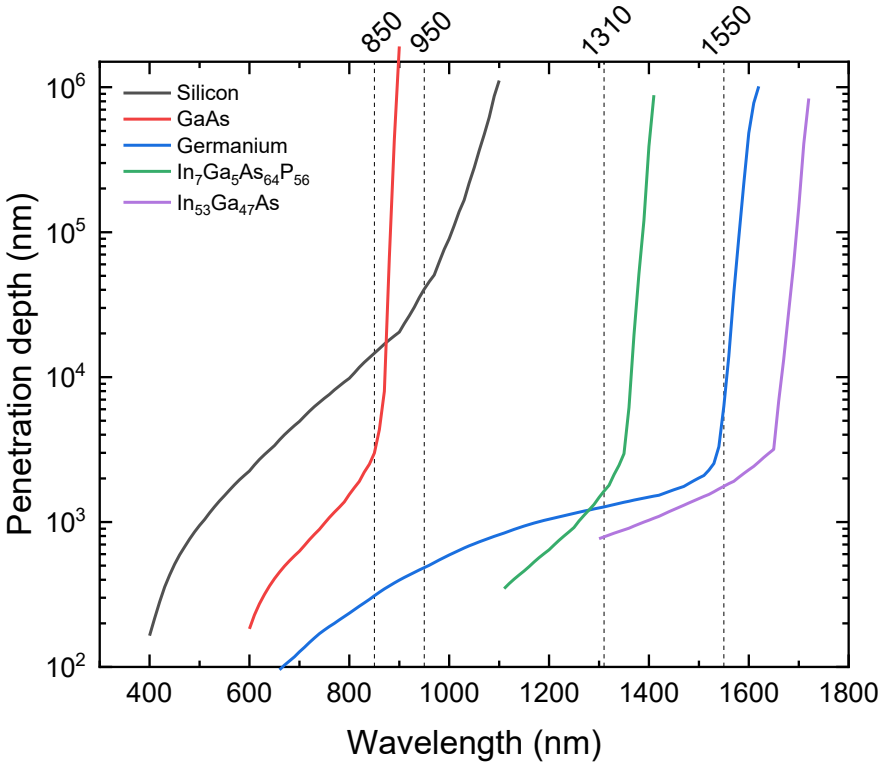

Comparative examples: InGaAs/InP versus Si-on-Ge

- Lattice constant
  - InP and $In_{0.53}Ga_{0.47}As$ = 5.87Å (matched) ✓
  - Si = 5.43Å and Ge = 5.66Å
    - 4.2% lattice mismatch ✗
- Energy bandgap
  - InP = 1.35eV and InGaAs = 0.75eV
    - $\Delta E_{Valence}$ = 0.347 eV
    - InP => holes for ionization ✗
  - Si = 1.11eV and Ge = 0.65eV
    - $\Delta E_{Conduction}$ = -0.34 eV
    - Si => electrons for ionization ✓

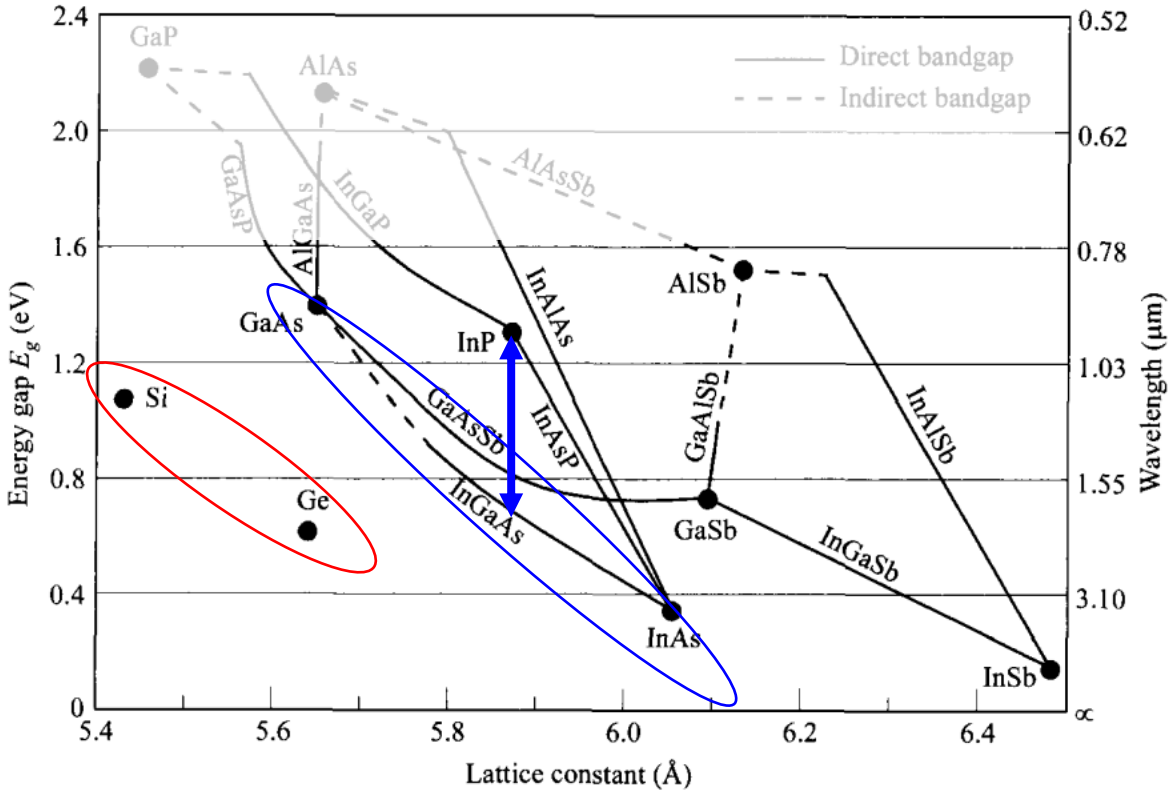

Fig. 32 Energy gap vs. lattice constant for some common elementary and binary semiconductors.

S.M. Sze 1969, Physics of semiconductor devices

Direct versus indirect band gap

- Dark noise (thermal carrier generation)
  - Proportional to $\exp(-E_g)$
  - Smaller gap leads to higher dark noise

- Divide and conquer: use two materials
  - One to **absorb** the photons: small band gap
  - One to **amplify** i.e. generate avalanche
  - Various designations:
    SAM (separate absorption multiplication), SAA, SACM, SAGCM...

- But silicon's dark noise is difficult to beat!
  - Silicon has an indirect band gap
  - 10^5 suppression of thermal generation
  - Dark noise dominated by mid-gap states
    - Shockley-Read-Hal ~ state density (not doping density)

- Germanium:
  - Is indirect but almost direct ($E_{\Gamma 1}$ ~ E_g)

InP	1.35 eV	0.8×
Silicon	1.11 eV	1×
$In_{53}Ga_{47}As$	0.75 eV	1.4×
Germanium	0.65 eV	1.6×

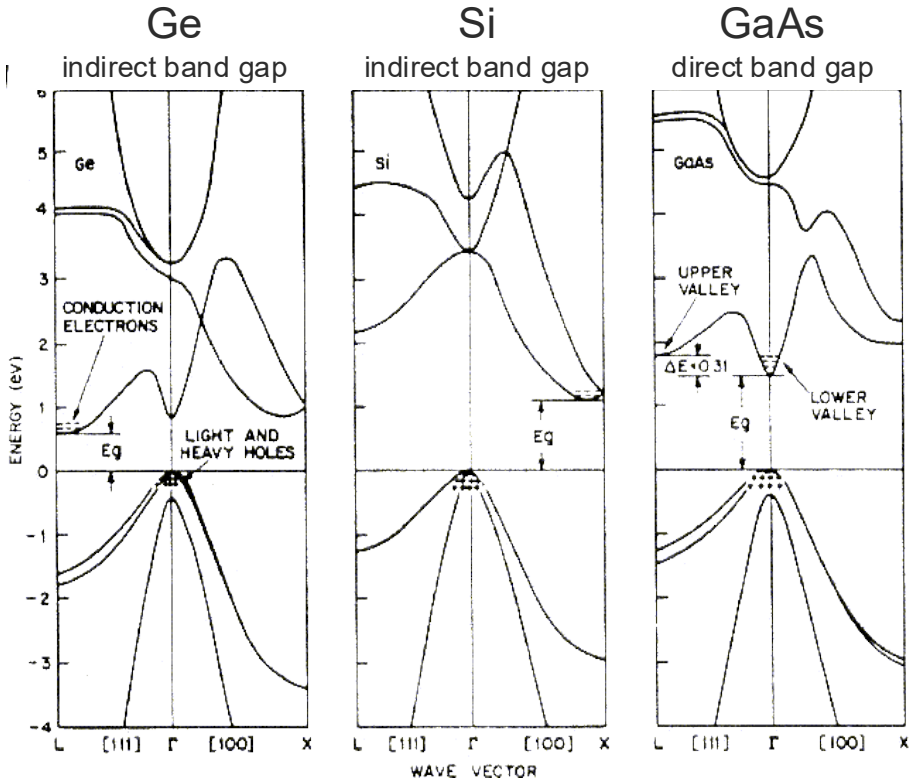

$E_g = E_L = 0.65$ eV
$\lambda = 1907$ nm
$E_{\Gamma 1} = 0.75$ eV

$E_g = E_X = 1.11$ eV
$\lambda = 1110$ nm
$E_{\Gamma 1} = 3.4$ eV

$E_g = E_{\Gamma 1} = 1.42$eV
$\lambda = 873$ nm

serge.charlebois@usherbrooke.ca

The band mismatch problem: InGaAs/InP versus Si-on-Ge

UDS

Type I heterostructure

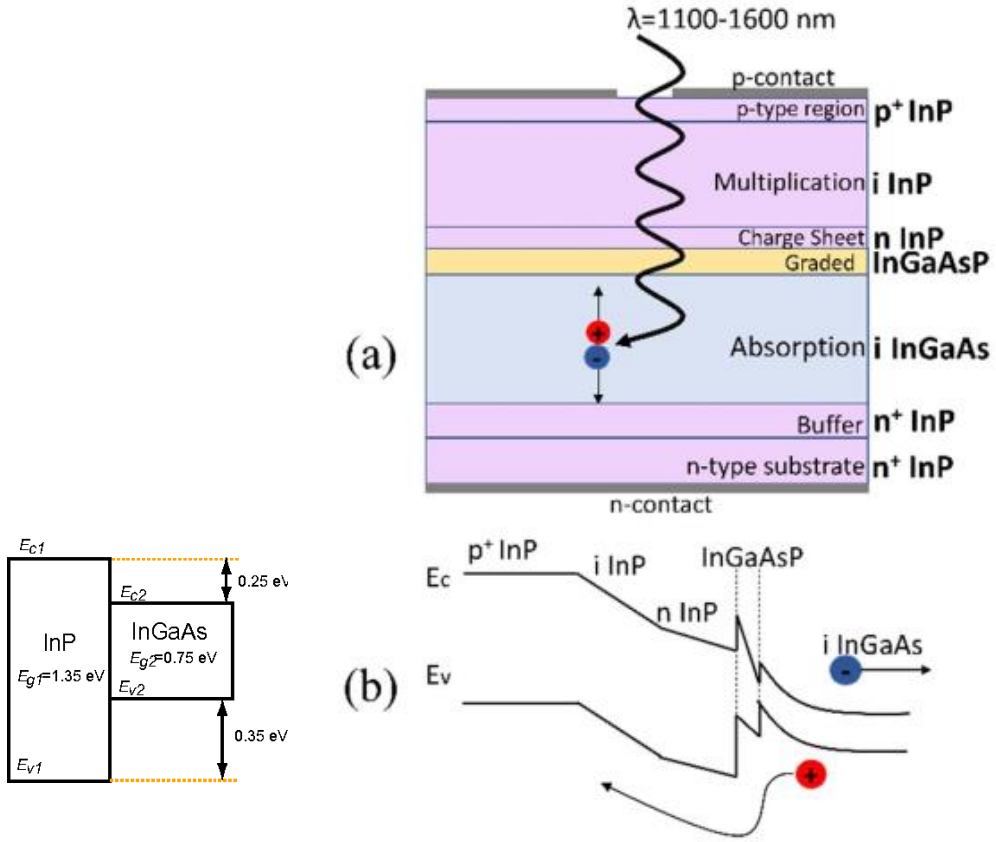

- InGaAs/InP SACM structure
- Holes need to overcome a barrier to reach InP
  - Graded InGaAsP to increase holes transfer/efficiency

Type II heterostructure

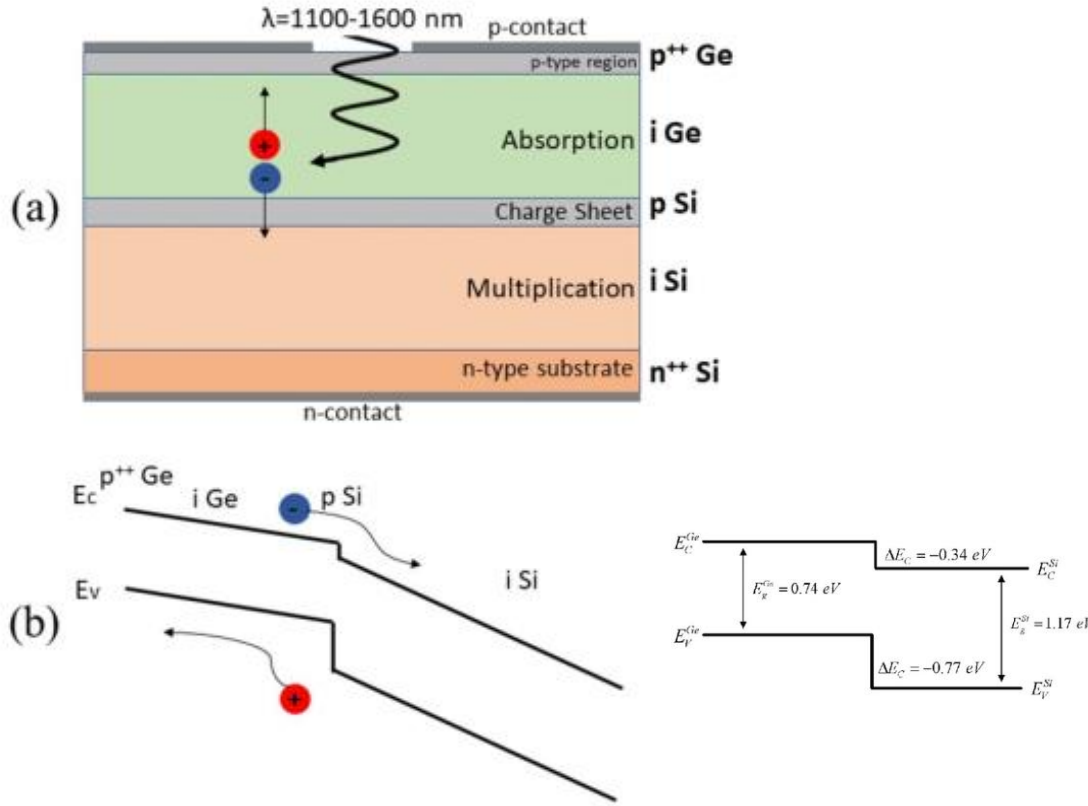

- Si-on-Ge SACM structure
- No barriers for photogenerated electrons
  - Electrons trigger the avalanche

serge.charlebois@usherbrooke.ca

Thorburn et al. 2022, “Ge-On-Si SPAD detectors for short-wave infrared”

In summary for the IR wavelengths

- Silicon is ineffective for detection above 1000 nm
  - Need to use a material with a higher absorption coefficient
- Small band gap semiconductors have high dark noise
- Divide and conquer: use two materials
  - One to **absorb**, one to **amplify (**SAM, SAA, SACM, SAGCM...)
- Ideal device would use silicon for amplification
  - No small gap semiconductors closely lattice matched
  - Ge (possibly Si_xGe_{1-x} alloys) seem ideal below 1550 nm
- Above 1550 nm is a material engineering challenge
  - Including industrialization and array integration
- Some reviews:
  - C. Liu, Chip, 1(1), 100005.
  - F. Thorburn, Journal of Physics: Photonics, 4(1):012001, 2021.

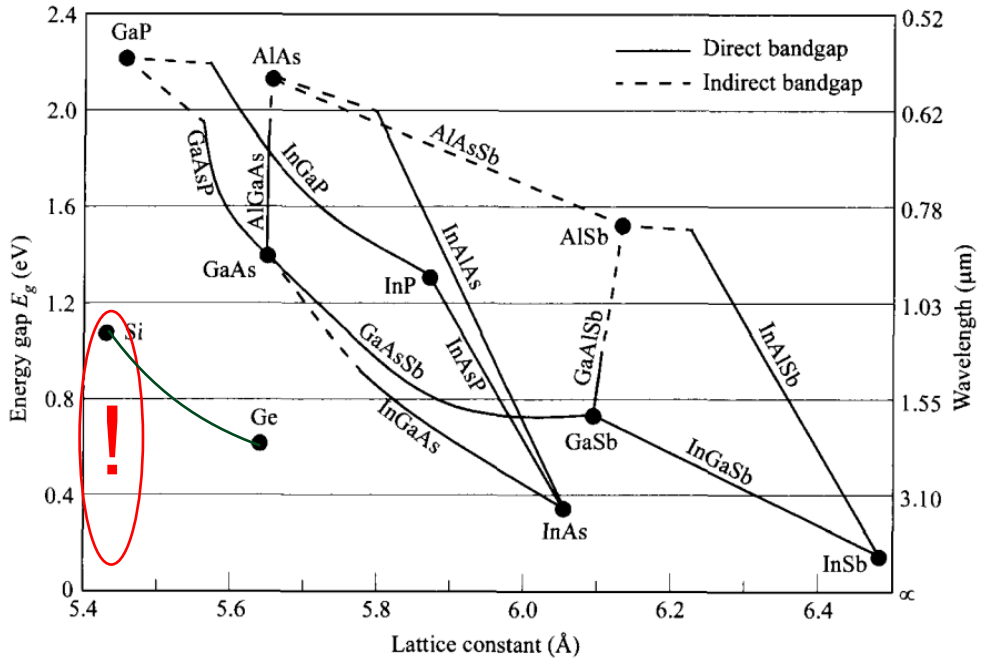

Fig. 32 Energy gap vs. lattice constant for some common elementary and binary semiconductors.